

AFIT/GA/ENY/92D-04

AD-A258 852



①

REWET PERFORMANCE OF A RECTANGULAR
GROOVED HEAT PIPE WICK AFTER
GRAVITATIONALLY INDUCED DRYOUT

THESIS

Lowell S. Hawthorne

Captain, USAF

AFIT/GA/ENY/92D-04

DTIC
SELECTE
JAN 07 1993
S B D

93-00052

Approved for public release; distribution unlimited

93 1 04 107

AFIT/GA/ENY/92D-04

REWET PERFORMANCE OF A RECTANGULAR GROOVED HEAT PIPE WICK
AFTER GRAVITATIONALLY INDUCED DRYOUT

THESIS

Presented to the Faculty of the School of Engineering
of the Air Force Institute of Technology

Air University

In Partial Fulfillment of the
Requirements for the Degree of
Master of Science in Astronautical Engineering

Lowell S. Hawthorne, B.S.M.E.

Captain, USAF

December 1992

Accession For	
NTIS GRA&I	<input checked="checked" type="checkbox"/>
DTIC TAB	<input type="checkbox"/>
Unannounced	<input type="checkbox"/>
Justification	
By	
Distribution/	
Availability Codes	
Dist	Avail and/or Special
A-1	

Approved for public release; distribution unlimited

NOT TO BE RELEASED

Acknowledgements

The process of designing, constructing, and performing an experimental thesis is a difficult task to say the least. It was an immense production at which I could not have succeeded if not for the assistance of a number of people.

I wish to thank Major Jerry Bowman, my thesis advisor, for his countless answers to my obvious questions and his support and encouragement throughout this effort. He is an outstanding instructor and advisor. I would also like to thank Jay Anderson and Andy Pitts, two laboratory experts without whom most AFIT students would never graduate. They both took the time to listen to what I wanted and then proceeded to construct an experimental set-up that performed exactly as I needed. Lastly, I would like to thank John Brohas of the AFIT model shop, who pulled me out of several jams, and Don Reinmuller down at the Wright Laboratory Thermodynamics Section, for his advice and supplies.

I also owe an enormous debt of gratitude to my incredible wife Lisa and her quiet encouragement. Even during the most trying times, she knew what it took to keep me going; but she also knew when to tell me to stop and smell the coffee. She is a remarkable woman and a great proof-reader. Ad Astra!

Lowell S. Hawthorne

TABLE OF CONTENTS

	Page
Acknowledgements	ii
List of Figures	vi
List of Tables	viii
List of Symbols	ix
Abstract	xii
I. INTRODUCTION	1
1.1 History	1
1.2 Background	1
1.3 Objectives	7
II. THEORY	9
2.1 The Heat Pipe Wick	9
2.2 The Pressure Balance Within a Heat Pipe	11
2.3 Capillary Pressure in Axial Groove Wicks	14
2.4 The Capillary Limit	16
2.5 Basic Heat Transfer Theory	22
III. EXPERIMENT DESIGN	27
3.1 Experiment Description	27
3.2 The Rectangular Groove	28
3.3 Inclination Control System	31
3.4 The Heater System	33
3.5 Working Fluid and Working Fluid Supply System	34

Supply System	34
3.6 Data Acquisition and Instrumentation	
System	38
3.7 Laboratory Environment	41
3.8 Overall Experimental Uncertainty	42
3.9 Experimental Procedure	44
IV. EXPERIMENTAL ANALYSIS	46
4.1 Thermocouple Mounting Procedure	
Validation	46
4.2 Thermocouple Calibration	48
4.3 Inclination System Calibration	49
4.4 Groove Heat Transfer Model	
Validation	51
4.4.1 Determining the Convective/ Radiative Heat Transfer Coefficient	51
4.4.2 Experimentally Validating the Groove Heat Transfer Model	54
4.5 Theoretical and Actual Capillary Limits on the Heat Transport Rate of the Groove	57
4.6 Experimental Test Sequence Descriptions	63
V. EXPERIMENTAL RESULTS	65
5.1 Nondimensionalizing the Heat Rates	65
5.2 Extent of Groove Dryout Under Varied,	

Increased Accelerations	67
5.3 Time Required for the Groove to Rewet Under Varied, Increased Accelerations .	69
5.4 Time Required for the Groove to Return to Steady-State Temperatures Under Varied, Increased Accelerations . . .	71
5.5 Observations of Dryout and Rewet Behavior	74
VI. CONCLUSIONS AND RECOMMENDATIONS	78
6.1 Conclusions	78
6.2 Recommendations	80
Bibliography	83
Appendix A. Plate Geometry	84
Appendix B. Convective/Radiative Heat Transfer Coefficient Test Data	88
Appendix C. Capillary Limit/Heat Transfer Model Validation Test Data	90
Appendix D. Working Fluid Properties	93
Appendix E. Experimental Test Data	94
Vita	128

LIST OF FIGURES

Figure	Page
1. Components and Operation of a Conventional Heat Pipe	2
2. Common Heat Pipe Wicks	10
3. Working Fluid Circulation Within a Heat Pipe . .	12
4. Meniscus Geometry of the Liquid-Vapor Interface .	15
5. Schematic of Gravitationally Induced Dryout Experiment	28
6. Schematic of Working Fluid Supply System	36
7. Heated Plate Heat Transfer Model	47
8. Groove/Plate Control Volume	55
9. Experimental and Theoretical Capillary Limit for the Axial Groove	62
10. Length of Groove's Dryout Region After Experiencing Short and Long Duration, Increased Acceleration	68
11. Time Required for the Groove to Rewet After Experiencing Short and Long Duration, Increased Acceleration	70
12. Time Required for the Groove to Return to Steady-State Temperatures After Experiencing Long-Duration, Increased Acceleration	73
13. Dryout Process in a Groove Experiencing Increased Acceleration	75

14.	Rewet Process in a Groove Experiencing	
	Increased Acceleration	76
A.1	Copper Plate and Groove; Right Side View	85
A.2	Copper Plate and Groove; Top View	86
A.3	Copper Plate and Groove; Front and Rear View	87

LIST OF TABLES

Table	Page
1. h_{cr} Values Corresponding to T_{ave}	53
2. q_{in} Versus q_{out} for Validating Groove Heat Transfer Model	56

LIST OF SYMBOLS

A	spatial area
a	acceleration force magnitude
Bi	Biot number; Eq (22)
c	specific heat
F_1	frictional coefficient
g	gravitational acceleration
h	convective heat transfer coefficient
h_{cr}	convective/radiative heat transfer coefficient
K	wick permeability
k	thermal conductivity
L	spatial length
L_a	groove adiabatic length
L_c	groove condenser length
L_e	groove evaporator length
L_t	groove length
L^*	nondimensional measure of the extent of dryout
L'	characteristic length
m	mass flow rate
P	pressure
P_{elec}	electric power
Q	heat transfer rate
Q_{cm}	capillary limit on the heat transfer rate
Q_{groove}	rate of heat transferred from system by the groove
Q_0	difference between the capillary limit at an

	angle θ and the input heat rate
Q_0	difference between the capillary limit at $\theta=0$ and the input heat rate
Q^*	nondimensional measure of the degree the input heat rate exceeds the capillary limit due to increased acceleration forces
(QL)	heat transport factor
R	radius of curvature
T	temperature
t	thickness
V	volume
w	width of groove
x	spatial coordinate; liquid flow direction
<i>Greek</i>	
Δ	difference, drop, or error
δ	groove depth
θ	angle between groove bottom and local horizontal
λ	latent heat of vaporization
μ	viscosity
ρ	density
σ	surface tension
τ	time constant
ψ	angle between acceleration vector and fluid flow direction

Subscripts

ave	average value
c	capillary value
cm	maximum, or limiting, capillary value
cr	convective/radiative value
dry	dryout region
evap	evaporative value
exp	experimental value
groove	out of or into groove
∞	free-stream condition
l	liquid value
min	minimum value
pc	phase change value
ref	reference value
rewet	rewet value
s	surface value
ss	steady-state value
theory	theoretical value
v	vapor value
w	wick, or groove, value

ABSTRACT

The effects of increased acceleration forces on the transient dryout and rewet performance of an axial groove heat pipe wick were experimentally studied using inclination to simulate increased acceleration forces. Two durations of increased acceleration forces were investigated, one being less than the time required for the groove to reach steady-state dryout conditions, the other being sufficient to ensure the groove had reached steady-state dryout conditions. The groove's extent of dryout was found to be greater at increased levels of acceleration force. The period of time required for the groove to rewet after an acceleration induced dryout increased as acceleration increased. The period of time for rewet was independent of duration for higher acceleration levels. The time period required for the groove to return to starting steady-state temperatures was zero for short durations of increased acceleration, and increased as acceleration increased for long durations.

REWET PERFORMANCE OF A RECTANGULAR GROOVED HEAT PIPE WICK AFTER GRAVITATIONALLY INDUCED DRYOUT

I. INTRODUCTION

1.1 History

Over the past 28 years, the heat pipe has been developed into a highly effective and reliable heat transmission device. First conceived and patented by R.S. Gaugler of the General Motors Corporation in 1944, the device was not developed beyond the patent stage until 1964 when G. M. Grover of the Los Alamos Laboratory independently reinvented the concept and began performing developmental research (4:1). Grover is credited with first coining the name "heat pipe" to describe this remarkable device. Since 1964, over a thousand papers and patents on heat pipes have been published (3:1).

1.2 Background

Though there are many references and papers describing the operation of heat pipes presently in publication (3,4), most people are still relatively unfamiliar with the operation of this device. Thus, a brief discussion of heat pipe operating principals should prove useful as background for this thesis.

The heat pipe is a passive heat transfer device which, though termed a 'pipe', can be constructed in a variety of

forms. The conventional form of the heat pipe is a closed tube or chamber with an interior surface that is lined with a porous capillary structure called the wick, which can take many forms. The wick is saturated with the liquid phase of a working fluid, while the rest of the heat pipe contains the vapor phase of this same working fluid.

In operation, as shown in Figure 1, heat is applied to

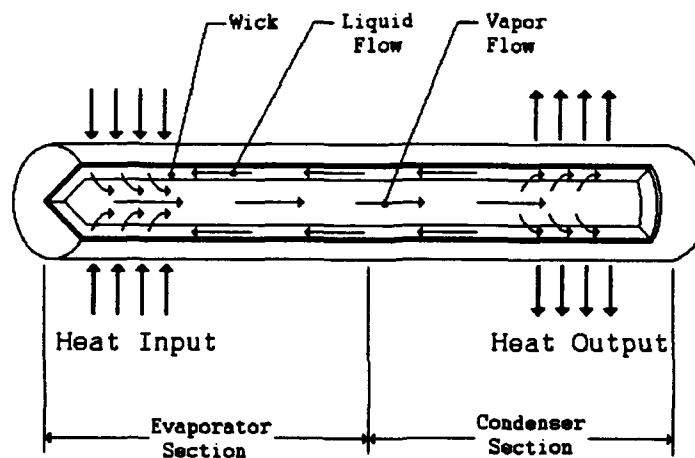


Figure 1. Components and Operation of a Conventional Heat Pipe

one end of the heat pipe, called the evaporator section, and rejected from the other end of the heat pipe, the condenser section. Within the evaporator section, input heat vaporizes the working fluid held in the wick, causing a pressure difference which drives the vapor to the condenser section. This vapor then condenses on the cooler surface of the condenser, releasing the latent heat of vaporization to a heat sink. Capillary pressure developed by the wick then

pumps the working fluid, in liquid form, through the wick back to the evaporator section. This simple cycle continuously transfers the working fluid's latent heat of vaporization from the evaporator section to the condenser section. This cycle has several limits. The *sonic limit* occurs when vapor leaves the evaporator at sonic speeds and the flow becomes choked. The *entrainment limit* occurs when the vapor flow actually tears liquid from the surface of the liquid-vapor interface and decreases the amount of working fluid which reaches the evaporator. The *capillary limit* is reached when the maximum capillary pressure is lower than the sum of the liquid and vapor pressure losses within the wick. And lastly, the *boiling limit* is reached when vapor production in the evaporator is so great that it hinders the return of liquid to the evaporator. The capillary limit is most important to this research. When the capillary limit is exceeded, the heat pipe's wick dries out, (appropriately termed 'dryout'), and the working fluid can no longer be pumped to the evaporator section, halting the heat transfer cycle.

Due to the simplicity of the above cycle, heat pipes offer several advantages over more conventional heat transfer devices: constructional simplicity, application flexibility, ability to transport heat at a high rate over a large distance with low temperature drop, and the benefit of requiring no external pumping power. Owing to their high

reliability and simplicity, heat pipes have been used to remove heat and smooth temperature gradients in a variety of earthbound and spaceborne applications. Examples are nuclear and isotope reactor cooling; cooling and isothermalization of spacecraft components and spacesuits; heat collection from exhaust gases; and the cooling of die cutting and casting tools in manufacturing (3:14).

Of more significance to the Air Force, however, is the proposed use of heat pipes to reduce peak temperatures and large thermal gradients at the leading edges of the wings and engine nacelles of hypersonic aircraft such as the National Aerospace Plane (NASP). Both on and off the stagnation line of an object in hypersonic flight, skin friction and heat transfer create enormous peak temperatures and temperature gradients. To enable the NASP to achieve the velocities its mission dictates without leading-edge cooling would require materials beyond the level of today's technology. However, by using innovative cooling schemes for the leading edges of hypersonic aircraft, the materials requirement can be brought back into the realm of materials available at the present level of technology.

In this concept, an array of heat pipes absorbs aerodynamic heat at the leading edges of the aircraft and transports the heat to the trailing upper and lower surfaces of the aircraft where it is rejected via convection and thermal radiation (8:1). The virtues of a heat pipe seem

almost custom-tailored to this purpose. Its inherent simplicity and lack of moving parts make the heat pipe a reliable choice for cooling in such critical areas. Additionally, the heat pipe's nearly isothermal behavior helps eliminate severe temperature gradients at the leading edges, thus lowering thermal stresses and allowing a lower-weight airframe.

Though the heat pipe seems perfectly suited to this use, little is known about the effects of increased accelerations on a heat pipe's performance. These accelerations could result from centripetal or lateral accelerations and decelerations brought about by aerial maneuvers, or by the re-entry into a planet's gravitational field from orbit. Knowledge of these effects would not only be useful in the design of the NASP, but also in designing heat pipes capable of withstanding varying satellite spin rates at arbitrary inclinations.

Since adverse accelerations primarily affect the wick's ability to pump working fluid to the evaporator section, an examination of how the wick itself is affected by increased accelerations would be the most valuable area to begin researching the overall problem. To this end, the present work is directed towards empirically examining the effects of increasing acceleration forces on a specific heat pipe wick.

There were two primary reasons for conducting this

research effort. The first reason was to experimentally investigate and document the transient performance of a heat pipe wick under increasing gravity loads to simulate increasing accelerations and aid in determining whether the heat pipe could operate in the constantly changing environment of an aircraft's flight regime. The second reason was to compile data for use in future efforts to model the transient behavior of the working fluid inside a wick experiencing varying accelerations.

A survey of current literature indicated that knowledge in this area is very limited. Though a great deal of research has been performed on the subject of using heat pipes to cool the leading edges of hypersonic aircraft, virtually all research dealt with the steady-state behavior of a heat pipe experiencing increased accelerations. Silverstein (8) addressed leading edge heat pipe performance under transient conditions, but failed to address capillary pressure or wick performance. Silverstein (8), Camarda (2), and Boman et al. (1) modelled increased accelerations by tilting the heat pipe to simulate an increased acceleration field corresponding to the effect of gravity at different tilt-angles. All papers, however, observed only the steady-state performance of the heat pipe at each angle and corresponding acceleration. A large body of knowledge was present on both the rectangular groove arterial wick design and the screen wick design. The grooved wick is simply a

series of grooves running longitudinally down the length of the heat pipe. Each groove transports working fluid via capillary pressure created by groove width. The screen wick is a layer of fine metal mesh lining the heat pipe and transporting fluid down the length of the heat pipe. For screen wicks, the capillary pressure is based on the fineness, or porosity, of the mesh. The amount of research performed on each wick being almost equal, the grooved wick design was chosen for several reasons discussed further in Chapter 2.

1.3 Objectives

The objectives of this research are as follows:

(1) Observe the extent of wick dryout in a rectangular grooved heat pipe wick under varied, increased gravity loads, simulating increased accelerations at different heat input levels.

(2) Observe the time required for the wick to rewet in a rectangular grooved heat pipe wick under varied, increased gravity loads and different heat input levels.

(3) Observe the time required for the wick to return to starting temperature in a rectangular grooved heat pipe wick under varied, increased gravity loads and different heat input levels.

The steps taken to meet these objectives are presented in this research thesis. Throughout the thesis, reference will be made to the basic theory involved in the

understanding of a heat pipe grooved wick contained in Chapter 2. An in-depth discussion of the experimental test apparatus, each component's purpose, and all construction techniques are presented in Chapter 3. Chapter 4 contains the experimental analysis required to determine the grooved wick's operating limits and validate all construction procedures and calibrations. Finally, the results from thirteen experiments are presented and discussed in Chapter 5, while Chapter 6 contains a summary of recommendations and conclusions with regards to the work performed during this research effort.

II. THEORY

The primary purposes of this chapter are to identify the governing equations used to determine the performance of a heat pipe grooved wick as well as the governing heat and mass transfer equations used throughout this effort. The full heat pipe governing equations do not completely apply to this experiment. This chapter shows which governing equations do apply and where the experiment differs from an actual heat pipe.

2.1 The Heat Pipe Wick

As stated in Chapter 1, the wick is the structure within the heat pipe which transports the working fluid, in its liquid form, from the condenser section of the heat pipe to the evaporator section. This movement of the working fluid is a very important heat pipe factor, making the wick a crucial component of the heat pipe. The heat transport capability of the heat pipe is directly linked to the ability of the wick to return the liquid from the condenser to the evaporator. Maximum heat transport corresponds to maximum fluid circulation.

There are an enormous number of different wicks currently in use within the heat pipe industry; many more than could be covered in this thesis. Figure 2 illustrates three of the most commonly used wicks. The first wick, a wrapped screen, is perhaps the most common. In a wrapped

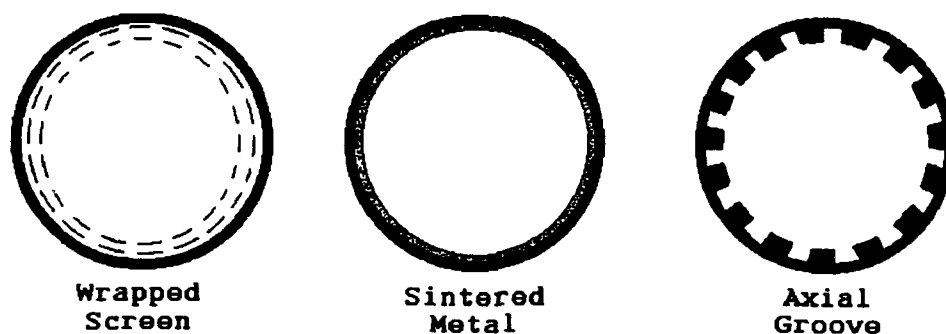


Figure 2. Common Heat Pipe Wicks

screen wick, very fine mesh screen is simply rolled into a tube and placed inside the pipe, where it is then unrolled so that the screen firmly contacts the pipe's walls. The pores of the screen draw the working fluid to the evaporator section. The sintered metal wick is a metal insert which has a fine metallic powder fused to its inner surface. This metal powder provides a porous medium that wicks the fluid back to the evaporator section of the heat pipe. The last wick in Figure 2, an axial groove wick, is simply a series of grooves milled into the inner surface of the heat pipe. These grooves run longitudinally down the length of the pipe. The axial groove wick has performed very well in

moderate-heat applications, and like the wrapped screen wick, is used extensively in the heat pipe industry (3:6).

The axial groove wick was chosen for this effort for several reasons. First, it has been tested and used extensively in numerous research projects and actual applications. Secondly, because it performs well in moderate-heat applications, it was well-suited for an AFIT laboratory. Lastly, of all the common wicks, only the axial groove wick allows the actual working fluid to be visually observed within the channel. The remainder of this chapter's discussion of heat pipe governing equations will apply to axial groove wicks unless otherwise indicated.

2.2 The Pressure Balance Within a Heat Pipe

Though a heat pipe is mechanically simple, its inner workings are amazingly complex. The heat pipe depends on a pressure balance to maintain its heat transport cycle. This section will briefly cover the basic heat pipe pressure balance, but the reader is referred to references (4) and (3) for a more complete explanation.

First, there exists an axial pressure variation along the vapor passage, shown in Figure 3, with maximum vapor pressure at the heat input end of the heat pipe and minimum vapor pressure usually occurring at the heat sink end of the heat pipe. At the same time, the axial pressure variation in the liquid saturated wick causes the working fluid to flow through the wick from the condenser back to the

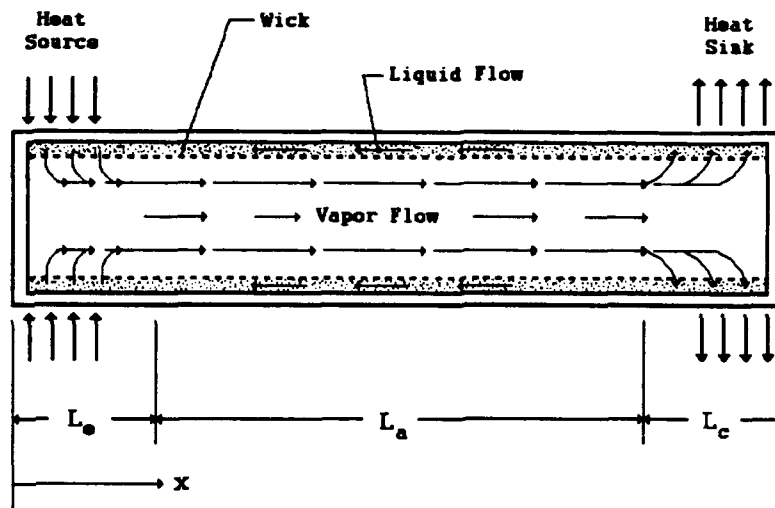


Figure 3. Working Fluid Circulation Within a Heat Pipe

evaporator. Since the heat pipe is a sealed system, the two pressures must be balanced. This balance requires that along the length of the heat pipe the pressure at the liquid side of the vapor-liquid interface within the wick must be different than the pressure at the vapor side of the interface, except in the condenser, where the two pressures are equal (3:33). This pressure difference is called the capillary pressure. A basic explanation of this pressure differences' origin would be helpful before continuing.

The difference in pressures at the liquid-vapor interface is established by the meniscus that forms at the liquid-vapor interface. Since molecules in a liquid attract

each other, the molecules at the liquid-vapor interface experience a force inward, forcing the liquid to take up a concave shape having minimum area (4:20). Surface tension is defined as the work required per unit area to increase the surface area of a fluid. A direct consequence of surface tension is that the pressure on a concave surface is less than that on a convex surface, resulting in a pressure difference, or capillary pressure, at the interface.

The pressure balance inside of a heat pipe can be described mathematically (3:33) as

$$[P_v(x_{ref}) - P_v(x)] + [P_v(x) - P_l(x)] + [P_l(x) - P_l(x_{ref})] + [P_l(x_{ref}) - P_v(x_{ref})] = 0$$

And the previously mentioned capillary pressure, P_c , is defined as the vapor pressure, P_v , minus the liquid pressure, P_l , or mathematically (3:33), as

$$P_c(x) = P_c(x_{ref}) + \Delta P_v(x - x_{ref}) + \Delta P_l(x_{ref} - x) \quad (1)$$

where

$$\begin{aligned} P_c(x) &= \text{capillary pressure at position } x \\ &= P_v(x) - P_l(x) \quad (\text{N/m}^2) \\ P_c(x_{ref}) &= \text{capillary pressure at reference position } x_{ref} \\ &= P_v(x_{ref}) - P_l(x_{ref}) \quad (\text{N/m}^2) \\ \Delta P_v(x - x_{ref}) &= \text{vapor pressure drop between } x \text{ and } x_{ref} \\ &= P_v(x) - P_v(x_{ref}) \quad (\text{N/m}^2) \\ \Delta P_l(x_{ref} - x) &= \text{liquid pressure drop between } x_{ref} \text{ and } x \\ &= P_l(x_{ref}) - P_l(x) \quad (\text{N/m}^2) \end{aligned}$$

The reference position, x_{ref} , is usually chosen to be at x_{min} , where P_c is equal to zero, so that Equation (1) reduces to

$$P_c = \Delta P_v(x - x_{min}) + \Delta P_l(x_{min} - x) \quad (2)$$

This simple equation is the basis of the inner workings of all heat pipes. As will be further demonstrated throughout this chapter, the capillary pressure of the groove used in this research depended only on the liquid pressure drop, $\Delta P_l(x - x_{min})$. This was because the experimental groove was not in a sealed system, but was in the open environment and thus could not experience a vapor pressure gradient along its length.

2.3 Capillary Pressure in Axial Groove Wicks

Just as the capillary pressure can be expressed in terms of the pressure balance within the heat pipe, it can also be expressed in terms of the meniscus of the liquid-vapor interface within the wick; a direct consequence of the working fluid's surface tension and the molecular attraction between its molecules.

The LaPlace-Young equation (4:22,3:34) may be used to calculate the pressure difference, or capillary pressure ($P_v - P_l$), across a liquid-vapor interface,

$$P_c(x) = \sigma \left(\frac{1}{R_1(x)} + \frac{1}{R_2(x)} \right) \quad (3)$$

where R_1 and R_2 , as shown in Figure 4, are the principal radii of curvature of the meniscus of the liquid-vapor

interface in meters, and σ is the surface tension of the fluid in N/m.

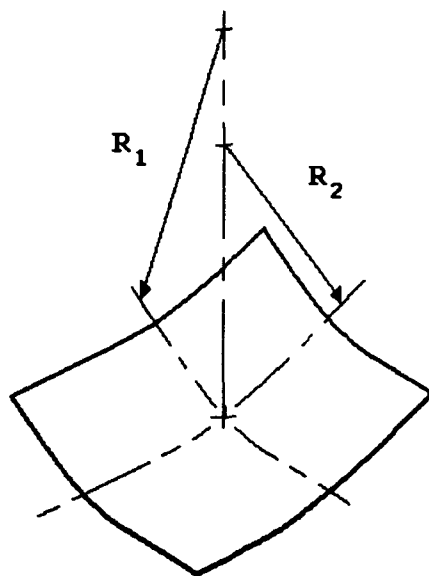


Figure 4. Meniscus Geometry of the Liquid-Vapor Interface

In an axial groove, one of the radii of curvature, (corresponding to the lengthwise meniscus), is infinity, while the other radius of curvature, (spanning the width of the groove), ranges from infinity to half the width of the groove depending on the amount of fluid in the groove (3:36). The maximum capillary pressure is

$$P_{cm} = \frac{2\sigma}{w} \quad (4)$$

Where w is the width of the groove. Armed with these expressions for capillary pressure, the liquid pressure drop along the length of the groove, and hence the groove's capillary limit, can be calculated.

2.4 The Capillary Limit

The capillary pressure developed by the wick provides the driving force for overcoming pressure losses for liquid and vapor flows. Therefore, for continued operation, the maximum capillary pressure, P_{cm} , must satisfy the following relationship:

$$P_{cm} \geq \Delta P_l + \Delta P_v \quad (5)$$

where ΔP_l is the liquid pressure drop experienced by the working fluid in returning from the condenser to the evaporator and ΔP_v is the vapor pressure drop causing the vapor to flow from the evaporator to the condenser. Again, this experiment differed from an actual heat pipe in that ΔP_v was equal to zero because the groove was open to the laboratory environment. However, because the vapor loss in heat pipes is usually small relative to the liquid pressure, the vapor pressure loss is typically neglected in heat pipe design, so the validity of this effort was not harmed by the difference between experiment and an actual heat pipe (6:24).

If Equation (5) is not satisfied, the wick will dry out in the evaporator section and the heat transfer cycle will halt. At the maximum operating condition the capillary

limit is expressed by

$$P_{cm} = \Delta P_l + \Delta P_v \quad (6)$$

or in the case of this experiment's groove,

$$P_{cm} = \Delta P_l \quad (7)$$

To determine the capillary limit, the liquid pressure drop must be determined. The liquid pressure drop in a wick arises from three sources: 1) frictional drag losses from flow in the wick, 2) inertial losses due to changes in momentum, and 3) changes in hydrostatic head resulting from body forces caused by gravity, aerobatic maneuvers or centripetal acceleration. The pressure loss associated with changes in momentum is generally neglected due to its relatively small magnitude (6:25).

Referring back to Figure 3, the liquid pressure drop in a wick can be obtained by integrating the liquid pressure gradient down the length of the pipe:

$$P_l(x_{min}) - P_l(x) = - \int_{x_{min}}^x \frac{dP_l}{dx} dx \quad (8)$$

The liquid pressure gradient in the direction of liquid flow is related to the frictional drag and hydrostatic head (3:42) by the equation

$$\frac{dP_l}{dx} = -F_l Q + \rho_l a \cos \psi \quad (9)$$

In the first term of Equation (9), Q is the local axial heat transfer rate, in Watts and F_l is the frictional

coefficient for the liquid flow in $(N/m^2)/W-m$, defined as

$$F_1 = \frac{\mu_1}{KA_w \lambda \rho_1} \quad (10)$$

where the variables in Equation (10) are defined as follows:

- μ_1 = liquid viscosity (kg/m-sec)
- ρ_1 = liquid density (kg/m³)
- λ = liquid latent heat of vaporization (J/kg)
- A_w = wick cross-sectional area (m²)
- K = wick permeability (m²)

Wick permeabilities are a property of the wick structure and are tabulated in several references (3:42).

The frictional loss in pressure is directly related to the axial heat flux, as seen in Equation (9). As the axial heat input increases, the mass flow of the liquid increases as more fluid evaporates. This increases the fluid's velocity and in turn increases the frictional pressure drop in the liquid flow. When this pressure drop in the liquid exceeds the maximum capillary pressure, Eq (5) is no longer satisfied and dryout of the wick begins.

In the second term of Equation (9), ρ_1 is the liquid density, a is the magnitude of the local body force acceleration in m/sec², and ψ is the angle between the local body acceleration vector and the direction of liquid flow. If the only acceleration acting on the wick is gravity, then:

$$\rho_l a \cos \psi = \rho_l g \sin \theta \quad (11)$$

where g is the acceleration due to gravity and θ is the magnitude of the angle between the direction of fluid flow and the local horizontal. This result can be substituted into Equation (9), yielding

$$\frac{dP_l}{dx} = -F_l Q \pm \rho_l g \sin \theta \quad (12)$$

The \pm is added to this equation because, depending on the orientation of the wick, gravity will either aid or hinder the liquid pressure drop. Additionally, if other accelerations, i.e. centripetal or lateral accelerations, are also acting on the wick in the same direction as gravity, their values need to be added to the value for the acceleration due to gravity in Equation (12). In this thesis, an increase in acceleration forces was simulated by increasing the angle θ .

All that remains now in order to find the axial pressure variation in the liquid filled groove is to perform a simple integration of Equation (12) down the length of the groove. Substituting Equation (12) into Equation (8) yields the following expression for the capillary limit of an axial groove wick:

$$P_{cm} = - \int_{x_{min}}^x \frac{dP_l}{dx} dx = - \int_{x_{min}}^x (-F_l Q \pm \rho_l g \sin \theta) dx \quad (13)$$

or, assuming x_{min} equal to zero,

$$P_{cm} = F_1 QL_t \pm \rho_1 g L_t \sin \theta \quad (14)$$

where L_t equals the entire length of the heat pipe in meters.

Substituting Equation (7) into Equation (14) gives:

$$\frac{2\sigma_1}{w} = F_1 QL_t \pm \rho_1 g L_t \sin \theta \quad (15)$$

Assuming inclinations only above the horizontal, QL_t in Equation (15) can be isolated to give an expression which is defined as the capillary limitation on the heat transport factor, $(QL)_{cm}$, (with units of W-m).

$$(QL)_{cm} = \frac{\frac{2\sigma_1}{w} - \rho_1 g L_t \sin \theta}{F_1} \quad (16)$$

Finally, the capillary limitation on the heat transport rate, Q_{cm} , can be derived from the heat transport factor, $(QL)_{cm}$. For the case of uniform heat flux along both the evaporator and the condenser

$$(QL)_{cm} = (0.5L_e + L_a + 0.5L_c) Q_{cm} \quad (17)$$

or,

$$Q_{cm} = \frac{(QL)_{cm}}{0.5L_e + L_a + 0.5L_c} \quad (18)$$

where

L_e = length of the heat pipe's evaporator section (m)

L_a = length of the heat pipe's adiabatic section (m)

L_c = length of the heat pipe's condenser section (m)

Equation (18), though precisely termed the capillary heat transport limit, is usually shortened to merely the capillary limit in most heat pipe literature. As will be seen in Chapter 3, the experimental groove used in this effort has no condenser length, thus $L_c = 0$. Substituting $L_c = 0$ into Equation (18), the capillary heat transport limit for this experiment becomes

$$Q_{cm} = \frac{(QL)_{cm}}{0.5L_e + L_a} \quad (19)$$

This expression for the capillary heat transport limit was used throughout this research effort. Of primary importance is the realization that the liquid velocity is very low, thus the fluid flow is assumed laminar and incompressible. By following the path of circulation of the working fluid, the maximum capillary pressure is seen to occur at the end of the evaporator and the minimum capillary pressure is seen to occur at the end of the condenser. From Equation (18) it can also be seen that as the body force accelerations or angle θ increase, the capillary limit decreases and the groove dries out at a lower input heat flux.

The preceding concepts and derivations were the basis for both the design and analysis of all portions of this thesis relating to heat pipe theory and practice. However, this research effort also required the application of several well known heat and mass transfer concepts.

2.5 Basic Heat Transfer Theory

To ensure an understanding of the heat transfer model detailed in Chapter 3, the subjects of convective and radiative heat transfer, conduction, and evaporation will be briefly presented.

Convection refers to heat transfer that will occur between a surface and a moving fluid when they are at different temperatures, *i.e.* a hair dryer warming air. Radiation, or thermal radiation, is the net radiant heat transfer between two surfaces at different temperatures, *i.e.* heating a metal plate with a high power light source (7:2). Both of these concepts were important factors in this effort.

For the purposes of this experiment, radiation and convection were both accounted for in one general constant termed the convective/radiative heat transfer coefficient, h_{cr} , with units of $W/^{\circ}C\cdot m^2$, defined for the entire surface area of an object at an average temperature, T_{ave} . Using this coefficient, the convective/radiative heat transfer rate for an object's entire surface, Q_{cr} , may be expressed as

$$Q_{cr} = h_{cr}A_s(T_s - T_{\infty}) \quad (20)$$

where A_s is the object's total surface area and T_{∞} is the temperature of the fluid flowing over the object's surface. This methodology is only valid when h_{cr} is empirically derived for a specific configuration, thus each experiment's

configuration, (including: room temperature, equipment position, and object orientation), must be kept consistent to maintain the validity of h_{cr} .

The lumped capacitance method was used throughout this effort to predict the time duration required for the experimental model to reach steady-state. This simple methodology dealt with the problem of predicting transient conduction through an object. Lumped capacitance basically assumes that the temperature of the object is spatially uniform at any instant in time, thus temperature gradients are assumed negligible and the rate of heat loss at the surface of the object can be related to the rate of change of the object's internal energy (7:228). Using this methodology, the thermal time constant, in seconds, is defined as

$$\tau = \left(\frac{\rho_v V c}{h_{cr} A_s} \right) \quad (21)$$

where

- ρ_v = density of the object's material (kg/m³)
- V = object's volume (m³)
- c = specific heat of object's material (kJ/kg-°C)
- A_s = object's surface area (m²)
- h_{cr} = object's convective radiative heat transfer coefficient (W/°C-m²)

The thermal time constant is of importance because three times the thermal time constant, (3τ), is regarded as

the duration of time required for an object to reach steady-state conditions. This analysis is only valid when the object's Biot number, Bi , a dimensionless measure of the temperature in the object relative to the temperature difference between the object's surface and its surroundings, is less than 0.1 (7:231). The Biot number is defined as

$$Bi = \frac{h_{cr} L'}{k} < 0.1 \quad (22)$$

where L' equals the ratio of the object's volume to surface area ($L' = V/A_s$) and k is the thermal conductivity of the object (7:231).

Since this effort also involved the supply, overflow, and evaporation of a working fluid, a brief survey of enthalpy and evaporative heat transfer was also thought valuable. First, when a liquid is supplied to a control volume and some overflow, or outflow, is allowed to leave, an accounting of the energy the outflow liquid removes from the system must be taken (7:646). This was achieved very simply by performing an energy balance on the liquid, yielding the overflow heat transfer rate, Q_{out} :

$$Q_{out} = \dot{m}_{out} c (T_{l_{out}} - T_{l_{in}}) \quad (23)$$

where,

\dot{m}_{out} = mass flow rate out (kg/sec)
 T_{lin} = inflow liquid temperature (°C)
 T_{lout} = outflow liquid temperature (°C)
 C = liquid specific heat (kJ/kg-°C)

The evaporative heat transfer rate, Q_{evap} , though a very important factor in this effort, was also easily found:

$$Q_{evap} = \dot{m}_{evap} \lambda \quad (24)$$

where,

\dot{m}_{evap} = evaporative mass flow rate (kg/sec)
 λ = liquid latent heat (J/kg)

For the liquid to evaporate, though, some energy must be input into the liquid to raise its energy level to the point where evaporation, or phase change, begins. The heat rate required to raise the liquid's energy level to the point of phase change, Q_{pc} , is expressed, in Watts, by

$$Q_{pc} = \dot{m}_{evap} C (T_{evap} - T_{lin}) \quad (25)$$

where T_{evap} is the temperature the liquid is evaporating at. Equations (24) and (25) can be combined to provide an expression describing the rate at which heat is being transferred out of the groove by evaporation of the working fluid. This heat transfer rate, Q_{groove} , is expressed as

$$Q_{groove} = \dot{m}_{evap} (C (T_{evap} - T_{lin}) + \lambda) \quad (26)$$

This equation was not only used throughout this effort to determine the rate at which the groove was removing energy, but also in empirically determining the capillary

limit on the heat transport rate. This was done by evaluating the heat rate required for dryout in Equation (26) from experimental measurements of the evaporative mass flow rate, the temperature the liquid was evaporating at, and the temperature of the input liquid.

The preceding heat transfer equations, though quite simple, were the basis for all mass and heat transfer analysis performed in this research effort.

III. EXPERIMENT DESIGN

This chapter provides a brief overview of this research effort's experimental system as a whole, as well as a thorough examination of the design of each component within the system. Pertinent construction techniques and methods are discussed to enable future duplication of the apparatus. Accuracy and experimental uncertainties are also detailed to determine error sources and provide an overall error range for the research effort's measurements and calculations. Finally, the general experimental procedure is detailed.

3.1 Experiment Description

The goal of this experiment was to simulate dryout due to varying acceleration or body forces on an axial groove by increasing the inclination of the groove until its capillary limit was exceeded and dryout occurred. Then, the transient dryout and rewet behavior of the groove would be observed. To this end, the experiment was purposefully designed to be simple in both operation and construction, while still providing the desired data. The five basic components of this experimental apparatus were combined as shown in Figure 5. First, the working fluid system supplied fluid to the groove and removed any unevaporated fluid in an overflow system. The groove was milled into a copper plate mounted to a rotating shaft, which positioned the plate at any inclination desired. Mounted to the plate was the heater

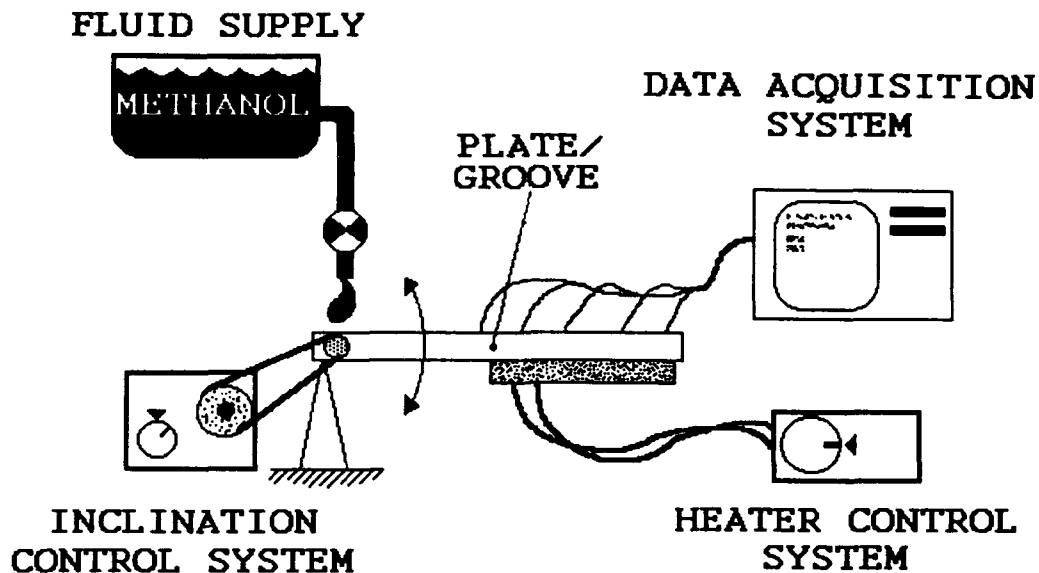


Figure 5. Schematic of Gravitationally Induced Dryout Experiment

which provided controllable heat flux input to the bottom of the plate. Completing the system was the data acquisition system and instrumentation, which recorded temperature data, inclination, and heat flux.

3.2 The Rectangular Groove

The rectangular groove used simulated an axial groove heat pipe wick. This groove was milled into a plate of pure, unalloyed, copper to enable attachment of thermocouples and heating elements in close proximity to the groove. The plate was 0.25 m long, 0.041 m wide, and 0.006 m thick. A fluid reservoir, 0.015 m long, 0.031 m wide, and 0.0006 m deep was milled into one end of the copper plate to act as a fluid supply point for the groove which originated

from the reservoir. This method of using a reservoir to supply fluid to the groove had worked successfully in earlier research efforts (9:1). As a result of using a fluid reservoir, though, the condenser length of the groove, or L_c , was equal to zero.

Several considerations were taken into account when the groove was designed. First, earlier research had shown that deep grooves exhibited a phenomenon, termed spattering, where boiling working fluid droplets splashed out of the groove and evaporated without contributing to the cooling of the groove itself (5:2). To avoid this, it was decided to make the groove as shallow as possible, thus making surface evaporation more likely than boiling within the groove. Conversely, to ensure adequate groove depth for maximum wetting, the groove's depth was constrained to be greater than half of the groove width (3:37).

Another consideration designing the groove was that it must function at a reasonable maximum inclination, and be a reasonable length in order to facilitate observing fluid behavior within the groove. To these ends several designs were considered. The design that suitably fulfilled all of the above constraints was found to be a groove that was 0.1995 m long, measured from the edge of the fluid reservoir, 0.001 m wide, and 0.0006 m deep. This groove's depth was slightly greater than half its width, thus ensuring maximum wetting while minimizing spattering. The

groove was long enough to allow observation of the fluid, and it had a reasonable maximum inclination of 2.02° .

As a result of heater size, discussed later in this chapter, and the earlier mentioned lack of a condenser, the groove possessed the following characteristics:

$$L_c = 0.0000 \text{ m}$$

$$L_a = 0.0979 \text{ m}$$

$$L_g = 0.1016 \text{ m}$$

Since both the measurement of the extent of dryout and the measuring of the time required for the groove to rewet pertain mainly to the groove itself, the methods for measuring them are covered in this section. First, to measure the extent of dryout, a small metric ruler was laid next to the groove to visually measure the length of the dried out portion of the groove, defined as the distance from the end of the groove to the liquid front of the liquid in the groove. The error in this measurement was determined to be $\pm 0.0025 \text{ m}$. Further, when the groove was returned to zero degrees inclination, the time duration required for the groove to rewet was determined by starting a stopwatch when the inclination began decreasing and halting the stopwatch when it was visually determined that the meniscus was completely re-established within the groove. The error in recording the time required to rewet was ± 2 seconds.

Upon design completion, the groove and reservoir were milled into the plate using a machine-steel burr turning at

slow rpm to ensure the smoothest possible surface inside the groove. Complete working plans for the groove and plate are contained in Appendix A.

3.3 Inclination Control System

To minimize experimental uncertainty, a very precise method of observing and controlling the groove's inclination was required. Since the different acceleration forces were going to be simulated by varying inclinations, imprecise inclinations would correspond to experimental error.

To this end, the plate was rigidly supported at one end of its length by a steel shaft connected to a controllable DC servo motor through a 10:1 reduction gear. This arrangement allowed the plate to rotate within the range of -30 to +90 degrees of inclination.

The system used a Model 5330 Direct Current servomotor manufactured by EG&G Torque Systems, with 500 steps, or angular positions, per one revolution. The motor's speed, acceleration, deceleration and angular position were all controllable through the use of an external controller. The motor was connected to the plate through a reduction gear which reduced the motor's output by a factor of ten. Metal collets, shims, and shafts were used throughout the system to reduce hysteresis as much as possible. Through use of the reduction gear and motor, the plate was able to be inclined in increments of 0.072° .

The controller was a Mini MC² Motion Control System,

manufactured by Delta Tau Data Systems. Using this controller, the angular velocity of the shaft turning the groove's plate was constrained to 0.072 degree-per-second ($0.072^{\circ}/\text{sec}$), and the angular acceleration and deceleration were reduced to a negligible amount. This speed was used to minimize momentum losses or gains in the working fluid as the plate rotated.

A Daytronic Model 3230 Linear Variable Displacement Transducer, or LVDT, was attached to the plate's shaft to determine the actual angular position of the plate and provide a redundant check on the motor controller. This device, through changes in voltage, was able to sense very small changes in linear displacement. These linear displacements were then mathematically manipulated to yield the plate's angular position. The LVDT's use was later halted when the controller's readout consistently agreed with the LVDT.

Prior to running each experiment, the plate's inclination would be set to zero degrees by use of a bubble balance and magnifying glass. The controller and LVDT were then both programmed to read this position as zero degrees.

The error in predicting and controlling inclination by the controller and LVDT were found to be $\pm 0.072^{\circ}$.

This inclination control system provided accurate inclination control, but was not without its faults in other areas. Due to the its high current flow during operation,

the motor necessitated that the instrumentation system to be grounded in a variety of ways to ensure accurate data collection.

3.4 *The Heater System*

The heater system was simple and effective. A simple strip heater, clamped to the bottom of the plate, supplied all heat required for the experiment.

The heater itself was the model PT-502/120 strip heater manufactured by Omegalux. This heater was a resistance type heater which heated to a temperature proportional to the amount of electrical power which flowed through it, much like an electric stove cooking element. Sheathed in chrome steel, the heater's heating area was 0.038 m wide and 0.1016 m long, operating at 120 V with a maximum heat rate of 250 W. This experiment never required the heater to operate at more than 30% of this maximum. The heater was clamped to the plate using four spring-loaded clamps, with no space between the heater and the plate and no thermal grease.

Power was supplied to the heater using a Adjust-A-Volt type 500-B 115 V power supply, manufactured by Standard Electronic Products, which lowered the commercially available 120 V electricity to the power level required for this experiment. A Hewlett Packard model 3466A digital multimeter was connected in parallel with the strip heater's terminals to read the voltage drop across the heating element, and a shunt and Simpson model 467 digital

multimeter were placed in series with the power supply lines to read current flow in amperes. Knowing the current and the voltage drop, power consumed by the heater could then be determined by the equation

$$P_{elec} = iV \quad (27)$$

where P_{elec} is electrical power in Watts, i is current flow in amperes, and V is voltage drop in volts.

Power consumed by the heater was only of use in maintaining consistency throughout the experiments, because plate temperatures were used for the actual computations of power used by the groove. Because of this, determination of error in computing power into, and out of, the heater was not needed as long as the heater's performance was consistent.

Overall, the heater system worked very well, but there was one problem in attaching the heater to the plate. The plate and heater, constructed of different materials, would expand and contract at different rates as the heater and the plate temperatures rose. Because the clamps held the heater against the plate so tightly, the plate would actually begin to bow at higher temperatures. To avoid this, a less rigid method of affixing the heater to the plate should be used in future research.

3.5 Working Fluid and Working Fluid Supply System

The working fluid could be likened to the blood of this experiment, and as such, it was treated very carefully. Of

utmost importance in the fluid supply system was the prevention of contamination of the fluid by the environment as well as the fluid supply system itself. Of equal importance was the supplying of working fluid to the groove in a consistent, controllable manner.

The working fluid used in this research effort was absolute, or 200 Proof, Ethyl Alcohol, also known as ethanol. The ethanol was not denatured and was 99.999% pure. For safety and cost reasons, demineralized water was originally chosen for this experiment, but after initial testing, it was observed that water did not wet the copper groove well, due to the immediate oxidation that occurred in the groove when the demineralized water contacted the copper. It was then discovered that water and copper had been observed to wet poorly in other experiments as well, so the working fluid was immediately switched to ethanol, which had a proven track record as a working fluid used with copper (9:360).

All surfaces that came in contact with the ethanol had to be tested for compatibility first, even control valves. Ethanol was found to be corrosive to almost all plastics and petroleum-based materials.

The supply system consisted of several components (Figure 6): a storage container, a supply buret, two control valves, and an overflow buret. The storage container held the supply of ethanol working fluid so that

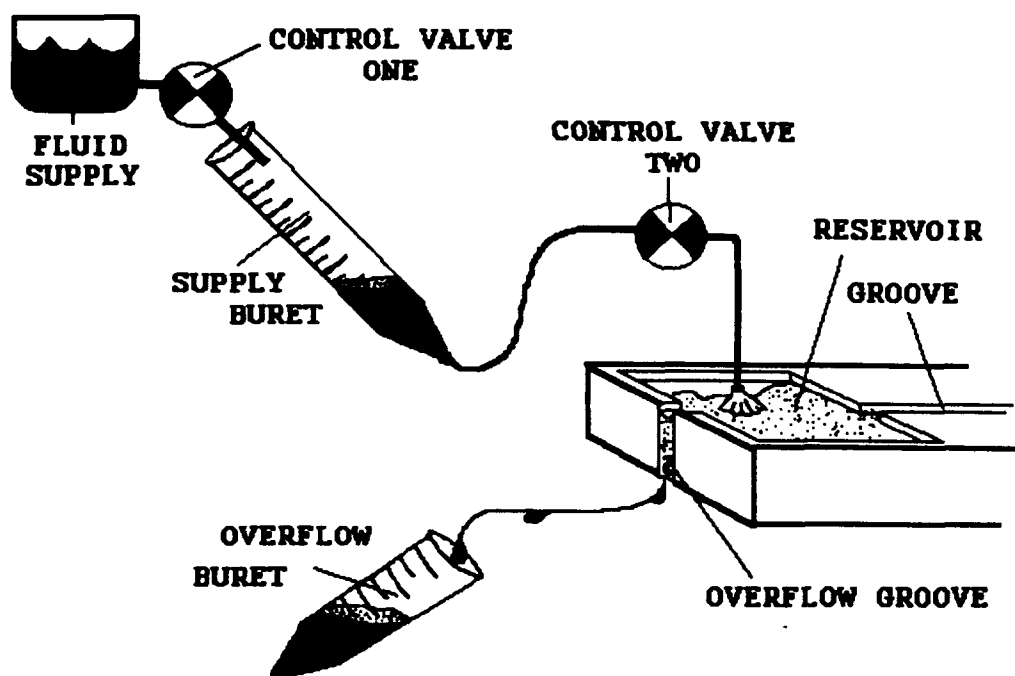


Figure 6. Schematic of Working Fluid Supply System

it was easily available throughout an experiment.

The ethanol was then fed into the supply buret by the first control valve at a steady flow rate. The supply buret was used throughout the experiments to check the flow rate by turning off control valve number one and observing the flow rate inside the buret by using a stopwatch and measuring the time required for a given amount of fluid to drain from the buret. The supply buret was also used to ensure the gravitational head of the liquid inside the buret was constant. This was done by maintaining the same level of ethanol within the buret throughout the experiment by allowing the flow into the supply buret to equal the flow out of the buret by adjusting control valve one as needed.

Once the ethanol exited the supply buret it flowed through Imperial Eastman poly-flo 44-P tubing, much like Cole Parmer's Viton tubing, into a second valve, control valve two. Control valve two was used to make minute adjustments to the flow rate prior to its entering the reservoir of the groove. Fluid flow rate for all experiments was maintained at a constant 1.33 mL/min through this valve for experimental consistency.

After exiting control valve two, the ethanol traveled through another length of tubing and flowed into the groove reservoir through a nylon wick structure; providing working fluid for the groove to draw up its length. This wick was simply a bundle of nylon fibers designed to spread the fluid evenly over the floor of the reservoir and prevent minor surges or droplets from forming. The nylon wick also minimized fluid level variations inside the reservoir.

An overflow groove at the rear of the reservoir prevented the formation of a bulge, or bubble, of liquid in the reservoir. This was because once a bubble formed, hydrostatic forces would also be driving the ethanol up the groove. Instead, once in the reservoir, excess ethanol flowed through the groove at the rear of the reservoir, down a guide-wire, and into a funnel which directed the excess fluid into an overflow buret. This buret was used to measure the fluid flow rate out of the system, in the same manner the supply fluid flow rate was determined, for later

use in determining evaporative fluid mass flow rate and overflow mass flow rate.

The burets used were graduated in increments of 0.1 mL, thus the error in reading fluid flows was determined to be 0.1 mL/min. Errors as a result of impurities in the ethanol were judged to be negligible.

There were many iterations in the evolution of this fluid supply system as it was repeatedly upgraded to increase its accuracy, make it less prone to contamination, and render the system easier to use during experiments. The final result was a system well suited to this effort.

3.6 Data Acquisition and Instrumentation System

The data acquisition system (DAS) and instrumentation system consisted of four components. A computer for recording the data, a DAS for acquiring the data, a network of thirteen thermocouples, and an inclination signal from the LVDT.

The computer used for recording experimental data was a Zenith 286 personal computer (PC), model ZWX 248, with a 16 MHz clock speed. This clock speed did not hinder data collection due to the relatively low number of thermocouples and because temperature and inclination readings were only recorded once every thirty seconds. A Keithley MetraByte DAS-8 analog/digital data acquisition system was used in conjunction with a Keithley Metrabyte EXP-16 multiplexer/thermocouple board to sample and record the

temperature and inclination data. The EXP-16 was adjustable so that the bias and ice point could be calibrated to render zero bias and ensure a zero degree ice point to compensate, via software, for the temperature of the hardware heated during operation. As earlier stated, data was collected every thirty seconds and recorded on hard disk within the PC. The EXP-16 itself sampled data at a 16 MHz sampling rate and provided an averaged value to the DAS.

Thirteen omegalux, T-type, thermocouples were used to collect temperature data. Ten thermocouples were arrayed down the left side of the actual groove at 0.02 m intervals, as shown in detail within Appendix A, to measure the surface temperature of the area of the plate near the groove. Due to the shallowness of the groove, 0.0006 m, the surface temperature of the plate adjacent to the groove was assumed to equal the temperature of the bottom of the groove. These thermocouples were inserted in 0.001 m diameter holes of 0.0006 m depth, (the same depth as the groove), and peened into the holes to ensure good contact between the thermocouples and the surrounding copper. A complete analysis was performed on various methods of mounting thermocouples and is presented in Chapter 4, Experimental Analysis. This analysis showed the peened thermocouples to be the best-suited mounting method to provide surface temperature readings for the plate. Of the remaining three thermocouples, one was suspended in the laboratory one meter

over the wick to monitor T_w , or freestream temperature. Another thermocouple was immersed within the working fluid inside the supply buret (Figure 6) to measure its temperature before it entered the fluid reservoir. The final thermocouple was peened into the copper above the overflow groove (Figure 6) to measure the excess fluid temperature as it flowed out of the plate.

As earlier stated, the LVDT output a voltage to indicate linear displacement. This voltage was sampled when the temperatures were sampled, every 30 seconds, and a computer program converted the voltage reading to a plate inclination in degrees, which was recorded along with the thirteen temperatures on the PC hard disk.

Time required for the groove to return to steady-state was measured by starting a stopwatch when the groove's inclination began decreasing and stopping the stopwatch when the groove's temperatures returned to their steady-state values. This was done by examining the data after each experiment. The error in determining t_{ss} , like t_{reset} , was found to be ± 2 seconds.

The DAS-8 was only able to operate to an accuracy of $\pm 2^\circ \text{C}$ in reading temperatures from each thermocouple. Thermocouple bias, as determined in Chapter 4, Experimental Analysis, was found to be only 0.4°C , thus the experimental uncertainty of the data acquisition and instrumentation system was the $\pm 2^\circ \text{C}$ range of the temperatures recorded by

the DAS-8. This temperature range was the largest error source in the experiment, and dominated the analysis of the determination of overall experimental uncertainty, as well. Despite this error source, the data acquisition and instrumentation system was still able to record data accurately enough for the purposes of this research effort, and did not unduly effect the validity of the experiment's results.

3.7 Laboratory Environment

All tests were performed on a laboratory workbench within a large, 15 m x 20 m, room with a ceiling at a height of 15 m. The largeness of this room helped ensure there were no rapid temperature changes during the course of an experiment. The ambient temperature and pressure were also continually monitored to ensure test conditions did not vary appreciably from experiment to experiment. Temperature fluctuations were never greater than one degree Celsius, and pressure fluctuations were below one millimeter of mercury, thus no error was attributed to the environment.

The workbench was mounted on a concrete slab, thus minimizing the intrusion of vibrations and ensuring a level environment for the experiment.

The only factor of the environment deemed noteworthy was the presence of air flows around the experiment due to heating and air conditioning ductwork. Occasionally an air current could be felt in the vicinity of the experiment.

Because of this possible change in air velocity over the plate, a 10% error range was qualitatively determined for the convective/radiative heat transfer coefficient found in Chapter 4, Experimental Analysis, based on typical convection approximations (7:326).

3.8 Overall Experimental Uncertainty

It was only necessary to determine the overall experimental uncertainty for the empirically determined capillary limit on the heat transport rate, Equation (18), and the expression for the overall heat transfer rate out of the groove, Equation (26). This was because only these factors were used in the analysis of this research effort. For an overall understanding of all sources of error in this thesis, all earlier mentioned error sources will be summarized in this section. In addition, the overall experimental uncertainties for the empirical capillary limit on the heat transport rate and the overall heat transfer rate out of the groove will also be presented.

The error sources were: 1) an error of $\pm 0.072^\circ$ in determining the zero degree inclination for the groove, 2) a $\pm 2^\circ$ C error reading each temperature, resulting in a $\pm 4^\circ$ C error in determining temperature differences, or ΔT s, 3) a ± 0.1 mL/min error in recording fluid flow rates, 4) ± 2 second error in determining time required for the groove to rewet and reach steady-state, 5) a ± 0.0025 m error in determining the length of the dried out region, and 6) 1

±10% error in determining h_{cr} .

To determine the overall experimental uncertainty, the root-sum square method of determining error was used.

Recall from Equation (26), shown here in expanded form

$$Q_{groove} = Q_{cm_{exp}} = \dot{m}_{evap} C (T_{evap} - T_{lin}) + \dot{m}_{evap} \lambda \quad (26)$$

In the work that follows, Q_{groove} will be abbreviated as Q .

The overall experimental uncertainty for Q was determined using the root-sum square formulation where the error in Q , ΔQ , is described by

$$\Delta Q = \left[\sum_{i=1}^N \left(\frac{\partial Q}{\partial (i)} \right)^2 \Delta_i \right]^{\frac{1}{2}}$$

where Δ_i equals error source i , and N is the total number of error sources.

Using this method to determine an expression for ΔQ yields

$$\Delta Q = \left[\left(\frac{\partial Q}{\partial \dot{m}_{evap}} \Delta \dot{m}_{evap} \right)^2 + \left(\frac{\partial Q}{\partial \Delta T} \Delta (\Delta T) \right)^2 \right]^{\frac{1}{2}} \quad (28)$$

or, performing the partial derivatives,

$$\Delta Q = \left[((C \Delta T + \lambda) \Delta \dot{m}_{evap})^2 + (\dot{m}_{evap} C \Delta (\Delta T))^2 \right]^{\frac{1}{2}} \quad (29)$$

Equation (29) applies to both the empirical capillary limit on the heat transport rate and the overall heat transfer rate from the groove, giving the equations used throughout this effort to determine error for each value:

$$\Delta Q_{cm_{exp}} = [((C\Delta T + \lambda)\Delta\dot{m}_{evap})^2 + (\dot{m}_{evap}C\Delta(\Delta T))^2]^{\frac{1}{2}} \quad (30)$$

and

$$\Delta Q_{groove} = [((C\Delta T + \lambda)\Delta\dot{m}_{evap})^2 + (\dot{m}_{evap}C\Delta(\Delta T))^2]^{\frac{1}{2}} \quad (31)$$

where,

$$\begin{aligned} \Delta\dot{m} &= \pm 0.1 \text{ mL/min} \\ \Delta(\Delta T) &= \pm 4^\circ \text{ C} \end{aligned}$$

3.9 Experimental Procedure

With each component of the experimental apparatus fully detailed, an explanation of the process of actually conducting an experiment and collecting data can now be provided.

In the case of several of the validations discussed in Chapter 4, Experimental Analysis, several experiments were conducted which varied from the primary experimental procedure. These experiments were each described in their appropriate section. The primary experiments conducted during this effort followed these basic guidelines.

Each experiment consisted of several basic steps. First, the input heat flux was set at a specific level so that the input heat rate from the heater was constant throughout the experiment. Next, the groove/plate was allowed to come to steady-state by waiting for a duration of time greater than three times the plate's time constant.

Once the plate was at steady-state conditions, temperature data collection by the DAS began as the inclination of the groove was increased to a specific angle that resulted in the input heater heat rate exceeding the groove's capillary limit on the heat transport rate, (simulating an increase in acceleration forces). The plate then remained at this inclination for a specified duration of time, simulating the groove experiencing increased acceleration forces for a set amount of time. The extent of dryout was measured while the plate was still inclined. When the plate's inclination was later returned to zero degrees inclination, (simulating a return to zero acceleration forces), both the time required for the groove to rewet and the time required for the groove to return to steady-state temperature conditions were recorded.

This procedure allowed the necessary data to be collected in fulfillment of the objective's specified in Chapter 1, and was used throughout the experimental portion of this research effort.

IV. EXPERIMENTAL ANALYSIS

This chapter presents the analysis required to determine the groove's theoretical capillary limit on the heat transport rate, or simply, the capillary limit, the calibration of the inclination and data acquisition systems, a validation of the groove's heat transfer model, and the groove's empirically determined, or actual, capillary limit. Additionally, detailed descriptions of the two test sequences conducted are presented.

4.1 Thermocouple Mounting Procedure Validation

To ensure accurate test results, an accurate method for measuring the temperature of the bottom of the groove had to be found. It was especially important to determine a method of mounting thermocouples which would provide the most accurate temperature readings, while being as insensitive to minor changes in the environment as possible.

To this end, five different methods of affixing thermocouples to a copper plate were examined. These methods were: 1) tying the thermocouple to the plate with copper wire, 2) spot welding the thermocouple to the surface of the plate, 3) spot welding the two thermocouple leads to the plate so that the plate surface between the two leads was considered part of the thermocouple, 4) affixing the thermocouple within a small hole in the plate with epoxy, and 5) peening the thermocouple into a small hole drilled

into the surface of the plate.

All thermocouples were mounted to the top of the plate and calibrated, and their respective biases recorded. The plate was then placed on a heating element where the temperature on the bottom of the copper plate could be controlled. The plate was allowed to come to steady-state conditions with the bottom of the plate, T_{bottom} , at a temperature of 195°C . As shown in Figure 7, the plate was modelled as an infinite plate, uniformly heated on one side and cooled by convection on the other. The mounted

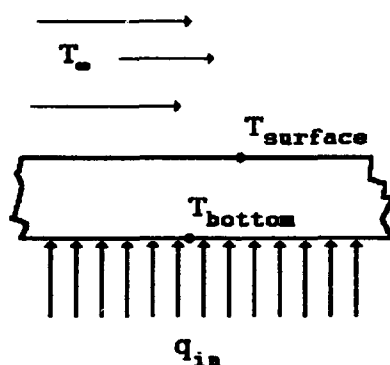


Figure 7. Heated Plate Heat Transfer Model

thermocouples recorded the following temperatures: 1) tied on thermocouple; $147^{\circ} \pm 4^{\circ}\text{C}$, 2) spot-welded thermocouple; $187^{\circ} \pm 4^{\circ}\text{C}$, 3) separate spot-weld thermocouple; $184^{\circ} \pm 4^{\circ}\text{C}$, 4) epoxied thermocouple; $162^{\circ} \pm 4^{\circ}\text{C}$, and 5) peened thermocouple; $184^{\circ} \pm 4^{\circ}\text{C}$. Based on these temperature

readings, methods 2), 3), and 5) were judged the most accurate.

Next, methods 2), 3), and 5) were exposed to a stream of moving air, where both of the spot welded methods were seen to respond very quickly to even slight exposure to the moving airstream. The peened method responded more slowly to continual air movement. Thus, the peened method was judged the best method for mounting the thermocouples in this research effort.

4.2 Thermocouple Calibration

Once the method of peening the thermocouples into the plate was validated, the thermocouples were calibrated. Prior to mounting, each thermocouple was checked on an electronic thermocouple calibrator to ensure it functioned properly. Furthermore, all thermocouples were of the same lot number and their leads of equal lengths. This ensured that all thermocouples had equal resistances across their lengths, with little or no variances. Additionally, no extension wire or quick connectors were used. Instead, each thermocouple lead was directly attached to the EXP-16 board. The EXP-16 board's electronic ice point was then calibrated, at standard operating temperatures, to ensure accurate temperature readings by the data acquisition system during normal operation. This was done by adjusting the electronic icepoint until it read the same temperature as a calibrated thermocouple.

The entire plate with its attached thermocouples and all other thermocouples were immersed in an ice bath and were allowed to come to a steady-state temperature of 0°C . At this temperature, the bias for all thermocouples was found to be -0.4°C , well within the error range of the data acquisition system itself, discussed in Chapter 3. Throughout the remainder of this effort, all temperatures stated have already taken this bias into account. Additionally, the raw data presented in Appendix B has also had the bias accounted for.

4.3 Inclination System Calibration

The last step in ensuring the experimental apparatus was ready to collect experimental data was to calibrate the inclination system. This was a relatively simple process which was repeated several times throughout this research effort to ensure the system's continued accuracy.

With knowledge of the exact position of the plate's pivot point and geometry, trigonometric functions were used to determine the exact height of the plate's edge at a corresponding inclination angle. Knowing the pivot point's depression, the distance between the pivot point and the end of the plate, and the vertical displacement of the end of the plate, use of the laws of right triangles yielded the angle which corresponded to a specific vertical displacement of the plate's end.

Using this relationship, the inclination system was

calibrated with a micrometer capable of measuring vertical displacements as small as 0.00003 m. The micrometer was placed at the end of the plate such that when the plate rotated, the end of the plate would strike the micrometer's blade. An electrical circuit was set up so that when the micrometer blade contacted the plate a small LED would light, indicating the plate's edge was at the vertical position indicated by the micrometer.

The plate was first placed at zero degrees inclination by use of a bubble balance and a magnifying glass. The plate's edge was then raised in 0.005 m increments, recording the LVDT's output at each 0.005 m increment. Thus, a table of LVDT output signals versus vertical displacements of the plate's end was constructed. Then for each vertical displacement, the corresponding angle of inclination was determined, yielding a table of inclination angles versus LVDT output signals. Using this table, an 8th order polynomial equation was computer-generated giving the plate's inclination angle as a function of the LVDT's output signal. This equation was then incorporated into the data acquisition system's computer program so that inclination angle could be computed from the LVDT output.

Using this methodology, the inclination system could be calibrated before each experiment, ensuring the inclination of the plate was controlled and recorded.

4.4 Groove Heat Transfer Model Validation

Before empirically determining the groove's actual capillary limit, the validity of the heat transfer model of the groove, Equation (26), had to be verified. The first step towards this goal was the actual determination of the plate's convective/radiative heat transfer coefficient, h_{cr} , discussed in Section 2.5.

4.4.1 Determining the Convective/Radiative Heat Transfer Coefficient. For this preliminary experiment, the research effort's apparatus was set up in the same configuration as would be utilized throughout the experimental test sequences. This configuration was discussed in detail in Section 3.9, Experimental Procedure. Thus, all systems were on and operating in order to duplicate the heat exchange that would be occurring between all of the heat generating machinery used in the experimental apparatus, such as the inclination system's motor, the computer, etc. Additionally, the DAS was used to collect temperature data as it normally would throughout the ensuing test sequences.

Three experiments were conducted at three different heater input power levels, or three specific input heat rates. These experiments were then used to create a graph depicting h_{cr} versus average temperature of the plate, T_{ave} .

In the first test, using no working fluid, the power supply was set to provide 30.24 W of power to the strip

heater mounted on the bottom of the dry plate. Then, using Equation (21),

$$\tau = \left(\frac{\rho_b V C}{h_{cr} A_s} \right) \quad (21)$$

an approximate time constant

$$\tau = 988 \text{ seconds } (16.5 \text{ minutes})$$

was determined using the plate's specifications from Appendix A and assuming the convective/radiative heat transfer coefficient, h_{cr} , was equal to $10 \text{ W/m}^2\text{-}^\circ\text{C}$. This assumed value for h_{cr} was very low and thus, very conservative. This ensured the approximate time constant would be larger than required, guaranteeing the plate would be at steady-state conditions after the required 3τ time period.

After a period of 49.5 minutes, or three times the time constant, the measured temperatures along the length of the groove were found to be constant, indicating the plate had reached steady-state conditions. The freestream air temperature as well as the temperatures along the length of the groove were then recorded at five second intervals for a period of 85 seconds.

This same process was repeated for input power levels of 60.14 W and 90.35 W to obtain a wide range of h_{cr} values for later use. All temperature data from these three experiments is contained in Appendix B, Convective/Radiative

Heat Transfer Coefficient Data Runs. The plate temperatures along the length of the groove were then averaged together for each separate experiment, to provide an average temperature of the bar, or T_{ave} , for each experiment. T_{ave} for the input power level of 30.24 Watts was found to be 79.5°C, 119°C for the input power level of 60.14 Watts, and 154°C for the input power level of 90.35 Watts.

Using the average temperature of the plate along with the known input power level, Equation (20)

$$Q_{cr} = h_{cr} A_s (T_s - T_\infty) \quad (20)$$

yielded a value for h_{cr} for each of the corresponding values of T_{ave} , where the freestream temperatures, T_∞ , for each experiment are presented within Appendix B, and the surface area of the plate, A_s , is contained in Appendix A. These values of h_{cr} were then tabulated for all three experiments.

Table 1. h_{cr} Values Corresponding to T_{ave}

T_{ave} (°C)	h_{cr} (W/°C-m ²)
79.5	21.18
119	24.79
154	27.29

It should be noted again that h_{cr} only applies to this configuration of the experimental apparatus. If any

component in the experimental apparatus was changed or even modified, h_{cr} would then have to be determined again for the new configuration. In this way, factors such as heater efficiency, contact resistance between the heater and the plate, and power supply efficiency could be accounted for within h_{cr} , as long as no variables within the experimental apparatus changed.

The convective/radiative heat transfer coefficient, h_{cr} , was also plotted versus the average plate temperature, T_{ave} , and the expression for h_{cr} was:

$$h_{cr} = -0.00027 T_{ave}^2 + 0.14459 T_{ave} + 11.37920 \quad (32)$$

where T_{ave} is in °C, was used throughout this effort to determine h_{cr} at the specific T_{ave} of the plate for each experiment, when required.

Once h_{cr} had been determined, it was possible to proceed and validate the heat transfer model for the groove. This validation was actually performed using the same experimental data collected to determine the groove's actual capillary limit.

4.4.2 Experimentally Validating the Groove Heat Transfer Model. The expression modelling the amount of energy removed by the evaporating fluid in the groove, Equation (26), was found to be valid. This was found by first constructing a control volume model of the plate, as shown in Figure 8. Conservation of energy required that the energy entering the control volume equal the energy exiting

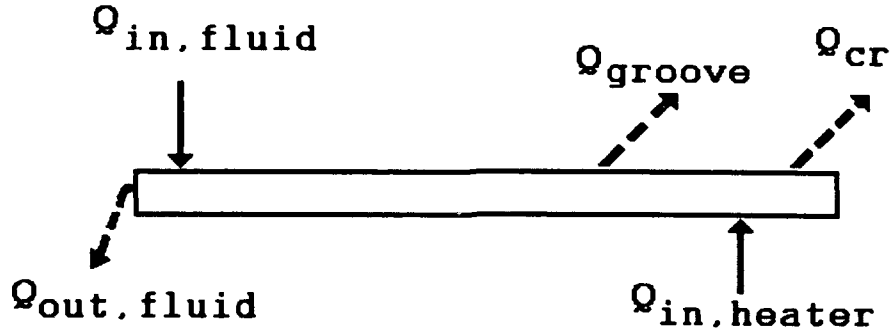


Figure 8. Groove/Plate Control Volume

the control volume for steady-state operation. Thus, Q_{in} , the sum of the energy entering the system via the input working fluid, $Q_{in,fluid}$, and the power input into the heater, $Q_{in,heater}$, had to equal Q_{out} , the sum of the energy exiting the system via the overflow working fluid, $Q_{out,fluid}$, the convective and radiative heat transfer, Q_{cr} , and the energy removed by the evaporating working fluid in the groove, Q_{groove} , modelled by Equation (26). Mathematically,

$$Q_{in} = Q_{in,fluid} + Q_{in,heater} \quad (33)$$

and,

$$Q_{out} = Q_{out,fluid} + Q_{cr} + Q_{groove} \quad (34)$$

Using the temperature data collected for determining the groove's actual capillary limit, (presented in Appendix C, Capillary Limit/Heat Transfer Model Validation Data Runs), all of the above heat rates were found and tabulated below in Table 2, where it can be readily seen why the expression for Q_{groove} , Equation (26) was judged to be accurate. In each experiment, Q_{out} , the energy predicted

Table 2. Q_{in} Versus Q_{out} for Validating Groove Heat Transfer Model

Test	Q_{in} Eq (33)	Q_{out} Eq (34)	Q_{cr} Eq (20)	$Q_{out, fluid}$ Eq (23)	Q_{groove} Eq (26)
A-1	28.15	26.25	18.91	0.81	6.53
A-2	26.87	25.48	18.49	0.72	6.27
C-1	11.63	10.69	8.27	0.60	1.82
C-2	15.47	14.69	11.19	0.72	2.78

to be exiting the control volume by Equation (34) was within 10% of the actual energy exiting the control volume; which had to equal the energy entering the control volume, Q_{in} .

These results indicated that the heat rate of the fluid evaporating within the groove could be calculated using Equation (26).

4.5 Theoretical and Actual Capillary Limits on the Heat Transport Rate of the Groove

Knowledge of the effect of tilt angle on the groove's capillary limit was vital in the fulfillment of this research effort's objectives. This was pivotal because this research effort simulated an increase in acceleration forces by inclining the groove and lowering the capillary limit.

The groove's capillary limit was experimentally measured and compared with the theoretical limit. Using the theory on capillary pressure in grooves presented in Chapter 2, Theory, the groove's theoretical capillary limit was easily found. All fluid properties for this analysis were tabulated in Appendix D, Working Fluid Properties and Manufacturer, and all groove characteristics were obtained from Appendix A, Plate Geometry.

Properties of Ethanol at 80° C (See Appendix D):

Liquid density:	$\rho_1 = 735 \text{ kg/m}^3$
Liquid viscosity:	$\mu_1 = 4.350 \times 10^{-4} \text{ N-sec/m}^2 \text{ (kg/m-sec)}$
Liquid surface tension:	$\sigma_1 = 2.105 \times 10^{-2} \text{ N/m}$
Liquid latent heat:	$\lambda = 841.547 \times 10^3 \text{ J/kg}$
Specific heat:	$c = 2.981 \times 10^3 \text{ J/kg-}^\circ\text{C}$

Liquid frictional coefficient, F_1 :

Groove cross-sectional area:	$A_w = 5.08 \times 10^{-7} \text{ m}^2$
Wick permeability:	$K = 3.57 \times 10^{-8} \text{ m}^2$
Liquid frictional coefficient (Eq (10)):	$F_1 = 38.779 \text{ (N/m}^2\text{)/W-m}$

Capillary limitation on the heat transport factor, $(QL)_{cm}$:

Groove width:	$w = 0.001 \text{ m}$
Groove inclination:	$\theta = \text{Variable}$

Acceleration due to gravity: $g = 9.81 \text{ m/sec}^2$
 Groove length: $L_t = 19.950 \times 10^{-2} \text{ m}$
 Liquid frictional coefficient (Eq (10)): $F_1 = 38.779 \text{ (N/m}^2\text{)}/\text{W-m}$
 Capillary limitation on the heat transport factor (Eq (16)): $(QL)_{cm} = 1.09 - 37.09 \sin \theta \text{ W-m}$

Capillary limit on the heat transport rate, Q_{cm}

Capillary limitation on the heat transport factor (Eq (16)): $(QL)_{cm} = 1.09 - 37.09 \sin \theta \text{ W-m}$
 Adiabatic length: $L_a = 9.790 \times 10^{-2} \text{ m}$
 Evaporator length: $L_e = 1.016 \times 10^{-1} \text{ m}$
 Condenser length: $L_c = 0.000 \text{ m}$
 Capillary limit (Eq (19)):

$$Q_{cm\text{Theory}} = 7.30 - 249.45 \sin \theta \text{ Watts (W)} \quad (35)$$

where θ is the angle of inclination between the groove and the local horizontal in degrees. Equation (35) is presented graphically in Figure 9.

Equation (35) was used throughout this effort to determine the theoretical capillary limit of the groove at any inclination. This theoretical limit would decrease in magnitude as the fluid temperature increased due to increased surface evaporation from the fluid in the open groove. Due to increased frictional effects caused by oxidation on the groove's surface and minor imperfections in the groove's surface, it was also expected that the groove's theoretical capillary limit would be slightly higher than the experimental limit at a given inclination. To verify the accuracy of the theory, the capillary limit of the groove was next determined experimentally.

As can be seen in Figure 9, the maximum angle this groove could theoretically function, θ_{\max} , equalled 1.68° . Conversely, at an inclination of zero degrees, the groove could theoretically achieve a maximum heat transport rate, Q_{cm} , of up to 7.3 watts. Though this heat transport rate seems small, it should be remembered that the groove is only 0.001 m wide and 0.0006 m deep.

To measure the capillary limit of the groove, a total of six experiments were conducted: two experiments to determine Q_{cm} at zero degrees inclination; two experiments to determine the θ_{\max} where the groove dried out with an input heat rate of approximately zero watts; and two experiments at intermediate angles. The results of these experiments, presented in Figure 9, verified that the experimental capillary limit of the groove was very close to the theoretical capillary limit.

The first two experiments conducted determined Q_{cm} at zero degrees inclination. With an inclination of zero degrees and the mass flow rate of working fluid into the reservoir maintained at a constant 1.33 mL/min, (the standard supply mass flow rate throughout this effort), the power supplied to the heater was increased incrementally until the groove dried out. With each increase in the power input, the plate was allowed to come to steady-state conditions, as determined by a 3 τ time duration and constant temperature values along the plate's length. Once steady-

state was reached the mass flow rate of working fluid out of the reservoir was measured and temperature measurements along the groove were recorded so that Q_{cm} , which equals Q_{groove} at dryout, could be determined using Equation (26). Once an approximate value of the Q_{cm} was determined, the size of the increments in which the power was supplied to the heater were lowered by smaller and smaller steps until a fine enough resolution was reached to enable the best possible value of Q_{cm} to be determined. This entire process was then reaccomplished to ensure repeatability and the uncertainty was computed using Equation (30).

From the first experiment, Q_{cm} at zero degrees was determined to be 6.53 ± 1.16 W, while from the second experiment, Q_{cm} was found to be 6.29 ± 1.16 W at zero degrees inclination. Both values for Q_{cm} , as expected, were lower than the theoretical Q_{cm} at zero degrees inclination.

Determining θ_{max} for the groove, where Q_{cm} equals zero watts, was experimentally easier. First, a very low amount of power was supplied to the heater to make dryout of the groove more observable. The experiments for this region of the capillary limit were first attempted with zero power being supplied to the heater, but the bottom of the groove tended to stay damp even when the groove had dried out, and made the exact angle at which the groove began drying out impossible to observe. To combat this, a small amount of power was supplied to the heater (1.5 W). This minute

amount of power resulted in a input heat rate low enough that it only caused the temperature of the bar to increase by 1°C , so Q_{groove} , and thus Q_{cm} , were assumed equal to zero watts. Once the plate had come to steady-state conditions, its inclination was increased in 0.072° increments until the groove dried out.

The inclination angle at which the groove dried out, or θ_{max} , was found to be 2.020° . After reaccomplishing the experiment to verify repeatability, the same value for θ_{max} was measured. The experimental θ_{max} was 0.34° greater than theory predicted.

Finally, to verify that the line between $Q_{\text{cm}}(\theta=0^{\circ})$ and $Q_{\text{cm}}(\theta_{\text{max}})$ was linear, two more experiments were conducted to determine Q_{cm} at two completely arbitrary angles. These experiments were conducted following the same procedure as the two experiments previously run to determine $Q_{\text{cm}}(\theta=0^{\circ})$, except that one experiment was conducted with the plate at an inclination of 1.152° and the other experiment was conducted at an inclination of 0.936° .

At the inclination of 1.152° , the groove's Q_{cm} was found to be $1.83 \pm 1.13\text{ W}$. At the inclination of 0.936° the groove's Q_{cm} was determined to be $2.79 \pm 1.16\text{ W}$.

When the experimentally determined values for Q_{cm} were plotted versus each corresponding inclination angle, as shown on the next page in Figure 9, it became obvious that the experimental capillary limit was approximately linear.

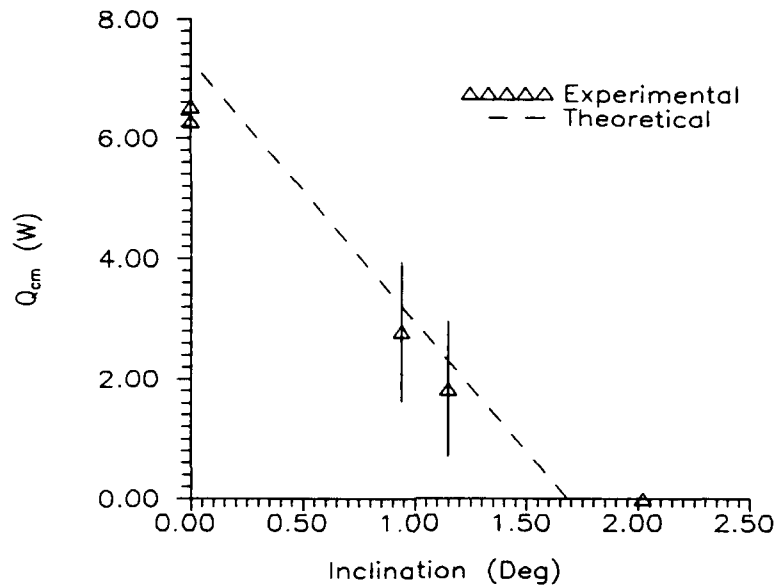


Figure 9. Experimental and Theoretical Capillary Limit for the Axial Groove

Furthermore, it also became obvious that the experimental capillary limit was very accurately predicted by theory, as evidenced by the fact that the line depicting the theoretical capillary limit as a function of inclination angle was always within the error range of each of the experimentally determined capillary limit points plotted. A best-fit line

$$Q_{cm_{exp}} = 6.20 - 3.30\theta \pm 1.16 \text{ Watts} \quad (36)$$

where θ is in degrees, was then computer-generated from the experimental capillary limit's data points for use in conducting the remaining research. This expression was used

throughout the research effort as the groove's capillary limit as a function of inclination.

4.6 Experimental Test Sequence Descriptions

After determining an expression for the groove's actual capillary limit as a function of inclination, all that remained was to answer the objectives of the thesis.

These objectives were achieved in two specific experimental sequences. The two sequences were identical to each other except for the duration of time the plate was inclined above the horizontal.

The first sequence left the plate inclined above the horizontal for a period of 1,000 seconds; a time duration less than the plate's 3τ time period and thus less than the time required for the plate to reach steady-state conditions.

The second test sequence left the plate inclined above the horizontal for a period of 3,000 seconds; a time duration exceeding the plate's 3τ time period and thus more than the time required for the plate to reach steady-state conditions.

Other than this difference, the two sequences were conducted in the same manner. Both had a working fluid supply mass flow rate of 1.33 mL/min and an input heater heat rate of approximately 28 Watts, which resulted in a Q_{groove} of approximately 5 Watts. Both started with the plate initially in the horizontal position. Then, both sequences

increased the inclination of the plate to several different inclinations to simulate a range of acceleration force magnitudes. A more detailed description of how each experiment was conducted was described in Section 3.9, Experimental Procedure.

V. EXPERIMENTAL RESULTS AND DISCUSSION

Chapter 5 presents the results of the research conducted to fulfil the objectives of this thesis. These objectives were, again, to: 1) observe the extent of dryout in the rectangular groove under varied, increased accelerations, 2) observe the time required for the rectangular groove to rewet after decreasing the acceleration levels, and 3) observe the time required for the groove to return to its starting, steady-state, temperatures. This chapter answers these objectives. First, by presenting a brief description of how the input heat rate was nondimensionalized to make the presented data more useful, then, by presenting the results of the two experimental test sequences, and finally, by presenting several observations on the dryout and rewet process. All data from each test sequence is presented in Appendix E, Experimental Test Data.

5.1 Nondimensionalizing the Heat Rates

In order to present the data collected during the two experimental test sequences in a more general, and thus applicable, manner, the input heat rate into the groove was nondimensionalized. A method of nondimensionalizing Q_{groove} was desired which would readily indicate the degree by which the capillary limit was exceeded by the input heat rate as

the groove experienced various acceleration forces, (or various inclinations).

First, the heat rate difference, Q_θ , was defined;

$$Q_\theta = Q_{groove} - Q_{cap}(\theta) \quad (37)$$

Q_θ measured the amount, in Watts, by which the input heat rate, Q_{groove} , exceeded the capillary limit at a specific angle of inclination. Q_θ would equal zero when Q_{groove} equalled the capillary limit and would be positive whenever Q_{groove} exceeded the capillary limit. This research effort did not explore the points where Q_{groove} was less than the capillary limit because the groove would not dry out in this regime, so Q_θ was always greater-than-or-equal-to zero.

The heat rate difference, Q_0 , was then defined,

$$Q_0 = Q_{cap}(0^\circ) - Q_{groove} \quad (38)$$

Q_0 measured the amount, in watts, by which the capillary limit at zero degrees inclination exceeded the input heat rate, Q_{groove} . Q_0 was also always greater than or equal to zero because Q_{groove} was always less than the capillary limit at zero degrees inclination.

The nondimensional parameter, Q^* , was now defined as

$$Q^* = \frac{Q_\theta}{Q_0} = \frac{Q_{groove} - Q_{cap}(\theta)}{Q_{cap}(0^\circ) - Q_{groove}} \quad (39)$$

Q^* was the ratio of the degree the capillary limit had decreased due to increased acceleration forces compared to

the maximum capillary limit at zero degrees inclination. Simply put, Q^* was a dimensionless measure of the extent that the capillary limit decreased due to increased acceleration forces. As Q^* grew in magnitude, the capillary limit was decreasing due to increased acceleration forces. As Q^* approached zero, acceleration forces were also approaching zero. Due to the previously described test conditions, Q^* was always greater-than-or-equal-to zero. Q^* proved to be a very useful parameter.

5.2 Extent of Groove Dryout Under Varied, Increased Accelerations

In general, the extent of dryout increased as Q^* increased for both short and long durations of increased acceleration. The extent of dryout for both sequences exhibited increased growth as Q^* increased, and both appeared to originate from the same origin. The long duration data, however, grew at a faster rate than the short duration data. The effect the duration of increased acceleration forces had on the extent of dryout appeared to be low at low levels of acceleration, but grew increasingly larger as the level of acceleration grew.

As shown in Figure 10, the length of the dried out region, L_{dry} , versus Q^* for the 1,000 second duration test sequence showed different behavior from the 3,000 second duration test sequence data, but the data from both test

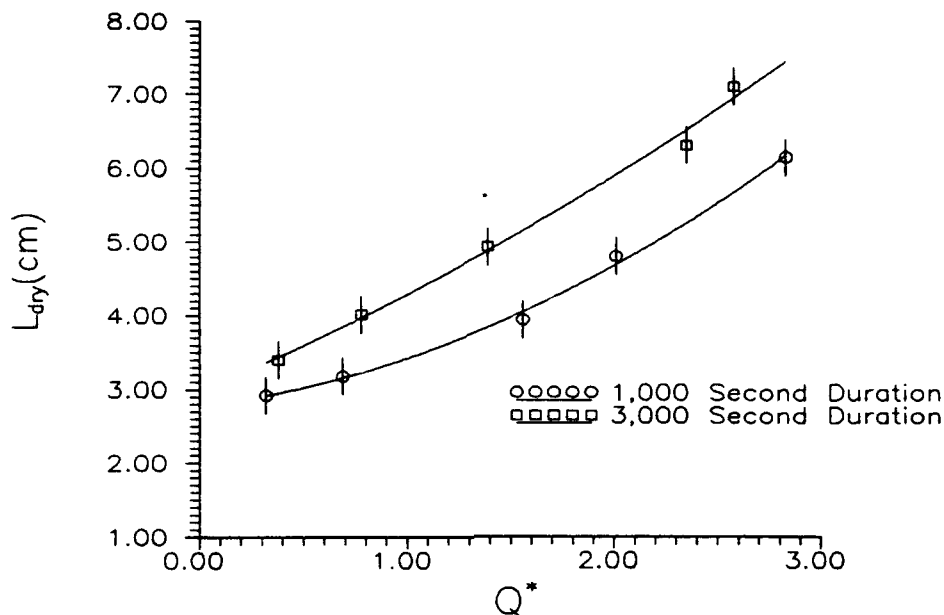


Figure 10. Length of Groove's Dryout Region After Experiencing Short and Long Duration, Increased Acceleration

sequences exhibited the same trends. All plotted curves fell within the error range of each data point (± 0.25 cm).

It seemed likely that the dryout length would equal zero at some point, but this case was not examined in these experiments. As observed in the laboratory, if q_{groove} did not exceed the capillary limit, the groove would not dry out. Thus, due to the nature of the dimensionless parameter Q^* , even when q_{groove} equalled Q_{ca} , (and Q^* equalled zero), there was still some length of the groove dried out. Q^* had to be negative for the extent of dryout to equal zero.

Several conclusions on the effects of increased acceleration, or increased inclination, on the extent of dryout in a groove were made from the above data. First, at relatively low inclinations, the extent of dryout was not greatly impacted by the duration of time the groove was inclined. Second, the extent of dryout grew larger as the inclination of the plate increased. Finally, the extent of dryout increased more rapidly at higher inclinations, and was more affected by the duration of time the groove was inclined at higher inclinations.

5.3 Time Required for Groove to Rewet Under Varied, Increased Accelerations

Simply put, the time required for the groove to rewet after experiencing increased acceleration showed trends similar to the extent of dryout data. The time required to rewet grew larger as Q^* , or accelerations, increased. However, where the extent of dryout data for the short and long durations of increased acceleration diverged as the accelerations increased, the time required to rewet data converged to a common value as acceleration increased.

Figure 11 shows t_{rewet} , the time required for the groove to rewet, versus Q^* for both the 1,000 and 3,000 second duration test sequences. Again, all curves fell within the error range of the test results.

As was expected, the time required to rewet increased

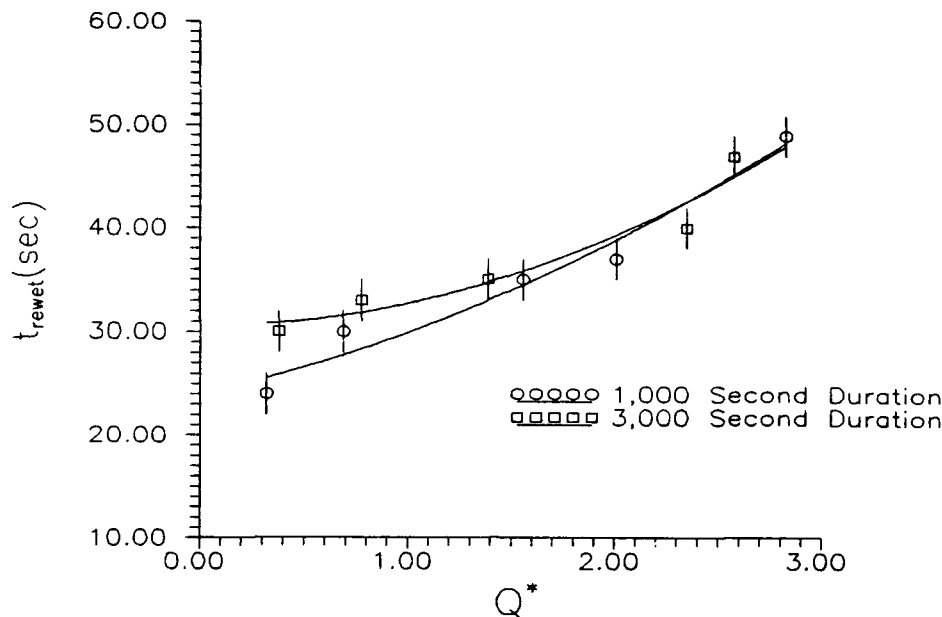


Figure 11. Time Required for the Groove to Rewet After Experiencing Short and Long Duration, Increased Acceleration

as the acceleration increased. Also, it was interesting to note that the time required to rewet grew larger as Q^* increased in much the same manner as the earlier discussed extent of dryout results. These two parameters were linked; if the extent of dryout increased to a very high value, then the groove would require more time to rewet.

This hypothesis, however, was not supported by the long duration test sequence data. At lower values of Q^* the time required for the groove to rewet data closely followed the trends exhibited by the extent of dryout data, but as Q^*

increased, the long duration test sequence data tended toward the same limiting t_{rewet} value as the short duration test data.

Several conclusions were made based on this data. First, the duration of time the groove was inclined greatly affected the time required for the groove to rewet after dryout caused by low inclinations. Secondly, the time the groove required to rewet was not greatly affected by the duration of the increased inclination after dryout caused by high inclinations.

5.4 Time Required for the Groove to Return to Steady-State Temperatures Under Varied Accelerations

Generally speaking, the groove's temperatures never changed during the short duration of increased acceleration test sequence. As a result, the time required for the groove to return to steady-state temperatures for the short duration test sequence was zero. The long duration test sequence yielded data in which the time required for the groove to return to steady-state temperatures grew linearly as Q' increased, but due to a tendency of the power supply to wander, or change settings over long periods of time, the data collected had a high level of uncertainty. Still, some general observations on the time required for the groove to return to steady-state temperatures were possible.

Temperatures along the groove changed at very slow

rates, thus, in the short duration test sequence the groove's average temperature increase was incremental; far less than could be deemed a departure from steady-state temperatures. This was reasonable behavior for the groove, as it was exposed to the increased acceleration for only 1,000 seconds. As covered earlier in this effort, 1,000 seconds were well below the amount of time required for the groove to approach steady-state values, and thus the groove did not have enough time for its temperatures to change before it was returned to the zero acceleration condition.

The 3,000 second duration test sequence did allow enough time for the groove's temperatures to increase, as shown in Figure 12. Figure 12 presents t_{ss} , the time required for the groove to return to steady state temperatures, versus Q^* . The error in determining t_{ss} was so small, (± 2 seconds), it could not be graphed. However, the plotted curve fell within the error range of each data point.

As can be seen in Figure 12, the time required for the groove to return to steady-state temperatures grew linearly as Q^* increased.

Even with the uncertainty in the power supply, several conclusions were made about the time required for the groove to return to steady-state temperatures. First, if the groove is only subjected to increased acceleration for a

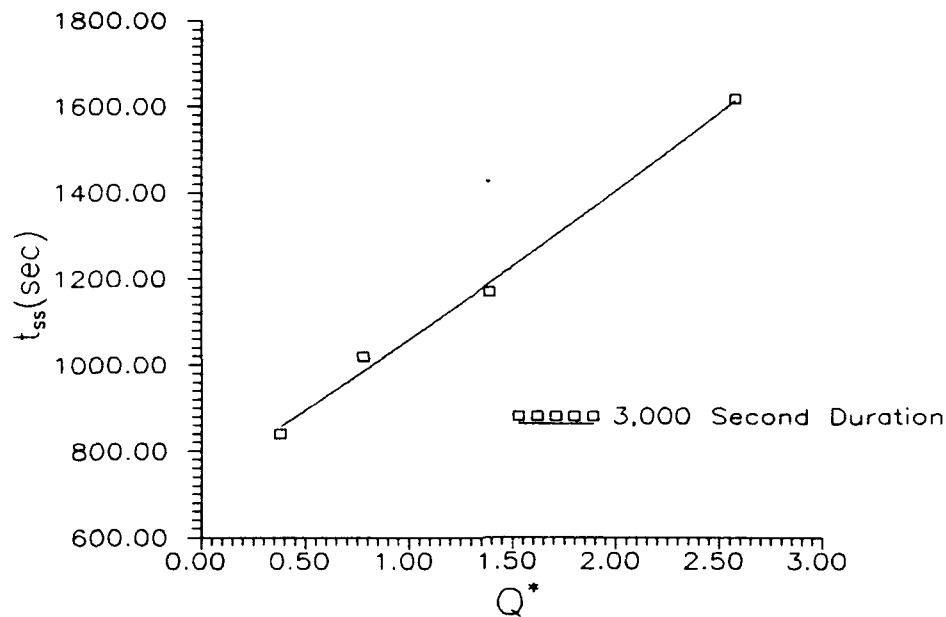


Figure 12. Time Required for the Groove to Return to Steady-State Temperatures After Experiencing Long-Duration, Increased Acceleration

short duration of time, the groove's temperatures will remain relatively unchanged and the groove does not depart significantly from the steady-state temperature it was at prior to experiencing the increased acceleration. Secondly, as the duration of time the groove experiences the increased accelerations grows, the groove does rise in temperature and the time required for it to return to steady-state temperatures grows almost linearly as acceleration levels increase.

5.5 Observations of Dryout and Rewet Behavior

Though the objectives of this research effort were met, there were still many other interesting observations on the processes of dryout and rewet of the groove that were observed.

One observation was the importance of maintaining a consistent mass flow rate of the working fluid into the groove's reservoir. Even a 0.1 mL/min change in flow rate could cause the fluid front of the fluid within the groove to move several millimeters, depending on the input heat rate into the groove. This was believed to be caused by the growth of a fluid bulge in the reservoir which resulted in an increase in hydrostatic pressure.

Of primary importance, though, was the observation that the dryout and rewet behavior in the groove were consistently identical to each other throughout every experiment conducted.

The process of dryout in the groove was examined first. This process was characterized by a drop in the ability of the groove to transport the bulk of the working fluid to the end of the groove. As shown below in Figure 13 a), the first indication of dryout was a rapid decrease in the radius of curvature of the fluid meniscus. This indicated that the pumping pressure was increasing, so fluid velocity was also increasing along with increased friction in the

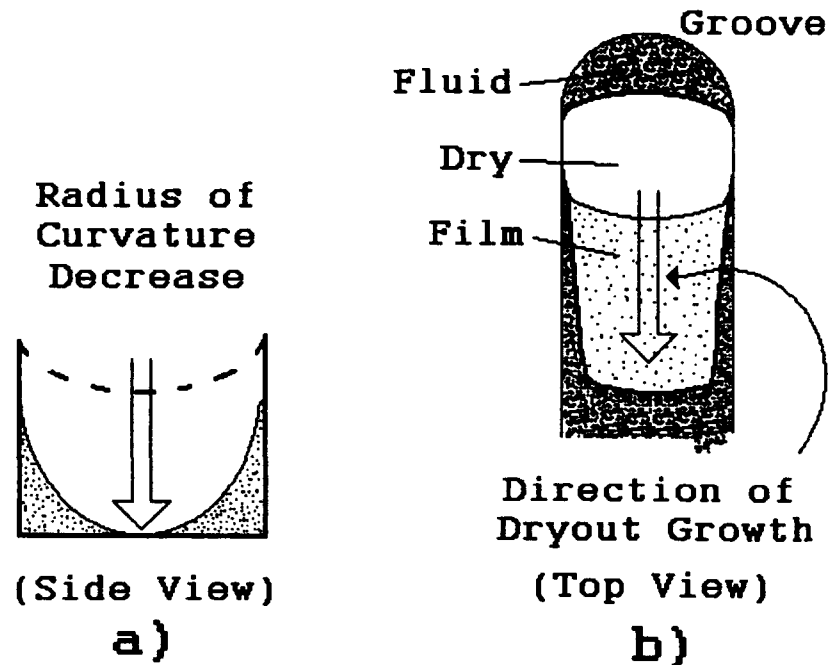


Figure 13. Dryout Process in a Groove Experiencing Increased Acceleration

groove. As the working fluid was depleted, the fluid level flattened out into a thin film on the floor of the groove, 13 b), with the bulk of the remaining fluid confined to thin streams of working fluid in the corners of the groove, which extended beyond the displaced working fluid front and into the dryout region. Some fluid would be trapped in the end of the groove, where it eventually evaporated as a result of it losing its fluid supply. This process continued as long as the acceleration and/or the input heat rate increased. The dryout front would move down the groove towards the condenser end of the groove until it reached the point where frictional and acceleration balanced the pumping force. The

actual working fluid front was the point where extent of dryout was measured.

The rewet process was very similar to the dryout process except for one difference. If the groove was still experiencing increased acceleration, the working fluid's front would assume the configuration shown in Figure 13 b), with the solid liquid front slightly offset behind the two streams of liquid travelling up the corners of the groove. But as the input heat rate and/or the acceleration were lowered, the groove would rewet as shown below in Figure 14

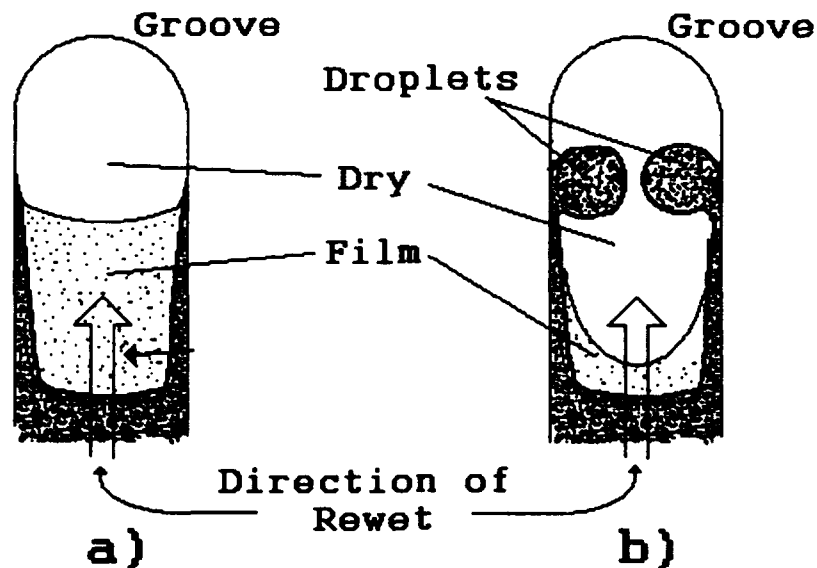


Figure 14. Rewet Process in a Groove Experiencing Increased Acceleration

a). First, the two streams of liquid in the corners of the groove would advance up the groove, then the bottom of the groove between the two streams would dampen and cover with a liquid film, and the area would rewet. This process would continue up the groove until the entire groove was rewet. However, in some experiments, the bottom of the groove would not dampen. In these cases, droplets of liquid would form at the ends of the two streams of working fluid, as shown in Figure 14 b); these droplets would grow in size until they coalesced, then the dry groove area enveloped by the working fluid would rapidly rewet. This process mainly occurred after long duration tests. However, this type of process always occurred when the very end of the groove was rewetting.

VI. CONCLUSIONS AND RECOMMENDATIONS

This chapter presents a concise overview of this research effort's conclusions and several recommendations for future research in this area of knowledge. Several recommendations for improving upon the experimental apparatus used in this thesis are also presented.

6.1 Conclusions

The effects of increased acceleration forces on the transient dryout and rewet performance of an axial groove heat pipe wick were experimentally studied using groove inclination to simulate increased acceleration forces on the groove. The following conclusions summarize the thesis results:

1. At low inclinations, the extent of dryout was not greatly impacted by the duration of time the groove was inclined.

2. The extent of dryout increased as the inclination of the groove was increased. At higher levels of simulated acceleration, the extent of dryout increased more rapidly than at lower levels.

3. After dryout caused by low inclinations, the duration of time the groove was inclined greatly affected the time required for the groove to rewet.

4. After dryout caused by high inclinations, the

duration of time the groove was inclined had little affect on the time required for the groove to rewet.

5. When the groove experienced increased inclinations for only a short duration of time, the groove's temperatures remained relatively unchanged throughout the period of simulated accelerations. As a result, the groove did not measurably depart from the original steady-state temperatures.

6. After experiencing increased inclinations for a long duration of time, the groove's temperatures did rise and the time period required for the groove to return to steady-state temperatures grew almost linearly as the simulated acceleration grew.

For use in the NASP or any other aircraft experiencing adverse acceleration forces resulting from aerobatic maneuvers or centripetal accelerations, a heat pipe employing this wick would best be used in lower heat areas and areas not susceptible to high levels of acceleration forces. Likewise, aerial maneuvers would have to be limited to very short time spans when the heat pipe was experiencing high heat loads and/or high acceleration forces. Thus, the heat pipe could not be used as the sole method of lowering the temperature along the aircraft's stagnation line.

This research demonstrates that the axial groove could only perform well in an environment characterized by low

levels of acceleration, such as a satellite or space station. In these applications the limitations described above would not impinge upon the design process.

In conclusion, this research indicates that the axial groove is strongly influenced by acceleration forces. Further research into the performance of other heat pipe wicks under adverse acceleration forces is recommended.

6.2 Recommendations

The areas recommended for further study are:

1. Examine the effects of acceleration on a screen wrapped wick using the same methodology employed in this effort. Attempt to correlate the data collected and compare it with the axial groove data to examine performance improvements as a result of the different wick.

2. Examine the effects of acceleration on a multi-grooved wick to determine whether performance data changes as a result of the majority of the input heat flux being removed by the grooves and not convection and radiation heat transfer.

3. Examine the possibilities of performing this research within a closed system, so that evaporation from the groove's reservoir and the adiabatic length of the groove are minimized.

4. Thoroughly investigate the performance of this groove on a centrifuge to see if the increased acceleration

forces simulated by increasing the inclination of the groove accurately model centripetal acceleration.

Recommendations for improving this research effort's experimental apparatus are as follows:

1. Build the plate/groove out of a material more compatible with deionized water so that the corrosive properties of ethanol can be avoided. This would also avoid difficulties in procuring absolute ethanol.

2. Construct the entire fluid supply system out of copper componentry if ethanol is used as a working fluid. This would preclude the possibility of corroded petroleum-based fluid control system materials contaminating the working fluid supplied to the groove.

3. Employ a solid-state power supply system to control the input heater power and ensure a steady supply of power throughout the experiment. The rheostat type power supply was prone to wander over long periods of time, resulting in experimental uncertainty.

4. Modify the present experimental apparatus with a different method of affixing the heater to the plate. The clamping method used in this effort would cause the plate to bow slightly at high temperatures when the plate and the heater expanded at different rates.

5. Modify the present experimental apparatus with a more accurate data acquisition system to lower the overall

experimental uncertainty. The $\pm 4^{\circ}$ C error was the largest error in this research effort.

Bibliography

1. Boman, B. L. et al. *Heat Pipes for Wing Leading Edges of Hypersonic Vehicles*, NASA CR-181922, December 1989.
2. Camarda, C. J. *Analysis and Radiant Heating Tests of a Heat Pipe Cooled Leading Edge*, NASA TN-D-8468, August 1977.
3. Chi, S. W. *Heat Pipe Theory and Practice: A Sourcebook*. Washington: Hemisphere Publishing Corporation, 1976.
4. Dunn, P. and D. A. Reay. *Heat Pipes*, 1st Ed. New York: Pergamon Press, 1976.
5. Fisher, M. A. et al. "Transient Heat-Pipe Studies, Documenting Wick Dryout and Rewet," AIAA 30th Aerospace Sciences Meeting and Exhibit. AIAA-92-0128 (January 1992).
6. Hendrix, W. A. *An Analysis of Body Force Effects on Transient and Steady-State Performance of Heat Pipes*. PhD dissertation. Georgia Institute of Technology, Atlanta GA, 1989.
7. Incropera, F. P., and D. P. DeWitt. *Fundamentals of Heat and Mass Transfer*, 3rd Ed. New York: John Wiley and Sons Inc., 1990.
8. Silverstein, C. C. *A Feasibility Study of a Heat-Pipe Cooled Leading Edge for Hypersonic Cruise Aircraft*, NASA CR-1857, November 1971.
9. Stroes, G. et al. "Heat Flux Induced Dryout and Rewet in Thin Films," *Proceedings of the 9th International Heat Transfer Conference*, 6: 359-36 (December 1990).
10. Vargaftik, N. B. *Tables on the Thermophysical Properties of Liquids and Gases*, 2nd Ed. New York: John Wiley and Sons Inc., 1975.

APPENDIX A. PLATE GEOMETRY

The plate used in this research effort was manufactured of pure copper. The following pages provide the necessary dimensions to accurately manufacture a duplicate of this plate and groove combination or to construct a computer model of the plate. Additionally, several important properties of copper and parameters of the plate are provided.

Properties of Copper at 300 K (7:A3):

k	=	401	W/m-K
c	=	385	J/kg-K
ρ	=	1358	kg/m ³

Plate Parameters:

A_s	=	2.527×10^{-2}	m ²	
V	=	7.257×10^{-5}	m ³	
Bi	=	$h(7.16 \times 10^{-6})$		(Eq 22)
τ	=	$(9877)/h$	sec	(Eq 21)

Figure A.1, shown on the next page, provides a side view of the plate and groove combination.

Right Side

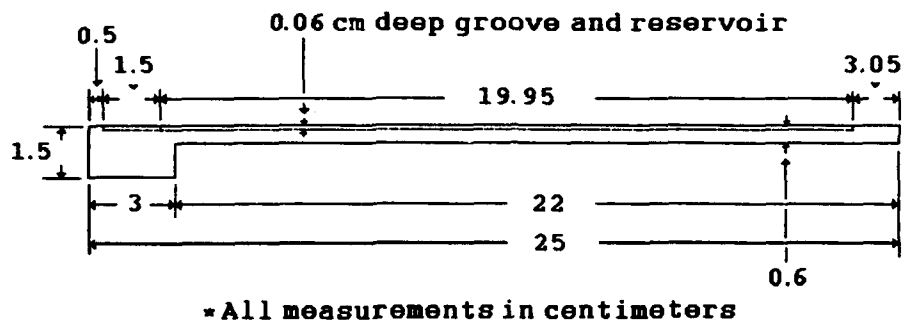


Figure A.1. Copper Plate and Groove; Right Side View

Figure A.2, below, provides a top view of the plate and groove combination.

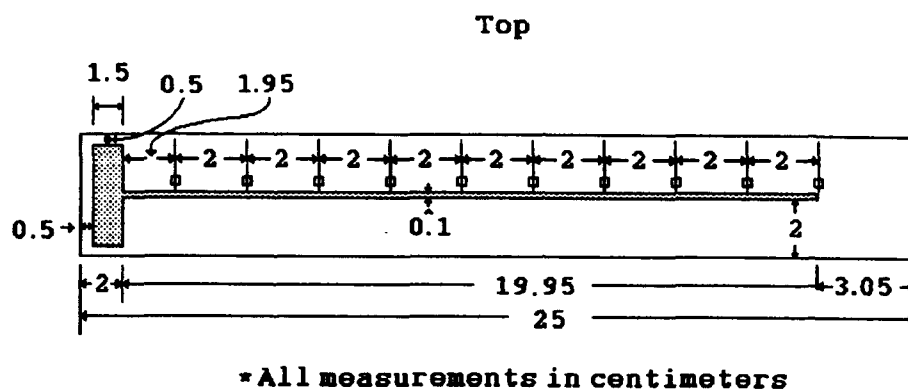
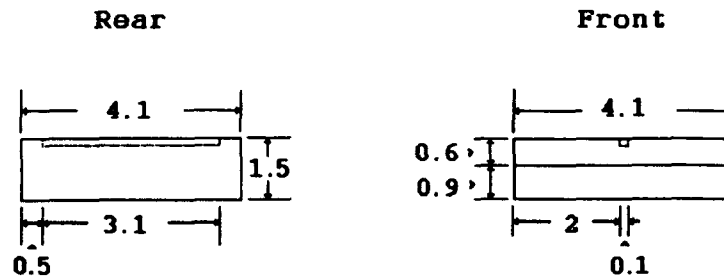


Figure A.2. Copper Plate and Groove; Top View

Figure A.3, below, provides a front and rear view of the plate and groove combination.



*All measurements in centimeters.

Figure A.3. Copper Plate and Groove; Front and Rear Views

APPENDIX B: CONVECTIVE/RADIATIVE HEAT TRANSFER COEFFICIENT

TEST DATA

The following pages contain the temperature data collected for use in determining the plate and groove combination's convective/radiative heat transfer coefficient.

DATE: 08-11-1992 TIME: 10:54:53

RUN NUMBER: HBAR-1

THE ATMOS. PRESSURE IS 28.9 MM OF MERCURY

HEATER POWER: 30.24 W

TIME	INC	T1	T2	T3	T4	T5	T6	T7	T8	T9	T10
0	0	70	72	73	77	80	83	86	88	88	89
5	0	70	72	73	77	80	83	86	88	88	89
10	0	70	72	73	77	80	83	86	88	88	89
15	0	70	72	73	77	80	83	86	88	88	89
20	0	70	72	73	77	79	83	86	88	88	89
25	0	70	72	73	77	79	83	86	88	89	89
30	0	70	72	73	77	79	83	86	88	88	89
35	0	70	72	73	77	80	83	86	88	88	89
40	0	70	72	73	77	79	83	86	88	88	89
45	0	70	72	73	77	79	83	86	88	88	89
50	0	70	72	73	77	79	83	86	88	88	89
55	0	70	72	73	77	79	83	86	88	88	89
60	0	69	71	73	77	79	83	86	88	88	89
65	0	69	72	73	77	79	83	86	88	88	89
70	0	69	72	73	77	79	83	86	88	88	89
75	0	70	72	73	77	79	83	86	88	88	89
80	0	70	72	73	77	79	83	86	88	88	89
85	0	70	72	73	77	79	83	86	88	88	89
Ave:		81	72	73	77	79	83	86	88	88	89
Tave:		70			T=:		23				

DATE: 08-11-1992 TIME: 11:58:48

RUN NUMBER: HBAR-2

THE ATMOS. PRESSURE IS 28.9 MM OF MERCURY

HEATER POWER: 60.14 W

TIME	INC	T1	T2	T3	T4	T5	T6	T7	T8	T9	T10
0	0	102	106	108	116	120	126	131	136	136	137
5	0	102	106	109	116	120	126	132	136	136	137
10	0	102	106	108	116	120	126	132	136	136	137
15	0	102	106	108	116	120	126	132	136	136	137
20	0	102	106	108	116	120	126	132	135	136	136
25	0	102	106	109	116	120	126	132	136	136	136

30	0	102	106	109	116	120	126	132	136	136	137
35	0	102	106	109	116	120	126	132	136	136	137
40	0	102	106	109	116	120	126	132	136	136	136
45	0	102	106	109	116	120	126	131	136	136	136
50	0	102	106	109	116	120	126	132	135	136	136
55	0	102	106	108	116	120	126	131	136	136	136
60	0	102	106	108	116	120	126	131	135	135	136
65	0	102	106	109	116	120	126	131	136	135	136
70	0	102	106	109	115	120	126	132	135	136	136
75	0	102	106	109	116	120	126	131	136	136	136
80	0	102	106	109	116	120	126	131	135	136	136
85	0	102	106	109	116	120	126	131	136	136	136
Ave:		102	106	109	116	120	126	132	136	136	136
Tave:		122			T:	23					

DATE: 08-11-1992 TIME: 13:19:48

RUN NUMBER: HBAR-3

THE ATMOS. PRESSURE IS 28.9 MM OF MERCURY

HEATER POWER: 90.35 W

TIME	INC	T1	T2	T3	T4	T5	T6	T7	T8	T9	T10
0	0	130	135	139	149	155	163	171	177	177	178
5	0	130	135	139	149	155	163	171	177	178	178
10	0	130	135	139	149	155	163	171	177	178	178
15	0	130	135	139	149	155	163	171	177	178	178
20	0	130	135	139	149	155	163	171	177	178	178
25	0	130	135	139	149	155	163	171	177	178	178
30	0	130	135	139	149	155	163	171	177	177	178
35	0	130	135	138	149	155	163	171	177	177	178
40	0	130	135	139	149	155	163	171	177	177	178
45	0	130	135	139	149	155	163	171	177	177	178
50	0	130	135	139	149	155	163	171	177	177	178
55	0	130	135	139	149	155	163	171	177	177	178
60	0	129	135	138	149	155	163	171	177	177	178
65	0	129	135	138	149	155	163	171	177	177	178
70	0	129	135	138	149	155	163	171	177	177	178
75	0	129	135	138	149	155	163	171	177	177	178
80	0	130	135	139	149	155	163	171	177	177	178
85	0	130	135	139	149	155	163	171	177	177	178
Ave:		130	135	139	149	155	163	171	177	177	178
Tave:		157		T:	23						

APPENDIX C: CAPILLARY LIMIT/HEAT TRANSFER MODEL VALIDATION

TEST DATA

The following pages contain the data used to determine the groove's experimental capillary limit and validate the heat transfer model used to model the input heat rate into the groove.

DATE: 09-10-1992 TIME: 16:23:24

RUN NUMBER: A-1

THE ATMOS. PRESSURE IS 29.0 MM OF MERCURY

HEATER POWER: 28.15 W EVAP. MASS FLOW: 0.54 mL/min
OUT MASS FLOW: 0.82 mL/min

TIME	INC	T1	T2	T3	T4	T5	T6	T7	T8	T9	T10	T11
0	0	51	52	54	57	60	63	66	68	69	70	48
10	0	51	52	54	57	60	63	67	68	68	69	48
20	0	51	52	54	58	60	63	67	68	69	70	48
30	0	52	52	54	57	60	63	66	68	68	69	48
40	0	51	53	54	57	60	63	67	68	69	69	48
50	0	52	52	54	57	60	63	66	68	69	69	48
60	0	51	53	54	57	60	63	66	67	68	68	49
70	0	51	53	54	57	60	62	67	67	69	68	48
80	0	51	52	54	57	60	63	68	68	68	69	50
90	0	51	52	54	57	60	63	66	68	68	69	48
100	0	51	52	54	57	60	63	67	68	69	69	48
110	0	51	53	54	57	60	63	66	68	68	69	48
120	0	51	52	55	57	60	63	66	68	69	69	48
130	0	51	52	54	57	60	63	66	68	69	70	48
140	0	51	53	54	57	61	63	67	68	70	69	48
150	0	51	53	53	57	60	63	67	68	70	69	48
160	0	51	52	54	57	60	63	67	68	68	69	48
170	0	51	52	55	57	60	63	66	68	68	69	48
180	0	51	53	54	57	61	63	66	68	69	69	49
190	0	52	53	54	57	60	63	66	68	68	69	48
AVE:		51	52	54	57	60	63	67	68	69	69	48
Tave:		61			Tl,in: 22			T-: 22				

DATE: 09-09-1992 TIME: 14:59:07

RUN NUMBER: B-1

THE ATMOS. PRESSURE IS 29.2 MM OF MERCURY

HEATER POWER: 1.794 W

TIME	INC	T1	T2	T3	T4	T5	T6	T7	T8	T9	T10	T11
------	-----	----	----	----	----	----	----	----	----	----	-----	-----

0	0	24	24	24	24	25	25	27	26	27	25	25
10	0	23	24	24	24	24	25	26	26	26	26	23
20	0	24	24	24	24	24	25	26	26	25	26	23
30	0	23	24	25	24	25	25	26	26	26	26	23
40	0	24	24	24	24	24	25	25	26	26	26	23
50	0	24	24	25	24	25	25	27	26	27	26	25
60	0	24	24	24	24	24	26	26	26	26	26	26
70	0	24	24	24	24	24	25	26	26	26	26	24
80	0	24	24	24	25	24	25	26	26	26	26	23
90	0	24	24	24	25	24	25	26	26	26	26	23
100	0	24	24	24	24	24	25	26	26	26	25	23
110	0	24	24	24	24	24	25	27	26	26	26	23
120	0	24	24	24	25	24	26	26	26	27	26	24
130	0	24	24	24	24	24	25	26	26	26	26	24
140	0	24	24	25	24	24	25	26	26	25	26	23
150	0	24	24	25	24	24	26	26	26	26	26	23
160	0	24	24	24	24	24	25	26	26	26	27	23
170	0	24	24	24	25	24	25	26	26	26	26	23
180	0	24	24	26	24	24	25	26	26	26	26	23
190	0	24	24	24	25	24	25	26	26	26	26	23

Ave: 24 24 24 24 24 25 26 26 26 26 26 24

Tave: 25 Tl,in: 23 T= 23

DATE: 09-10-1992 TIME: 10:09:37

RUN NUMBER: B-2

THE ATMOS. PRESSURE IS 28.9 MM OF MERCURY

HEATER POWER: 1.62 W

TIME	INC	T1	T2	T3	T4	T5	T6	T7	T8	T9	T10	T11
0	0	24	24	24	24	24	25	26	26	26	25	24
10	0	24	24	25	24	25	25	26	26	26	25	23
20	0	24	24	24	24	24	25	26	26	25	26	23
30	0	23	24	24	24	24	25	25	26	25	25	23
40	0	23	24	24	24	24	25	26	26	25	25	23
50	0	23	24	24	24	24	25	25	26	25	26	23
60	0	23	23	24	24	24	25	25	25	26	25	23
70	0	23	24	24	24	24	25	25	26	26	25	24
80	0	23	23	24	24	24	25	25	26	26	26	23
90	0	23	23	23	24	24	25	25	26	26	27	25
100	0	23	24	25	24	24	25	26	26	25	25	23
110	0	23	24	24	24	24	25	26	26	27	26	23
120	0	23	24	24	24	24	25	26	25	25	25	23
130	0	23	23	24	24	24	25	26	26	25	25	23
140	0	23	24	24	24	24	25	26	26	26	26	23
150	0	23	24	24	24	24	25	26	26	26	25	24
160	0	24	23	24	24	24	25	26	26	25	26	23
170	0	24	24	24	24	24	25	25	26	26	25	23
180	0	24	23	24	24	25	25	26	26	26	25	25
190	0	23	24	23	24	24	25	25	26	26	25	24

Ave: 23 24 24 24 24 25 26 26 26 26 25 23

Tave: 25 Tl,in: 23 T= 23

DATE: 09-10-1992 TIME: 15:26:39

RUN NUMBER: C-1

THE ATMOS. PRESSURE IS 29.1 MM OF MERCURY

HEATER POWER: 11.63 W EVAP. MASS FLOW: 0.160 mL/min

OUT MASS FLOW: 1.200 mL/min

TIME	INC	T1	T2	T3	T4	T5	T6	T7	T8	T9	T10	T11
0	0	37	37	38	39	40	42	44	45	47	45	35
10	0	37	37	38	39	41	42	44	45	44	45	34
20	0	37	37	38	39	41	42	44	44	45	45	35
30	0	37	37	38	39	41	43	44	45	45	46	35
40	0	37	37	38	40	41	43	45	45	45	46	35
50	0	37	37	37	39	40	42	44	45	47	45	34
60	0	36	37	38	39	40	42	44	45	45	45	34
70	0	37	37	38	39	40	42	44	45	45	45	37
80	0	36	37	38	39	40	42	44	45	45	45	38
90	0	36	37	38	40	41	42	44	45	46	45	35
100	0	37	37	38	40	41	42	44	45	45	45	35
110	0	37	37	38	40	40	43	44	45	45	45	35
120	0	37	38	38	40	41	43	44	45	45	47	35
130	0	37	37	38	39	41	42	44	45	45	45	35
140	0	37	37	38	39	40	42	44	45	45	46	36
150	0	37	37	38	39	41	42	44	45	46	46	35
160	0	37	37	38	40	41	43	44	45	45	46	35
170	0	37	37	38	40	40	43	44	45	45	46	36
180	0	37	37	38	40	41	42	44	45	45	45	35
190	0	36	37	38	39	41	42	45	45	45	47	35
200	0	37	37	38	39	41	42	44	45	45	45	34
210	0	37	37	38	40	40	42	44	45	45	46	36
220	0	36	37	38	39	40	42	44	45	45	45	35
AVE:		37	37	38	39	41	42	44	45	45	46	35
Tave:		41	Tl,in:			22	T=:			22		

DATE: 09-10-1992 TIME: 17:14:00

RUN NUMBER: C-2

THE ATMOS. PRESSURE IS 29.0 MM OF MERCURY

HEATER POWER: 15.47 W EVAP. MASS FLOW: 0.240 mL/min
OUT MASS FLOW: 1.120 mL/min

TIME	INC	T1	T2	T3	T4	T5	T6	T7	T8	T9	T10	T11
0	0	42	43	44	46	47	49	51	52	53	53	40
10	0	42	42	44	46	47	49	52	53	53	53	40
20	0	42	43	45	45	47	49	52	53	53	53	40
30	0	42	42	43	45	47	49	51	52	53	54	40
40	0	42	42	43	46	47	49	51	53	52	53	39
50	0	42	42	44	46	47	50	51	52	55	53	39
60	0	42	42	43	45	47	49	52	52	52	55	39
70	0	42	43	43	47	47	50	51	53	53	53	40
80	0	41	43	43	45	47	50	51	52	53	53	39
90	0	42	43	44	45	47	49	51	52	52	53	41
100	0	42	42	43	46	47	49	51	52	54	53	39
110	0	42	42	43	46	48	50	51	52	52	53	40
120	0	41	42	43	45	47	49	52	52	52	53	39
130	0	42	42	44	45	47	49	51	52	52	53	41
140	0	42	43	44	45	48	49	51	52	52	52	41
150	0	41	42	43	46	47	49	51	52	52	53	39
160	0	42	42	43	45	47	49	51	52	53	53	41
170	0	42	42	44	45	47	49	51	52	52	53	39
180	0	42	42	44	45	47	50	51	52	52	54	39
190	0	41	42	43	45	47	49	51	51	52	52	39
AVE:		42	42	44	46	47	49	51	52	53	53	40
Tave:		48	Tl,in:			23	T=:			23		

APPENDIX D. WORKING FLUID PROPERTIES

All fluid properties used in this endeavor are presented below at the average temperature of the plate.

Properties of Ethanol at 80° C (10:407-415):

Liquid density:	ρ_1	=	735 Kg/m ³
Liquid viscosity:	μ_1	=	4.350×10 ⁻⁴ N-sec/m ²
Liquid surface tension:	σ_1	=	2.105×10 ⁻² N/m
Liquid latent heat:	λ	=	841.547×10 ³ J/Kg
Specific heat:	c	=	2.981×10 ³ J/Kg-°C

APPENDIX E. EXPERIMENTAL DATA

The following pages contain the research test data used throughout this research effort to formulate conclusions and recommendations.

DATE: 09-15-1992 TIME: 14:56:16

RUN NUMBER: 1

THE ATMOS. PRESSURE IS 29.2 MM OF MERCURY

HEATER POWER: 10.64 W Evap. Mass Flow: 0.29 mL/m

TIME	INC	T1	T2	T3	T4	T5	T6	T7	T8	T9	T10	T11
0	0	34	35	35	36	37	39	41	41	42	42	33
20	0	34	34	35	36	38	39	40	42	42	42	33
40	0	34	34	35	37	37	39	40	41	42	42	33
60	0	34	35	36	36	38	39	40	42	42	42	33
80	0	34	34	36	36	38	39	40	42	42	42	32
100	0	35	34	36	36	37	40	40	42	42	43	33
120	0	34	34	35	36	37	39	41	42	42	44	32
140	0	34	34	35	36	38	39	41	42	42	42	33
160	0	34	34	35	36	38	39	41	41	44	42	36
180	0	34	35	35	36	38	39	41	42	42	42	33
200	0	34	34	35	37	37	39	40	42	42	42	33
Ave:		34	34	35	36	38	39	40	42	42	42	33
T _{ave} :		38		T _{1,1n} :		22		T _u :		22		
220	0	34	35	35	37	38	39	42	42	42	42	33
240	0.15	34	34	35	36	37	39	40	42	42	42	33
260	1.21	34	34	35	36	38	39	41	42	45	42	33
280	1.59	34	34	35	36	38	39	41	41	42	43	34
300	1.59	34	35	35	36	38	39	41	41	42	42	33
320	1.59	34	3	35	37	37	39	41	42	42	42	32
340	1.59	35	35	35	36	37	39	40	41	42	42	33
360	1.59	34	34	35	36	37	39	40	42	42	42	34
380	1.59	34	34	36	36	38	40	42	42	43	42	33

400	1.59	34	34	35	37	37	39	41	42	42	42	33
420	1.59	34	35	35	36	38	39	41	42	43	42	34
440	1.59	34	34	35	36	37	39	41	42	42	42	34
460	1.59	35	35	36	37	38	40	41	42	42	43	33
480	1.59	34	35	35	37	38	39	41	42	44	43	33
500	1.59	34	35	36	37	38	40	42	42	44	42	33
520	1.59	34	35	35	37	38	40	41	42	43	43	34
540	1.59	34	35	35	37	38	39	41	42	42	42	35
560	1.59	34	35	36	37	38	40	42	42	43	43	34
580	1.59	34	35	38	37	38	40	41	42	45	43	34
600	1.59	34	35	36	37	38	41	41	43	43	44	33
620	1.59	35	35	36	37	38	40	42	42	46	43	34
640	1.59	34	35	35	37	38	40	42	42	43	43	33
660	1.59	35	35	36	37	39	40	41	42	42	43	35
680	1.59	34	35	36	37	38	40	42	42	43	42	33
700	1.59	35	35	36	37	38	41	41	42	42	43	33
720	1.59	35	36	36	37	38	40	41	42	43	43	34
740	1.59	34	35	35	37	38	40	43	42	42	44	34
760	1.59	35	35	36	38	38	40	41	42	44	43	33
780	1.59	35	35	36	38	38	41	42	43	43	43	36
800	1.59	35	35	36	37	38	40	41	42	42	43	33
820	1.59	35	35	36	38	38	40	42	43	44	43	34
840	1.59	35	35	36	37	39	40	42	42	43	43	34
860	1.59	35	36	37	37	38	40	42	43	43	43	34
880	1.59	35	36	36	37	38	40	43	43	44	43	34
900	1.59	35	36	36	38	38	41	42	43	43	45	34
920	1.59	35	35	36	37	39	40	41	43	43	43	34
940	1.59	35	35	36	38	39	40	41	42	44	43	35
960	1.59	35	36	36	37	38	40	42	43	43	43	34
980	1.59	35	36	36	37	38	40	42	43	43	43	34
1000	1.59	35	35	38	37	38	40	42	42	45	44	34
1020	1.59	35	35	36	37	38	40	42	42	43	43	35
1040	1.59	36	35	36	37	39	40	41	42	43	43	33
1060	1.59	35	35	36	37	38	40	42	42	44	43	34
1080	1.59	35	35	36	38	39	40	42	43	43	44	34
1100	1.59	35	35	36	38	38	40	43	42	43	43	34

1120	1.59	35	35	36	37	38	40	42	42	43	44	35
1140	1.59	35	35	36	37	38	41	42	43	44	43	35
1160	1.59	35	35	36	38	38	40	41	42	43	43	34
1180	1.59	35	35	36	37	38	40	42	42	43	43	33
1200	1.59	35	35	36	37	38	40	42	42	43	43	34
1220	1.59	35	36	36	38	38	40	42	43	43	43	33
1240	1.59	35	35	36	37	38	40	42	43	43	43	34
1260	1.59	35	35	36	37	38	40	42	42	43	43	36
1280	1.59	34	35	36	37	39	40	44	43	44	43	34
1300	1.59	35	35	37	38	38	41	42	43	44	43	34
1320	0.55	35	35	36	38	38	40	42	42	44	43	34
1340	0	35	35	36	37	38	41	41	42	44	43	33
1360	0	35	35	36	38	38	40	42	43	43	43	35
1380	0	35	35	36	38	38	40	42	42	43	44	34
1400	0	35	36	36	37	39	40	42	42	43	44	34
1420	0	35	35	36	37	38	40	41	42	44	44	34
1440	0	34	35	36	37	38	40	41	42	43	44	34
1460	0	35	35	36	37	38	40	41	42	43	44	34
1480	0	35	36	36	37	38	40	42	43	43	43	34
1500	0	35	36	36	37	38	40	41	43	45	43	34
1520	0	35	36	36	38	38	40	41	42	43	44	34
1540	0	35	36	36	37	38	40	42	43	43	43	34
1560	0	35	35	36	37	38	40	41	42	43	43	33
1580	0	35	35	36	37	38	40	41	42	44	43	33
1600	0	35	35	37	37	38	40	41	42	42	44	35
1620	0	35	35	36	37	38	40	42	42	43	43	33
1640	0	34	36	37	37	39	40	43	42	43	43	37
1660	0	35	35	36	37	38	40	41	42	43	44	34
1680	0	35	35	36	37	38	40	41	42	43	43	34
1700	0	35	35	36	37	38	40	41	42	42	43	33
1720	0	35	35	36	37	38	40	41	43	43	43	33
1740	0	35	35	36	37	39	40	41	43	42	44	36
1760	0	34	35	36	37	38	40	42	42	42	43	33
1780	0	35	35	35	38	38	40	41	42	43	43	34
1800	0	35	35	36	37	38	40	41	42	44	44	34
1820	0	35	35	37	37	38	40	41	42	42	43	34
1840	0	35	35	36	37	38	40	41	42	43	44	35

1860	0	34	35	36	37	38	40	41	42	43	43	33
1880	0	34	35	35	37	38	40	41	42	43	43	34
1900	0	35	35	35	37	38	40	41	42	42	42	33
1920	0	34	35	36	37	38	40	41	43	42	43	34
1940	0	35	35	35	37	38	40	41	42	42	42	33
1960	0	35	35	35	37	39	40	43	42	42	43	35
1980	0	34	35	36	38	38	40	41	42	43	43	33
2000	0	35	35	37	37	38	40	41	42	42	42	33
2020	0	35	35	36	37	38	40	42	42	43	43	34
2040	0	35	35	36	37	38	40	41	42	43	43	35
2060	0	34	35	35	37	38	40	42	42	42	43	33
2080	0	35	35	36	37	38	40	41	42	43	43	34
2100	0	35	35	36	37	38	40	41	42	43	43	35
2120	0	35	35	36	37	38	40	42	42	43	43	34
2140	0	35	35	36	37	38	40	42	42	43	43	38
2160	0	35	35	36	37	38	40	43	42	43	43	34
2180	0	34	35	36	37	38	40	41	42	42	42	33
2200	0	35	35	36	37	38	40	41	42	42	42	34
2220	0	35	35	35	37	38	39	41	42	42	42	34
2240	0	34	35	36	37	38	40	41	42	42	43	33
2260	0	34	35	36	37	38	40	41	42	42	43	33
2280	0	34	35	35	36	38	40	41	42	42	42	33
2300	0	34	35	36	37	38	39	42	42	42	42	33
2320	0	34	35	35	37	38	40	41	42	44	42	33
2340	0	34	35	35	37	38	39	41	42	42	42	34
2360	0	34	35	35	37	38	40	41	42	43	43	34
2380	0	35	35	35	37	38	40	42	42	44	42	35
2400	0	34	35	36	37	38	39	41	42	42	42	33
2420	0	34	35	35	36	38	39	42	42	43	43	33
2440	0	35	35	36	37	38	39	41	42	42	42	33
2460	0	34	35	35	37	38	39	42	42	42	42	33
2480	0	34	35	35	36	38	39	42	42	43	42	34
2500	0	34	35	36	37	38	39	42	42	42	42	33
2520	0	34	35	35	36	38	40	41	41	42	44	33
2540	0	34	34	35	37	38	40	41	42	43	43	33
2560	0	34	35	35	37	38	40	41	42	42	42	33

2580	0	34	35	35	37	38	39	41	42	44	42	33
2600	0	34	35	35	36	38	40	41	42	42	42	33
2620	0	35	34	35	37	38	40	42	42	43	42	33
2640	0	34	35	36	37	38	40	42	42	42	44	33
2660	0	34	35	35	37	38	40	41	42	42	43	33
2680	0	34	35	35	36	38	39	41	42	42	43	33
2700	0	34	34	35	37	38	39	41	42	42	43	33
2720	0	34	35	35	37	38	39	41	42	42	43	34
2740	0	35	35	35	37	38	39	41	42	43	44	33
2760	0	34	35	36	37	38	40	40	42	42	42	34

DATE: 09-21-1992 TIME: 10:32:22

RUN NUMBER: 2

THE ATMOS. PRESSURE IS 29 MM OF MERCURY

HEATER POWER: 22.8 W Evap. Mass Flow: 0.46 mL/min

TIME	INC	T1	T2	T3	T4	T5	T6	T7	T8	T9	T10	T11
0	0	48	49	50	53	55	57	60	62	62	62	46
30	0	48	49	50	53	56	57	61	62	62	63	44
60	0	48	49	50	53	55	57	61	62	63	63	44
90	0	47	49	50	52	55	57	60	61	62	64	44
120	0	48	49	50	53	55	58	60	62	63	63	45
Ave:		48	49	50	53	55	57	60	62	62	63	45
Tave:		56	T1, in:				22	T=:		22		
150	0	48	49	51	53	55	58	60	62	63	63	45
180	0.28	48	49	50	53	55	58	60	62	62	63	44
210	0.28	48	49	50	53	55	58	61	62	63	63	45
240	0.28	48	49	50	52	55	57	60	61	63	63	44
270	0.28	48	49	50	52	55	57	60	62	62	63	44
300	0.28	47	48	50	53	55	57	60	62	62	63	44
330	0.28	48	49	50	53	55	58	60	62	62	63	44
360	0.28	48	48	50	53	55	57	61	62	63	63	44
390	0.28	48	49	50	53	55	58	60	62	62	64	44
420	0.28	48	49	50	52	55	57	60	62	64	63	45
450	0.28	48	48	50	53	55	57	60	62	62	63	44
480	0.28	48	49	50	53	55	57	61	62	63	63	44

510	0.28	48	49	51	53	55	58	61	62	63	63	44
540	0.28	48	49	50	53	55	58	60	62	62	63	45
570	0.28	48	49	50	53	55	58	60	62	63	63	44
600	0.28	48	49	50	53	55	58	61	62	63	63	44
630	0.28	48	49	51	53	55	58	61	62	63	63	46
660	0.28	48	49	51	53	55	58	61	62	63	63	45
690	0.28	48	49	50	53	55	58	61	62	63	63	46
720	0.28	48	49	50	53	55	58	61	62	63	63	44
750	0.28	48	49	51	53	55	58	60	62	63	63	44
780	0.28	48	49	50	53	55	58	61	62	63	63	44
810	0.28	48	49	51	53	55	58	60	62	63	63	45
840	0.28	48	49	50	53	55	58	60	62	62	63	45
870	0.28	48	49	50	53	55	58	61	62	63	63	44
900	0.28	48	49	50	53	55	58	60	62	63	63	44
930	0.28	48	49	50	53	55	58	61	62	63	63	45
960	0.28	48	49	50	53	55	58	62	62	64	63	45
990	0.28	48	49	50	54	55	58	60	62	63	64	44
1020	0.28	48	49	50	53	55	58	60	62	63	63	45
1050	0.28	48	49	50	53	55	58	60	62	62	63	44
1080	0.28	48	49	51	53	55	58	61	62	63	63	45
1110	0.28	48	49	50	53	56	58	61	62	63	63	44
1140	0.28	48	49	50	53	55	58	60	62	63	63	44
1170	0	48	49	50	53	55	57	60	61	63	63	45
1200	0	48	49	50	53	55	58	60	61	63	63	44
1230	0	48	49	51	53	55	57	60	61	63	62	44
1260	0	48	49	50	53	55	57	60	61	61	62	45
1290	0	48	49	50	53	55	57	60	62	63	63	44
1320	0	48	49	50	53	55	57	60	62	62	63	46
1350	0	48	49	50	53	55	58	60	62	63	63	46
1380	0	48	49	50	53	55	57	60	62	62	62	44
1410	0	47	49	50	52	55	57	60	61	62	63	44
1440	0	47	49	50	53	55	58	60	62	64	63	44
1470	0	47	49	50	53	55	58	60	62	62	64	45
1500	0	47	49	50	53	55	57	61	62	63	63	44
1530	0	48	49	50	52	55	57	60	61	62	62	45
1560	0	47	49	50	53	55	57	60	62	62	62	44
1590	0	48	48	50	53	55	57	60	62	62	62	44

1620	0	48	49	50	53	55	57	60	62	63	63	44
1650	0	48	49	50	53	55	58	60	62	62	63	44
1680	0	48	49	50	53	55	58	60	62	63	62	44
1710	0	48	49	50	53	55	58	60	62	62	63	44
1740	0	48	49	50	53	55	57	60	62	62	63	45
1770	0	48	49	50	53	55	58	60	62	63	63	45
1800	0	48	49	50	53	55	58	60	62	63	63	44
1830	0	48	49	50	53	55	58	60	62	63	63	44
1860	0	48	49	50	53	55	58	61	62	62	63	44
1890	0	49	49	50	53	56	58	60	62	63	63	44
1920	0	48	49	50	53	55	58	60	62	63	63	46
1950	0	48	49	51	53	55	58	61	62	62	63	44
1980	0	48	49	50	53	55	58	61	62	63	63	44
2010	0	48	49	50	53	55	58	60	62	63	62	44
2040	0	48	49	51	53	55	58	60	62	62	63	44
2070	0	48	49	50	53	55	58	60	62	62	63	44
2100	0	48	49	50	53	55	58	61	62	62	63	44
2130	0	48	49	50	53	55	58	60	62	62	63	44
2160	0	48	49	50	53	55	58	60	61	64	63	44
2190	0	48	49	51	53	55	58	60	62	62	63	44
2220	0	48	49	50	53	55	57	61	62	63	63	45
2250	0	48	49	50	53	55	58	61	62	63	63	44
2280	0	48	49	50	53	55	58	60	62	62	63	44
2310	0	48	49	50	53	55	57	60	62	63	62	45

DATE: 09-21-1992 TIME: 13:20:43

RUN NUMBER: 3

THE ATMOS. PRESSURE IS 29 MM OF MERCURY

HEATER POWER: 24.8 W Evap. Mass Flow: 0.46 mL/min

TIME	INC	T1	T2	T3	T4	T5	T6	T7	T8	T9	T10	T11
0	0	48	50	51	54	56	59	63	64	64	64	44
30	0	48	49	51	54	56	60	61	64	64	64	44
60	0	48	49	51	54	56	59	62	64	66	65	48
90	0	48	49	52	54	56	59	62	64	63	65	45
120	0	48	49	50	54	56	59	62	63	64	64	45
150	0	48	50	51	54	56	59	63	63	67	64	45

180	0	48	49	51	53	56	59	62	63	64	64	45
210	0	49	49	51	54	56	59	61	64	64	65	45
240	0	48	50	52	54	56	59	62	64	64	65	46
Ave:		48	49	51	54	56	59	62	64	64	64	45
T _{ave} :		57		T _{l, in} :		22		T _a :		22		
270	0	48	49	51	54	56	60	61	64	63	65	45
300	0.65	48	49	50	54	56	59	61	64	64	64	45
330	0.65	48	50	51	54	56	59	62	64	64	65	45
360	0.65	48	49	51	54	56	60	62	64	64	65	46
390	0.65	48	50	51	54	56	59	62	64	64	64	46
420	0.65	48	49	51	54	57	59	64	64	64	64	46
450	0.65	49	49	51	54	57	59	62	64	65	65	44
480	0.65	48	49	51	54	56	59	64	64	65	65	45
510	0.65	48	50	51	54	56	59	62	64	65	65	45
540	0.65	48	50	51	54	56	59	62	64	64	66	45
570	0.65	48	50	51	54	57	59	62	64	65	65	47
600	0.65	48	49	51	54	56	60	62	63	63	65	44
630	0.65	48	49	51	55	56	59	62	64	64	65	45
660	0.65	48	50	51	54	56	60	62	63	64	66	46
690	0.65	49	50	51	54	56	59	62	64	64	65	45
720	0.65	48	50	51	54	57	59	62	64	64	65	47
750	0.65	48	50	51	54	56	60	63	64	64	66	46
780	0.65	48	50	51	54	57	60	62	64	64	65	45
810	0.65	48	50	51	54	57	59	62	64	64	65	46
840	0.65	49	50	52	54	57	59	62	64	64	65	45
870	0.65	48	50	51	54	56	59	64	64	64	65	46
900	0.65	48	50	52	54	57	59	63	64	65	65	47
930	0.65	49	50	51	54	57	59	63	64	65	65	48
960	0.65	49	50	51	54	57	59	62	64	66	65	46
990	0.65	50	50	51	55	57	59	64	64	65	65	46
1020	0.65	49	50	51	54	57	60	63	64	64	65	47
1050	0.65	49	50	52	54	57	60	63	64	65	66	48
1080	0.65	49	50	51	54	57	60	63	64	65	66	46
1110	0.65	49	50	51	55	57	60	63	64	66	65	46
1140	0.65	49	50	51	54	57	60	62	65	64	66	45
1170	0.65	49	50	52	54	57	60	62	64	65	66	45

1200	0.65	49	50	51	54	57	59	63	64	66	66	48
1230	0.65	49	50	51	54	57	60	62	64	65	66	45
1260	0.65	49	50	51	55	57	60	63	65	66	65	45
1290	0	49	50	52	54	56	59	62	64	66	65	47
1320	0	49	50	52	54	57	59	62	64	64	65	45
1350	0	49	50	51	54	56	59	63	63	64	64	45
1380	0	48	50	51	54	56	59	63	63	64	65	45
1410	0	49	49	52	54	56	60	63	63	63	65	45
1440	0	48	50	51	54	57	59	62	64	63	65	45
1470	0	48	50	51	54	57	60	62	63	64	65	45
1500	0	48	50	51	54	57	59	62	64	63	64	44
1530	0	48	50	51	54	56	59	62	64	64	65	45
1560	0	48	50	52	54	56	59	62	64	64	65	45
1590	0	49	50	51	54	56	59	62	64	64	64	44
1620	0	48	50	51	54	57	60	62	63	64	65	45
1650	0	49	50	51	54	57	59	62	63	64	64	45
1680	0	48	50	51	54	57	59	62	64	63	65	44
1710	0	49	50	51	54	57	59	63	63	64	65	45
1740	0	49	50	51	54	57	59	62	64	64	64	48
1770	0	48	49	52	54	56	60	62	63	65	65	45
1800	0	49	50	51	54	57	59	62	64	64	64	45
1830	0	48	50	51	54	56	59	62	64	65	65	46
1860	0	49	50	51	54	57	59	62	64	64	65	46

DATE: 09-22-1992 TIME: 14:15:41

RUN NUMBER: 4

THE ATMOS. PRESSURE IS 29 MM OF MERCURY

HEATER POWER: 24.96 W Evap. Mass Flow: 0.51 mL/min

TIME	INC	T1	T2	T3	T4	T5	T6	T7	T8	T9	T10	T11
0	0	48	49	51	54	56	59	62	64	64	64	46
30	0	49	50	51	54	56	59	62	64	64	65	46
60	0	48	50	51	54	56	59	62	64	64	65	46
90	0	48	50	51	54	56	59	63	64	64	65	46
120	0	48	50	51	54	56	59	62	64	64	64	46
150	0	49	50	51	54	57	59	62	64	64	65	47
180	0	49	50	51	54	56	59	62	64	65	65	46

210	0	49	50	51	54	56	59	62	64	64	66	46
240	0	48	50	51	54	57	59	62	64	65	64	46
270	0	49	50	51	54	57	59	62	64	64	65	46
300	0	49	49	51	54	56	59	63	64	64	64	45
330	0	48	50	51	54	56	59	62	64	64	64	46
Ave:		49	50	51	54	56	59	62	64	64	65	46
T _{ave} :		57		T _{1, in} :		22		T _a :		22		
360	0	49	50	51	54	56	59	62	64	64	65	46
390	0	48	50	51	54	56	59	62	64	64	64	46
420	0.72	48	49	51	54	57	59	62	64	64	65	46
450	0.72	49	49	51	54	56	59	62	64	63	64	45
480	0.72	48	49	51	53	56	59	62	63	64	64	45
510	0.72	48	49	50	53	55	59	62	63	63	64	45
540	0.72	48	49	51	53	56	60	62	63	64	64	46
570	0.72	48	49	51	54	56	59	62	63	64	64	47
600	0.72	48	49	51	53	56	58	62	63	64	64	46
630	0.72	48	49	51	54	56	59	62	64	64	64	47
660	0.72	48	49	51	53	56	58	62	63	64	64	47
690	0.72	49	49	51	54	56	59	62	63	66	64	46
720	0.72	48	50	51	54	56	59	63	64	64	65	46
750	0.72	48	49	51	54	56	59	62	63	64	64	46
780	0.72	49	49	51	54	56	59	62	63	64	65	46
810	0.72	48	50	51	54	56	59	62	64	64	64	46
840	0.72	48	50	51	54	56	59	62	64	64	64	46
870	0.72	49	49	51	54	56	59	62	64	64	65	46
900	0.72	48	49	51	54	56	59	62	64	64	64	46
930	0.72	48	50	51	54	56	59	62	64	64	64	46
960	0.72	48	50	51	54	56	59	62	64	64	64	46
990	0.72	49	50	51	54	56	59	62	64	64	65	46
1020	0.72	48	50	51	54	56	59	63	64	64	64	46
1050	0.72	49	50	51	54	56	59	62	64	64	64	46
1080	0.72	49	50	51	54	57	59	62	64	64	65	46
1110	0.72	48	50	51	54	56	59	62	64	64	64	47
1140	0.72	49	50	51	54	56	59	62	64	64	65	46
1170	0.72	49	50	52	54	56	59	63	64	64	65	46

1200	0.72	49	50	51	54	57	59	62	64	64	65	46
1230	0.72	49	50	51	54	56	59	64	64	64	65	46
1260	0.72	49	50	52	54	56	59	62	64	64	65	46
1290	0.72	49	50	51	54	56	59	62	64	64	65	47
1320	0.72	49	50	52	54	57	60	62	64	65	65	47
1350	0.72	49	50	51	54	56	59	62	64	64	66	48
1380	0.72	48	50	51	54	56	59	62	64	65	65	47
1410	0.72	48	50	51	54	56	59	62	64	64	64	47
1440	0.72	49	49	51	54	56	59	62	63	65	65	49
1470	0.72	49	50	51	54	56	59	62	63	64	65	47
1500	0.72	48	50	51	54	56	59	62	64	64	66	46
1530	0.72	49	50	51	54	56	59	62	64	64	65	47
1560	0.72	49	50	51	54	56	59	62	64	64	64	48
1590	0.72	49	50	51	54	56	59	62	64	64	64	46
1620	0.72	48	50	52	54	57	59	62	64	64	65	46
1650	0.72	49	50	51	54	56	59	62	64	65	65	47
1680	0.72	49	50	52	54	56	59	62	63	64	65	46
1710	0.72	48	50	51	54	56	59	62	64	64	64	47
1740	0.72	48	50	52	54	57	59	63	63	64	64	49
1770	0.72	49	50	51	54	57	59	63	64	64	64	47
1800	0.72	49	50	51	54	56	60	62	64	64	65	48
1830	0.72	49	50	52	55	56	59	64	64	64	65	46
1860	0.72	49	50	51	54	57	59	63	64	64	65	50
1890	0.72	49	50	51	54	57	59	62	64	64	64	46
1920	0.72	49	50	51	54	56	60	62	64	67	65	47
1950	0.72	49	50	52	54	57	59	63	64	64	64	47
1980	0.72	49	50	52	54	56	59	62	64	64	65	46
2010	0.72	50	50	51	54	56	59	64	64	64	65	46
2040	0.72	50	50	51	54	57	60	62	64	64	65	46
2070	0.72	51	50	51	54	56	59	63	64	64	65	47
2100	0.72	49	50	52	54	57	60	63	64	65	65	46
2130	0.72	49	50	52	54	57	59	63	64	64	65	47
2160	0.72	50	50	52	54	57	59	63	64	65	65	47
2190	0.72	49	50	52	54	57	59	63	64	64	66	47
2220	0.72	49	50	52	54	57	59	63	64	64	65	46
2250	0.72	49	50	52	54	57	60	62	64	65	65	46
2280	0.72	49	50	52	54	57	60	63	65	64	65	47

2310	0.72	50	50	52	54	57	60	62	64	65	65	47
2340	0.72	49	50	52	54	57	60	62	64	66	65	47
2370	0.72	49	50	52	55	57	59	63	64	64	65	47
2400	0.72	49	50	53	55	58	60	63	64	65	65	49
2430	0.72	49	51	52	54	58	60	63	64	65	65	49
2460	0.72	49	50	52	54	57	60	63	64	65	66	47
2490	0.72	49	50	51	55	57	60	63	65	64	65	48
2520	0.72	49	50	52	55	57	60	64	64	66	65	47
2550	0.72	50	51	53	55	57	60	63	65	65	65	47
2580	0.72	49	51	51	54	57	60	63	65	65	66	47
2610	0.72	49	51	52	55	57	60	63	65	66	65	47
2640	0.72	49	50	52	54	58	60	63	65	67	65	47
2670	0.72	49	51	51	55	57	60	63	65	65	65	47
2700	0.72	49	50	51	54	57	60	63	64	64	65	48
2730	0.72	49	50	51	55	57	60	64	64	65	65	50
2760	0.72	49	50	52	54	57	60	62	65	64	66	46
2790	0.72	50	50	53	54	57	60	63	64	65	65	47
2820	0.72	50	50	52	55	57	60	63	65	64	67	50
2850	0.72	49	50	52	55	57	60	63	65	65	65	47
2880	0.72	50	50	52	55	57	60	63	64	65	66	47
2910	0.72	50	50	51	55	57	60	62	64	65	66	48
2940	0.72	49	50	52	55	57	60	63	65	65	66	47
2970	0.72	49	50	52	54	57	60	63	65	65	66	48
3000	0.72	49	50	52	54	56	60	62	64	64	65	47
3030	0.72	50	50	51	55	57	60	63	64	64	65	47
3060	0.72	50	50	52	55	57	60	62	64	65	66	50
3090	0.72	49	51	51	55	57	60	62	64	65	65	47
3120	0.72	50	50	52	55	57	60	62	64	65	65	47
3150	0.72	49	50	53	55	57	60	63	65	65	66	47
3180	0.72	49	50	52	55	57	60	64	65	65	66	47
3210	0.72	49	50	52	54	57	60	63	64	65	65	47
3240	0.72	50	50	53	54	57	59	63	64	64	65	47
3270	0.72	49	50	52	55	57	60	62	65	64	66	47
3300	0.72	49	50	51	55	57	60	62	64	64	66	47
3330	0.72	49	50	51	55	57	59	63	64	65	66	47
3360	0	49	50	51	54	57	60	62	64	65	65	47

3390	0	50	50	52	54	57	60	63	65	64	65	47
3420	0	49	50	51	54	57	60	63	64	64	65	47
3450	0	49	50	51	54	57	60	62	64	66	65	46
3480	0	49	50	51	54	57	59	62	64	65	65	47
3510	0	49	50	52	54	57	59	63	64	64	65	47
3540	0	49	50	51	54	57	59	62	64	64	64	46
3570	0	49	50	51	55	57	59	62	64	66	65	47
3600	0	50	50	51	54	57	60	63	64	64	64	47
3630	0	49	50	51	54	56	59	62	64	64	65	46
3660	0	49	50	51	54	56	60	63	64	64	65	46
3690	0	49	50	51	54	57	59	63	64	64	64	47
3720	0	48	50	52	54	56	58	61	63	63	64	46
3750	0	48	50	51	54	57	59	62	63	64	64	46

DATE: 09-22-1992 TIME: 17:35:12

RUN NUMBER: 5

THE ATMOS. PRESSURE IS 29 MM OF MERCURY

HEATER POWER: 24 W

Evap. Mass Flow: 0.43 mL/min

TIME	INC	T1	T2	T3	T4	T5	T6	T7	T8	T9	T10	T11
0	0	46	47	48	51	53	56	58	60	60	60	43
30	0	46	47	48	51	53	56	59	60	63	61	46
60	0	46	47	48	51	54	56	58	60	60	61	44
90	0	46	47	48	51	53	56	58	60	60	61	44
120	0	46	47	48	51	53	56	58	61	61	61	44
150	0	46	47	49	51	53	56	59	60	61	61	44
180	0	46	47	48	51	53	56	59	60	60	61	45
Ave:		46	47	48	51	53	56	58	60	61	61	44
T _{ave} :		54		T _{1,in} :		22		T ₂ :		22		
210	0	46	47	49	51	53	56	58	60	60	61	44
240	0.86	46	47	49	51	53	56	60	60	62	61	46
270	0.86	47	47	49	51	53	56	59	60	61	61	44
300	0.86	46	47	49	51	54	56	59	60	61	61	44
330	0.86	46	47	48	51	54	56	59	60	61	62	44
360	0.86	46	47	49	51	54	56	59	61	61	61	44
390	0.86	46	48	49	51	53	56	59	60	60	61	44

420	0.86	46	48	49	51	54	56	59	61	61	61	45
450	0.86	47	48	49	52	54	57	59	61	61	62	44
480	0.86	48	48	49	52	53	56	59	61	61	61	44
510	0.86	47	48	49	52	54	56	59	61	61	61	44
540	0.86	46	48	49	51	54	56	59	61	61	61	45
570	0.86	47	48	49	52	53	57	59	61	62	62	45
600	0.86	47	48	49	52	54	57	59	61	61	62	44
630	0.86	47	48	49	51	54	56	59	61	61	62	47
660	0.86	47	48	49	52	54	57	60	61	62	62	45
690	0.86	47	48	49	51	54	56	59	61	61	61	45
720	0.86	47	48	49	52	54	57	59	61	61	62	44
750	0.86	48	48	49	52	54	57	59	61	61	62	45
780	0.86	46	47	48	52	53	57	59	61	61	62	44
810	0.86	47	48	49	52	54	57	59	61	61	61	44
840	0.86	47	48	49	51	54	56	60	60	61	63	44
870	0.86	48	48	50	52	54	57	59	61	61	63	47
900	0.86	47	47	49	52	53	56	59	61	61	61	44
930	0.86	47	48	50	52	54	57	60	61	61	62	44
960	0.86	47	48	50	52	54	56	59	61	61	62	45
990	0.86	47	47	49	52	54	56	59	61	62	62	44
1020	0.86	47	48	50	52	54	57	59	61	61	62	44
1050	0.86	46	48	49	52	53	57	59	61	61	62	44
1080	0.86	47	48	49	52	54	57	59	61	62	61	45
1110	0.86	46	48	49	51	54	57	59	61	62	61	44
1140	0.86	46	48	50	52	54	56	60	61	61	62	45
1170	0.86	46	47	49	51	53	56	59	60	60	61	44
1200	0.86	46	47	49	51	54	56	59	61	60	61	44
1230	0.1	46	47	48	51	53	56	59	61	61	61	45
1260	0	46	47	48	51	53	56	59	61	60	61	43
1290	0	46	47	48	51	53	56	59	60	60	61	45
1320	0	46	47	48	51	53	56	58	60	60	61	43
1350	0	46	47	48	51	53	56	59	60	60	61	43
1380	0	45	47	48	51	53	55	59	60	60	61	43
1410	0	46	47	49	51	53	56	61	60	60	61	44
1440	0	46	47	48	51	53	56	58	60	60	61	44
1470	0	46	47	48	51	53	56	58	60	62	61	43
1500	0	46	47	49	51	53	56	59	60	60	61	43

1530	0	46	47	48	51	53	56	58	60	60	61	44
1560	0	46	47	48	51	53	56	58	60	60	60	43
1590	0	46	47	48	51	53	56	59	60	61	61	44
1620	0	46	47	48	51	53	56	59	60	61	60	44
1650	0	46	47	48	51	53	56	58	60	60	60	43
1680	0	46	47	48	51	53	56	58	60	61	60	44

DATE: 09-22-1992 TIME: 18:04:20

RUN NUMBER: 6

THE ATMOS. PRESSURE IS 29 MM OF MERCURY

HEATER POWER: 24.2 W Evap. Mass Flow: 0.43 mL/min

TIME	INC	T1	T2	T3	T4	T5	T6	T7	T8	T9	T10	T11
0	0	46	47	48	51	53	55	58	60	60	61	43
30	0	47	47	48	51	53	56	58	60	60	61	44
60	0	46	47	48	51	53	56	58	60	60	61	43
90	0	46	47	48	51	53	56	58	60	60	62	44
120	0	46	47	48	51	53	56	58	60	60	60	45
150	0	46	47	49	51	53	56	59	59	61	60	45
180	0	46	47	48	51	53	56	59	60	60	61	44
210	0	47	47	49	51	53	56	59	60	60	60	45
240	0	46	47	48	51	53	56	59	60	60	60	44
Ave:		46	47	48	51	53	56	58	60	60	61	44
T _{ave} :		54	T _{1,in} :		22		T _o :		22			
270	0	46	47	48	51	53	56	58	60	60	61	44
300	1.3	47	47	48	51	53	56	59	60	61	61	44
330	1.3	46	47	48	51	53	56	59	61	62	61	44
360	1.3	46	47	49	51	53	56	59	60	62	62	43
390	1.3	46	47	49	51	53	56	59	61	60	61	44
420	1.3	46	47	48	51	53	56	59	60	60	61	45
450	1.3	46	48	48	51	53	56	59	60	60	61	45
480	1.3	46	47	48	51	53	56	59	60	60	61	43
510	1.3	46	47	49	51	53	56	59	60	60	61	44
540	1.3	46	47	49	51	53	56	59	60	61	61	43
570	1.3	46	47	49	51	53	56	59	60	61	62	45
600	1.3	46	47	48	51	53	56	58	60	60	61	44

630	1.3	46	47	48	51	53	56	59	61	60	61	45
660	1.3	46	48	48	51	53	56	59	60	61	61	44
690	1.3	46	47	48	51	53	56	58	60	61	62	44
720	1.3	46	47	49	51	54	56	59	61	61	61	45
750	1.3	47	47	49	51	53	56	60	61	62	61	44
780	1.3	46	47	49	51	54	57	60	61	60	62	44
810	1.3	47	47	49	51	54	56	59	61	61	61	44
840	1.3	46	47	49	52	54	57	60	61	61	61	44
870	1.3	47	47	48	52	54	56	59	61	61	62	44
900	1.3	46	47	48	52	53	57	59	60	62	61	44
930	1.3	46	47	49	52	54	56	59	61	61	61	45
960	1.3	47	47	49	52	54	56	59	61	61	62	44
990	1.3	46	48	49	52	54	56	60	61	61	62	46
1020	1.3	47	47	49	52	54	56	60	61	61	61	46
1050	1.3	47	48	49	51	54	56	60	61	61	61	45
1080	1.3	47	47	49	52	54	56	60	60	61	61	44
1110	1.3	47	47	49	52	54	56	59	61	61	61	45
1140	1.3	47	47	49	51	54	56	59	60	61	61	44
1170	1.3	47	47	49	51	54	56	59	61	61	63	44
1200	1.3	46	47	48	52	53	56	59	61	60	61	44
1230	1.3	46	47	48	51	53	56	59	61	60	61	44
1260	1.3	46	47	48	52	53	57	60	61	60	61	47
1290	0.14	46	47	48	51	53	56	59	61	60	61	46
1320	0	46	46	48	51	53	56	58	61	60	61	44
1350	0	45	46	48	50	53	55	58	60	59	60	43
1380	0	45	47	48	50	53	55	58	59	60	60	43
1410	0	45	46	47	50	53	55	58	59	59	59	44
1440	0	45	46	47	50	51	53	56	57	57	58	43
1470	0	45	46	47	49	51	53	55	56	56	56	42

DATE: 09-23-1992 TIME: 10:41:02

RUN NUMBER: 7

THE ATMOS. PRESSURE IS 29 MM OF MERCURY

HEATER POWER: 24 W

Evap. Mass Flow: 0.42 mL/min

TIME	INC	T1	T2	T3	T4	T5	T6	T7	T8	T9	T10	T11
0	0	46	47	49	51	55	56	60	61	62	62	43
30	0	46	48	49	51	53	56	59	61	63	62	43
60	0	47	47	49	51	54	57	60	61	61	63	43
90	0	47	47	49	52	54	57	59	61	62	62	45
120	0	46	48	49	51	54	57	60	61	62	62	44
150	0	47	48	49	52	54	57	59	61	62	64	43
180	0	47	48	49	52	54	57	59	61	62	62	44
210	0	47	48	49	52	54	57	60	62	62	63	43
240	0	48	48	49	52	54	57	59	62	62	62	44
270	0	47	48	49	52	54	57	59	61	62	62	43
300	0	47	48	49	52	54	57	59	62	62	63	43
330	0	47	48	49	52	54	57	59	61	62	62	43
Ave:		47	48	49	52	54	57	59	61	62	62	43
T _{ave} :		55		T _{1,1n} :		21		T _u :		21		
360	0	47	48	49	52	54	57	60	61	63	62	44
390	0.5	47	48	50	53	54	57	60	61	61	62	45
420	0.5	47	48	49	52	54	57	60	61	62	62	44
450	0.5	47	48	49	51	55	57	60	61	62	62	45
480	0.5	47	48	49	52	54	57	60	62	62	62	43
510	0.5	47	48	49	52	54	57	60	61	62	63	46
540	0.5	47	48	49	52	54	57	60	62	62	62	45
570	0.5	47	48	50	52	54	57	60	61	62	63	43
600	0.5	47	48	49	52	54	57	60	62	62	63	44
630	0.5	47	48	49	52	54	57	60	62	62	62	43
660	0.5	47	48	49	52	54	57	61	62	62	63	44
690	0.5	47	48	50	52	54	57	60	62	63	63	45
720	0.5	47	48	49	52	55	57	61	62	62	63	44
750	0.5	47	48	50	52	54	57	60	62	62	63	43
780	0.5	47	48	49	52	55	57	61	62	62	63	43
810	0.5	47	48	49	52	54	57	60	62	62	63	44

840	0.5	47	48	49	52	54	57	60	62	62	63	44
870	0.5	47	48	49	52	54	57	60	62	63	63	45
900	0.5	47	48	49	52	54	57	60	62	62	63	44
930	0.5	47	48	49	53	54	58	60	62	62	63	44
960	0.5	47	48	49	52	54	57	60	62	62	62	45
990	0.5	47	48	50	52	54	58	60	62	64	63	44
1020	0.5	47	48	50	52	55	57	60	62	63	64	44
1050	0.5	47	48	50	52	55	57	60	62	63	63	46
1080	0.5	47	48	50	52	54	57	61	61	62	64	46
1110	0.5	47	48	49	52	55	57	60	62	62	62	46
1140	0.5	47	48	49	52	54	57	60	62	62	63	44
1170	0.5	47	48	50	52	5	57	60	62	62	62	44
1200	0.5	47	48	50	53	54	57	60	62	62	63	43
1230	0.5	48	48	50	52	55	57	60	62	62	62	44
1260	0.5	47	48	50	52	55	57	61	62	62	62	45
1290	0.5	47	48	49	52	54	57	61	62	63	63	45
1320	0.5	47	48	50	52	54	57	61	62	63	63	44
1350	0.5	47	48	50	52	55	57	61	62	62	63	44
1380	0.5	47	48	50	53	54	57	60	62	62	63	44
1410	0.5	47	48	49	52	54	57	60	62	62	63	44
1440	0.5	47	48	50	52	54	57	60	61	62	63	44
1470	0.5	47	48	50	52	55	57	60	62	62	63	44
1500	0.5	47	48	50	52	54	57	60	62	62	63	44
1530	0.5	48	48	50	52	54	57	60	62	63	63	44
1560	0.5	47	48	50	52	54	57	60	62	63	63	45
1590	0.5	48	48	50	53	54	57	61	62	62	63	45
1620	0.5	47	48	50	52	55	57	60	62	63	63	45
1650	0.5	48	48	50	53	55	58	60	62	63	63	45
1680	0.5	48	49	50	52	54	57	61	62	62	63	44
1710	0.5	47	49	49	53	54	58	61	62	63	63	44
1740	0.5	47	48	50	53	55	57	61	62	62	64	44
1770	0.5	47	48	49	53	54	58	60	62	62	64	45
1800	0.5	48	48	50	53	54	58	60	62	62	64	44
1830	0.5	47	49	49	53	54	57	60	62	62	63	45
1860	0.5	47	48	50	53	55	57	61	62	63	63	45
1890	0.5	47	49	50	53	55	58	61	62	62	64	45

1920	0.5	47	49	50	53	55	58	60	62	62	63	45
1950	0.5	48	49	50	53	55	58	61	62	63	63	45
1980	0.5	47	48	49	53	55	58	60	62	62	63	44
2010	0.5	48	48	50	52	54	57	60	62	63	63	45
2040	0.5	47	48	50	52	54	58	60	62	62	63	44
2070	0.5	47	48	49	52	54	57	60	61	62	63	46
2100	0.5	47	48	50	53	55	58	61	62	63	63	46
2130	0.5	48	49	50	53	55	57	61	62	63	63	45
2160	0.5	48	49	50	53	55	58	61	62	63	63	44
2190	0.5	47	48	49	52	55	57	60	62	62	63	44
2220	0.5	47	49	49	53	54	58	60	62	62	63	44
2250	0.5	47	48	50	53	55	57	60	62	63	63	44
2280	0.5	48	49	50	53	55	57	61	62	62	63	45
2310	0.5	47	49	50	53	54	58	60	62	62	63	44
2340	0.5	47	48	50	52	54	57	60	62	62	63	45
2370	0.5	48	48	50	53	55	58	60	62	63	63	44
2400	0.5	47	48	50	52	55	57	60	62	62	63	46
2430	0.5	48	49	50	52	55	57	60	62	63	63	44
2460	0.5	47	48	50	52	55	58	60	62	62	64	44
2490	0.5	47	48	50	52	54	57	61	62	63	63	46
2520	0.5	48	48	50	52	55	57	60	62	62	63	44
2550	0.5	47	48	50	52	55	58	61	62	63	64	44
2580	0.5	47	48	50	52	55	57	60	62	63	63	48
2610	0.5	47	48	50	52	55	57	60	62	63	63	44
2640	0.5	47	48	50	52	55	57	60	62	63	64	44
2670	0.5	47	48	49	52	55	57	60	62	63	63	44
2700	0.5	47	48	50	52	54	57	60	62	63	63	44
2730	0.5	47	48	51	52	55	57	62	62	63	63	44
2760	0.5	47	48	50	52	55	57	60	62	63	63	45
2790	0.5	47	48	50	52	55	57	60	62	63	63	45
2820	0.5	48	49	50	52	55	57	60	62	62	63	45
2850	0.5	47	48	50	52	55	57	61	62	63	63	44
2880	0.5	47	48	50	53	55	57	61	62	63	63	44
2910	0.5	47	48	50	53	55	57	60	62	62	63	46
2940	0.5	48	48	50	53	55	58	60	63	63	63	44
2970	0.5	47	49	50	53	55	58	61	62	63	63	45
3000	0.5	47	48	50	52	55	57	61	62	63	64	44

3030	0.5	48	48	50	53	55	57	61	62	63	63	44
3060	0.5	48	48	50	52	55	58	61	63	63	63	44
3090	0.5	48	48	50	52	55	57	61	62	62	63	45
3120	0.5	47	49	50	53	55	57	61	62	63	63	45
3150	0.5	47	48	51	52	55	57	61	62	63	63	44
3180	0.5	48	49	50	53	55	58	60	62	63	63	44
3210	0.5	47	48	50	52	55	58	60	63	63	63	45
3240	0.5	47	49	50	53	55	58	61	62	64	63	44
3270	0.5	47	48	50	53	55	57	60	62	62	64	44
3300	0.5	47	48	50	53	55	58	61	62	63	63	44
3330	0.5	47	48	50	52	55	57	60	62	62	63	44
3360	0.5	47	48	50	52	54	58	61	62	63	64	44
3390	0	47	48	49	52	54	58	61	62	63	63	44
3420	0	47	48	49	52	54	57	60	62	62	63	43
3450	0	46	48	49	52	54	57	60	62	62	63	44
3480	0	46	48	50	52	54	57	60	62	62	63	44
3510	0	47	48	49	52	54	57	60	62	62	63	44
3540	0	47	48	49	52	54	57	60	62	62	63	44
3570	0	47	48	49	52	54	57	60	62	62	62	44
3600	0	47	48	49	52	54	57	60	62	62	63	45
3630	0	47	48	49	52	54	57	60	62	63	63	43
3660	0	47	48	49	52	55	57	60	62	62	63	44
3690	0	47	48	49	52	55	57	61	62	62	63	43
3720	0	48	48	50	52	54	57	60	62	63	63	44
3750	0	47	48	49	52	54	58	60	62	63	63	44
3780	0	47	48	50	52	55	57	61	62	62	63	44
3810	0	48	48	49	52	54	57	60	62	63	63	45
3840	0	47	48	50	52	55	57	60	62	62	63	44
3870	0	47	48	50	52	54	57	60	62	62	63	43
3900	0	47	48	50	52	54	57	60	62	62	63	44
3930	0	47	48	49	52	55	57	61	61	63	62	46
3960	0	47	48	49	52	54	57	60	62	63	62	44
3990	0	47	48	49	52	54	57	60	62	63	62	44
4020	0	47	48	49	52	54	57	60	62	62	63	44
4050	0	47	48	49	52	54	57	60	61	62	62	45
4080	0	47	48	49	52	55	57	61	62	62	63	44

4110	0	47	48	50	52	54	57	60	61	62	64	44
4140	0	47	49	50	52	54	57	60	62	63	63	44
4170	0	47	48	49	52	54	57	60	62	62	64	44
4200	0	47	48	49	52	54	57	60	61	63	63	44
4230	0	47	48	49	52	54	57	60	62	62	63	43
4260	0	47	48	49	52	54	57	61	62	62	63	44
4290	0	47	48	49	52	54	57	61	62	62	63	45
4320	0	48	48	49	53	54	57	60	62	62	63	44
4350	0	47	48	49	52	54	57	60	62	62	63	44

DATE: 09-23-1992 TIME: 12:00:02

RUN NUMBER: 8

THE ATMOS. PRESSURE IS 29 MM OF MERCURY

HEATER POWER: 24 W Evap. Mass Flow: 0.42 mL/min

TIME	INC	T1	T2	T3	T4	T5	T6	T7	T8	T9	T10	T11
0	0	47	48	49	52	54	57	61	61	62	63	43
30	0	47	48	49	52	54	57	60	61	62	62	43
60	0	47	48	50	52	54	57	60	61	62	62	44
90	0	47	48	49	52	54	57	60	61	62	62	44
120	0	47	48	50	52	54	57	60	61	61	62	43
Ave:		47	48	49	52	54	57	60	61	62	62	43
T _{ave} :		55		T _{1, in} :		21		T _{in} :		21		
150	0.65	47	48	49	52	54	57	60	61	61	63	45
180	0.65	47	48	49	52	54	56	60	61	62	62	43
210	0.65	47	48	49	52	54	57	60	61	62	63	44
240	0.65	47	48	50	52	54	57	61	61	62	62	44
270	0.65	47	48	49	52	54	57	60	62	63	62	46
300	0.65	47	48	50	52	54	57	60	62	62	62	44
330	0.65	47	48	50	52	54	57	61	62	62	63	44
360	0.65	47	48	50	52	55	57	61	62	63	63	44
390	0.65	47	49	50	53	54	58	60	62	62	63	45
420	0.65	48	48	49	52	54	57	61	62	62	63	44
450	0.65	47	48	49	53	54	57	60	62	62	63	45
480	0.65	47	48	50	53	54	57	60	62	62	63	44
510	0.65	47	49	50	52	55	57	60	62	63	63	44

540	0.65	47	49	49	52	55	58	61	62	62	63	46
570	0.65	47	48	49	53	55	58	60	62	62	63	44
600	0.65	47	49	50	53	55	57	60	62	62	63	45
630	0.65	48	48	50	53	55	58	62	62	62	63	44
660	0.65	47	48	50	53	55	58	60	62	62	63	44
690	0.65	47	48	50	52	55	57	60	62	62	63	44
720	0.65	48	49	50	53	56	58	61	62	64	64	46
750	0.65	48	49	50	53	55	58	60	62	62	64	44
780	0.65	48	48	50	53	55	58	60	62	63	63	45
810	0.65	47	49	51	53	55	58	60	62	63	63	44
840	0.65	47	49	50	53	55	57	61	62	62	63	44
870	0.65	47	49	50	53	55	58	61	62	62	63	45
900	0.65	47	49	50	53	55	58	60	62	63	63	45
930	0.65	47	49	50	53	55	58	60	62	62	63	44
960	0.65	48	49	50	53	55	58	60	63	64	63	44
990	0.65	47	49	50	53	55	58	61	62	63	64	44
1020	0.65	47	49	50	53	55	58	60	62	63	63	45
1050	0.65	47	48	50	53	55	58	60	62	63	63	44
1080	0.65	48	49	50	53	55	58	61	62	63	64	44
1110	0.65	48	49	50	53	55	58	60	62	62	63	44
1140	0.65	47	49	50	53	55	57	61	62	63	63	46
1170	0.65	47	49	50	53	55	58	61	62	63	63	44
1200	0.65	48	49	50	53	55	58	60	62	63	63	45
1230	0.65	47	49	50	53	55	58	61	63	63	63	45
1260	0.65	48	49	51	53	56	58	61	63	63	63	44
1290	0.65	48	49	50	53	55	58	61	62	63	63	46
1320	0.65	48	49	50	53	55	58	61	63	63	63	45
1350	0.65	47	48	50	53	56	58	60	62	62	63	44
1380	0.65	48	49	50	53	55	58	61	63	62	63	44
1410	0.65	47	48	50	53	55	58	61	63	62	63	44
1440	0.65	47	48	49	53	55	58	60	62	62	63	44
1470	0.65	47	49	50	53	55	58	60	62	63	63	44
1500	0.65	47	48	50	52	55	57	61	63	62	63	44
1530	0.65	47	49	50	53	55	58	61	63	63	63	45
1560	0.65	48	49	51	53	55	58	61	63	64	63	47
1590	0.65	48	49	50	53	55	58	61	63	63	64	45
1620	0.65	47	49	50	53	55	58	61	62	63	63	44

1650	0.65	48	49	50	53	55	58	61	63	63	63	47
1680	0.65	48	49	50	53	55	58	61	63	63	64	45
1710	0.65	48	49	50	53	55	58	61	63	63	64	45
1740	0.65	48	49	50	53	55	58	61	63	63	64	44
1770	0.65	48	49	50	53	55	58	61	63	63	63	44
1800	0.65	48	49	50	53	55	58	61	63	63	63	45
1830	0.65	49	49	50	53	56	58	61	63	63	63	44
1860	0.65	48	49	50	53	55	58	61	63	63	63	45
1890	0.65	48	49	50	53	56	58	61	63	63	64	46
1920	0.65	48	49	50	53	55	58	61	63	63	64	45
1950	0.65	48	49	51	53	55	58	61	63	63	64	45
1980	0.65	48	49	50	53	55	58	61	63	63	64	45
2010	0.65	48	49	50	53	55	59	61	63	63	64	45
2040	0.65	48	49	50	53	55	58	61	63	63	64	45
2070	0.65	48	49	50	53	55	58	61	63	63	63	45
2100	0.65	48	49	50	53	55	58	61	62	63	64	45
2130	0.65	48	49	50	53	55	58	61	63	62	63	44
2160	0.65	48	49	50	53	55	58	61	63	63	64	45
2190	0.65	48	49	51	53	56	58	61	62	64	63	45
2220	0.65	48	49	51	53	55	58	61	63	63	64	44
2250	0.65	48	49	50	53	55	58	61	63	63	63	45
2280	0.65	48	49	51	53	55	58	61	63	63	63	45
2310	0.65	48	49	50	53	55	58	61	62	63	64	45
2340	0.65	48	49	50	53	55	58	61	63	63	63	47
2370	0.65	48	49	50	53	55	58	62	63	63	63	45
2400	0.65	48	49	50	53	56	58	61	63	64	64	45
2430	0.65	48	49	51	53	55	58	61	63	63	63	45
2460	0.65	48	49	51	53	55	58	62	63	63	64	46
2490	0.65	48	49	50	53	55	58	61	63	63	64	44
2520	0.65	48	49	51	54	55	58	61	63	63	64	44
2550	0.65	48	49	50	53	55	58	61	63	63	64	45
2580	0.65	48	49	50	53	55	58	61	63	64	64	44
2610	0.65	48	49	50	53	55	58	61	63	64	64	45
2640	0.65	48	49	51	53	55	58	61	63	63	64	44
2670	0.65	48	49	50	53	55	58	61	63	63	64	44
2700	0.65	48	49	50	53	55	58	61	63	63	63	44

2730	0.65	48	49	51	53	55	58	61	63	63	64	44
2760	0.65	48	49	50	53	55	58	61	63	64	63	44
2790	0.65	48	49	51	53	55	58	61	63	63	63	45
2820	0.65	48	49	50	53	55	58	61	63	63	64	44
2850	0.65	48	49	50	53	55	58	61	63	64	64	44
2880	0.65	48	49	50	53	56	58	61	62	64	63	45
2910	0.65	48	49	50	53	55	58	61	63	63	63	45
2940	0.65	48	49	50	53	55	58	61	63	64	64	44
2970	0.65	48	49	51	53	56	58	61	63	63	64	45
3000	0.65	48	49	50	54	56	58	61	63	63	64	45
3030	0.65	48	49	50	53	55	58	61	63	63	64	45
3060	0.65	48	49	50	53	56	58	61	63	63	63	46
3090	0.65	48	49	50	53	55	58	61	63	64	64	45
3120	0.65	48	49	50	53	55	58	61	63	63	64	44
3150	0.65	48	49	50	53	56	58	61	63	63	64	46
3180	0.65	48	49	51	53	55	58	61	63	63	64	45
3210	0.65	48	49	50	53	55	58	61	63	64	64	45
3240	0.65	48	49	50	53	55	58	61	63	64	64	45
3270	0.65	48	49	50	53	56	58	62	63	63	63	45
3300	0.65	48	49	50	53	55	58	61	62	63	64	45
3330	0.65	48	49	50	53	55	58	61	63	64	64	45
3360	0.17	48	48	50	53	55	58	61	63	62	63	44
3390	0	47	48	50	52	55	57	61	62	62	63	43
3420	0	47	48	50	53	55	57	60	62	62	63	47
3450	0	48	48	50	52	55	57	60	62	62	63	44
3480	0	47	48	50	52	55	57	61	62	62	63	44
3510	0	47	48	50	52	55	57	61	62	63	63	46
3540	0	47	48	50	53	55	57	60	62	62	63	44
3570	0	47	48	50	53	55	57	60	62	62	62	46
3600	0	48	48	51	53	55	58	61	63	63	63	44
3630	0	48	49	50	53	55	57	61	63	62	63	45
3660	0	48	49	50	53	55	58	61	62	63	63	45
3690	0	48	49	50	53	55	58	61	62	63	63	45
3720	0	48	49	50	53	55	58	60	62	63	63	45
3750	0	48	49	50	53	55	57	61	62	64	63	45
3780	0	48	49	50	53	55	58	62	63	63	63	44
3810	0	48	49	50	53	55	58	61	62	62	64	44

3840	0	48	49	51	53	55	58	60	62	62	63	44
3870	0	48	49	51	53	55	58	61	62	63	63	44
3900	0	48	49	50	53	55	58	61	62	62	64	44
3930	0	48	49	50	53	55	58	61	62	62	63	44
3960	0	48	49	50	53	56	58	62	62	62	63	46
3990	0	48	49	50	53	55	58	61	62	63	64	44
4020	0	48	49	50	53	55	58	62	62	63	63	45
4050	0	48	49	50	53	55	58	62	62	62	63	44
4080	0	48	49	50	53	55	58	61	62	62	63	44
4110	0	48	49	50	53	55	58	62	62	63	63	45
4140	0	48	49	50	53	55	58	61	62	63	63	45
4170	0	47	49	50	53	55	58	63	62	62	63	44
4200	0	48	49	50	53	55	58	61	62	62	63	44
4230	0	48	49	51	53	55	58	60	62	62	63	45
4260	0	48	49	50	53	55	58	60	62	62	63	45
4290	0	48	49	50	53	55	58	62	62	62	63	45
4320	0	48	49	50	53	55	57	61	62	62	64	44
4350	0	48	49	50	53	55	58	61	62	62	63	44
4380	0	48	49	50	53	55	58	60	63	63	63	45
4410	0	48	49	50	53	55	58	60	62	62	63	44
4440	0	48	49	50	53	55	58	61	62	63	63	45
4470	0	48	49	50	53	55	58	60	62	63	63	44
4500	0	48	49	50	53	55	58	60	62	62	63	45
4530	0	48	49	50	53	55	58	61	62	63	63	44
4560	0	48	49	50	53	55	58	61	63	62	63	46
4590	0	48	49	50	53	55	58	60	62	62	63	44
4620	0	48	49	50	53	55	58	61	63	62	64	44
4650	0	48	48	50	53	55	58	61	62	62	63	45
4680	0	48	48	50	53	55	57	61	62	62	63	44
4710	0	48	48	50	53	55	58	60	62	62	63	45
4740	0	48	48	50	53	55	57	61	62	62	62	47
4770	0	48	49	50	53	55	58	61	62	62	63	44
4800	0	48	48	50	53	55	57	61	62	63	63	45
4830	0	48	48	50	53	55	57	61	62	62	63	46
4860	0	48	49	50	52	55	57	61	62	62	63	44
4890	0	47	49	50	53	55	57	62	62	62	63	44

4920	0	48	48	50	53	55	57	60	62	62	63	44
4950	0	48	49	50	53	55	57	61	62	64	63	46
4980	0	48	49	50	52	55	57	61	62	63	64	44
5010	0	48	48	50	53	55	57	60	62	62	63	44

DATE: 09-23-1992 TIME: 13:29:01

RUN NUMBER: 9

THE ATMOS. PRESSURE IS 29 MM OF MERCURY

HEATER POWER: 24 W Evap. Mass Flow: 0.42 mL/min

TIME	INC	T1	T2	T3	T4	T5	T6	T7	T8	T9	T10	T11
0	0	47	48	50	53	55	57	60	62	63	63	44
30	0	47	49	50	53	55	57	61	62	62	63	44
60	0	47	49	51	53	55	58	61	62	63	63	45
90	0	47	49	50	53	55	58	60	62	63	63	44
120	0	48	49	50	53	55	58	61	62	62	63	45
150	0	47	49	50	53	55	57	61	62	63	63	44
180	0	48	49	50	53	55	58	60	62	63	63	44
210	0	48	49	50	53	55	58	60	62	63	63	46
240	0	47	49	50	53	55	57	61	62	62	62	45
Ave:		47	49	50	53	55	58	61	62	63	63	45
T _{ave} :		56		T _{1,in} :		21		T _{in} :		21		
270	0	47	48	50	53	55	58	61	62	62	63	44
300	0.86	48	48	50	52	54	58	60	62	62	63	44
330	0.86	48	48	50	52	55	57	61	62	62	63	44
360	0.86	48	48	49	52	55	57	60	62	62	63	44
390	0.86	47	48	50	53	55	57	61	62	62	63	45
420	0.86	48	48	50	53	55	57	61	62	62	63	44
450	0.86	48	48	50	52	55	57	60	62	62	62	46
480	0.86	48	48	50	53	55	57	60	62	63	63	45
510	0.86	47	48	50	52	55	58	60	62	62	63	44
540	0.86	47	48	50	52	55	58	60	62	63	63	44
570	0.86	47	48	50	52	55	58	60	62	63	63	45
600	0.86	47	48	50	52	55	57	60	62	62	63	44
630	0.86	47	49	50	52	55	57	62	62	62	63	45
660	0.86	47	48	50	53	55	57	61	62	63	63	44

690	0.86	48	48	50	52	55	57	61	63	63	63	44
720	0.86	47	48	50	52	55	57	61	62	62	63	45
750	0.86	48	49	50	53	55	58	60	63	62	64	44
780	0.86	47	49	50	53	55	58	61	62	62	63	44
810	0.86	48	48	50	53	55	58	61	63	63	64	44
840	0.86	48	49	50	53	55	58	61	62	62	63	46
870	0.86	48	48	50	53	55	57	61	62	62	63	45
900	0.86	47	48	49	53	55	58	60	62	63	63	44
930	0.86	47	48	50	52	55	58	61	62	62	63	44
960	0.86	48	48	50	52	55	57	61	62	62	63	44
990	0.86	48	49	50	52	55	58	60	62	62	63	46
1020	0.86	47	48	50	53	55	58	60	62	63	63	44
1050	0.86	48	48	50	53	55	58	61	63	62	64	44
1080	0.86	47	49	50	53	55	58	61	63	64	63	44
1110	0.86	48	49	50	53	55	58	61	63	63	63	45
1140	0.86	48	49	50	53	55	58	61	63	63	64	44
1170	0.86	48	49	50	53	55	58	61	63	63	63	46
1200	0.86	48	49	51	53	56	58	61	63	63	63	44
1230	0.86	48	49	51	53	55	58	61	63	63	63	46
1260	0.86	48	49	50	53	55	58	61	63	63	63	45
1290	0.86	48	49	50	53	55	58	61	63	63	63	45
1320	0.86	48	49	50	53	55	58	61	62	63	64	47
1350	0.86	48	49	50	53	55	58	61	63	62	64	44
1380	0.86	48	49	50	53	55	58	61	62	63	63	45
1410	0.86	48	49	51	53	56	58	61	63	64	63	45
1440	0.86	49	49	51	53	56	58	61	63	63	63	44
1470	0.86	48	49	51	53	55	59	61	63	63	64	44
1500	0.86	48	49	51	53	56	58	61	63	63	63	45
1530	0.86	48	49	51	53	56	58	62	63	64	63	45
1560	0.86	48	49	50	53	56	58	61	63	63	64	45
1590	0.86	48	49	51	54	56	58	61	63	63	63	45
1620	0.86	48	49	50	54	56	58	61	63	63	63	45
1650	0.86	48	49	50	53	55	58	61	63	63	63	44
1680	0.86	48	49	51	53	56	58	62	63	63	63	45
1710	0.86	48	49	50	53	55	58	62	63	63	63	45
1740	0.86	48	49	50	53	55	58	61	62	64	63	44
1770	0.86	48	49	50	53	55	58	61	63	63	63	44

1800	0.86	48	49	50	53	55	58	61	63	63	64	44
1830	0.86	49	49	51	53	56	58	62	63	63	64	45
1860	0.86	48	49	50	53	56	58	61	62	63	65	45
1890	0.86	48	49	50	53	56	58	63	63	63	64	45
1920	0.86	48	49	50	53	55	58	62	63	64	64	44
1950	0.86	48	49	51	53	56	58	61	63	63	64	44
1980	0.86	48	49	51	53	56	58	61	63	63	63	46
2010	0.86	49	49	51	53	56	59	61	63	63	64	45
2040	0.86	48	49	50	54	56	58	62	63	64	64	45
2070	0.86	48	49	51	53	56	58	61	63	63	63	45
2100	0.86	48	49	51	54	56	59	62	63	63	64	45
2130	0.86	48	49	51	53	56	58	61	63	63	64	46
2160	0.86	48	49	50	54	56	58	62	63	63	63	45
2190	0.86	48	49	51	53	56	59	61	63	63	64	45
2220	0.86	48	49	50	53	56	58	61	63	63	64	45
2250	0.86	48	49	51	54	56	58	61	63	63	64	45
2280	0.86	48	49	51	53	56	58	61	62	63	64	44
2310	0.86	48	49	51	53	56	58	61	63	63	64	45
2340	0.86	48	49	51	53	56	58	61	63	64	64	47
2370	0.86	48	49	51	53	56	58	61	63	65	63	45
2400	0.86	48	49	51	53	56	58	63	63	64	64	45
2430	0.86	48	49	52	54	56	58	61	63	63	64	45
2460	0.86	48	49	51	53	56	58	61	63	63	64	45
2490	0.86	49	49	51	53	56	59	61	63	63	64	47
2520	0.86	48	50	51	53	56	58	61	63	63	64	45
2550	0.86	48	49	51	54	56	59	61	63	63	64	45
2580	0.86	48	49	51	53	56	59	62	63	63	64	45
2610	0.86	49	49	51	54	56	58	61	63	63	64	45
2640	0.86	48	49	51	54	55	59	61	63	63	64	44
2670	0.86	48	49	51	54	56	59	61	63	63	64	44
2700	0.86	48	49	51	54	56	59	62	63	63	64	45
2730	0.86	49	49	51	54	56	59	61	63	63	64	44
2760	0.86	49	49	51	54	56	59	61	63	63	64	45
2790	0.86	49	49	51	54	56	59	62	63	65	64	45
2820	0.86	49	49	51	53	56	58	61	63	64	64	44
2850	0.86	48	49	50	53	56	58	61	63	63	64	45

2880	0.86	48	49	51	53	55	59	61	63	63	64	44
2910	0.86	48	49	51	53	56	58	62	63	63	63	45
2940	0.86	48	49	50	53	55	59	61	63	63	64	44
2970	0.86	48	49	51	53	56	58	61	63	63	64	45
3000	0.86	48	49	51	53	56	58	62	63	63	63	48
3030	0.86	48	49	50	53	56	58	61	63	63	64	47
3060	0.86	48	49	51	54	56	59	61	63	64	64	45
3090	0.86	49	49	50	53	56	58	61	63	64	64	45
3120	0.86	48	49	52	53	56	58	61	63	63	65	45
3150	0.86	48	49	51	53	56	58	61	63	63	64	45
3180	0.86	48	49	51	53	55	59	61	63	63	64	44
3210	0.86	48	50	51	53	56	58	61	63	64	64	45
3240	0.86	48	49	51	54	56	58	62	63	65	63	46
3270	0.86	48	49	51	53	56	58	62	63	63	64	45
3300	0	48	49	50	53	55	58	61	63	63	64	44
3330	0	48	49	50	53	55	58	60	63	62	64	45
3360	0	47	49	50	53	55	58	61	62	63	63	44
3390	0	48	49	50	53	55	58	61	62	62	64	44
3420	0	49	49	50	53	55	58	62	62	62	64	44
3450	0	48	49	50	53	55	58	61	62	62	63	45
3480	0	48	49	50	53	55	58	61	63	63	63	44
3510	0	48	49	51	53	55	58	61	62	63	63	45
3540	0	48	49	50	53	55	58	62	62	63	64	45
3570	0	48	49	50	53	55	58	62	63	63	63	45
3600	0	48	49	50	53	55	58	61	62	62	63	45
3630	0	48	49	50	53	55	58	61	63	64	63	44
3660	0	48	49	50	53	55	58	61	62	62	63	46
3690	0	48	49	50	53	55	58	61	63	62	63	45
3720	0	48	49	50	53	55	58	61	62	62	63	44
3750	0	48	49	50	53	55	58	61	62	62	63	45
3780	0	48	49	51	53	55	58	61	62	62	63	45
3810	0	48	49	50	53	55	58	62	62	63	63	45
3840	0	48	49	51	53	55	58	61	62	63	64	44
3870	0	48	49	50	53	57	58	61	63	62	64	46
3900	0	49	49	50	53	55	58	61	62	63	63	46
3930	0	48	49	50	53	55	58	61	63	62	64	44
3960	0	48	49	50	53	55	58	61	62	63	63	44

3990	0	48	49	50	53	56	58	61	62	62	63	45
4020	0	48	49	50	53	55	58	60	63	62	63	45
4050	0	48	49	50	53	55	58	61	62	62	63	45
4080	0	48	49	50	53	55	58	62	63	63	63	45
4110	0	48	49	51	53	55	58	61	63	62	63	45
4140	0	48	49	50	53	55	58	61	63	62	63	45
4170	0	48	49	50	53	55	58	60	62	62	63	44
4200	0	48	49	50	53	55	58	61	62	62	64	45
4230	0	48	49	50	53	55	58	61	63	63	63	45
4260	0	48	48	50	53	55	58	60	62	62	63	45
4290	0	47	48	50	53	55	58	60	62	62	63	43
4320	0	47	49	50	52	55	57	60	62	62	63	44
4350	0	48	49	50	53	55	58	60	62	62	63	44
4380	0	48	49	50	53	55	58	61	63	63	63	44
4410	0	48	49	50	53	55	57	61	62	62	63	45
4440	0	48	49	50	53	55	57	60	62	63	62	47

DATE: 09-23-1992 TIME: 14:56:30

RUN NUMBER: 10

THE ATMOS. PRESSURE IS 29 MM OF MERCURY

HEATER POWER: 24 W Evap. Mass Flow: 0.42 mL/min

TIME	INC	T1	T2	T3	T4	T5	T6	T7	T8	T9	T10	T11
0	0	47	48	50	52	55	57	60	62	62	62	45
30	0	47	48	50	53	55	57	61	62	62	63	47
60	0	48	48	50	53	55	58	61	62	63	63	44
90	0	48	48	50	52	55	57	60	62	62	63	44
120	0	48	49	50	53	55	58	61	62	62	63	44
Ave:		48	48	50	53	55	57	61	62	62	63	45
T _{ave} :		56		T _{1,in} :		22		T _m :		22		
150	1.3	47	49	50	53	55	58	60	62	62	63	44
180	1.3	48	48	50	52	55	57	60	62	62	63	44
210	1.3	47	49	50	53	55	58	61	62	63	63	45
240	1.3	47	49	50	53	55	58	61	62	62	63	44
270	1.3	48	49	51	53	55	58	61	63	63	63	45
300	1.3	49	49	50	53	55	58	61	63	64	64	44

330	1.3	48	49	50	53	55	58	61	63	63	63	45
360	1.3	48	49	51	53	55	58	61	63	62	64	44
390	1.3	48	49	51	53	55	58	61	63	63	63	45
420	1.3	48	49	50	53	55	58	61	63	63	63	44
450	1.3	49	49	50	53	55	58	62	63	63	63	45
480	1.3	48	49	50	53	55	58	61	63	63	64	45
510	1.3	48	49	50	53	55	58	61	62	63	63	46
540	1.3	48	49	50	53	55	58	61	63	62	64	44
570	1.3	48	49	51	53	56	58	61	62	63	63	45
600	1.3	48	49	50	53	55	58	61	63	64	63	45
630	1.3	48	49	50	53	55	59	61	63	63	63	47
660	1.3	48	49	50	53	56	58	61	63	63	63	46
690	1.3	48	49	50	53	55	58	61	63	63	63	44
720	1.3	48	49	51	54	56	58	62	63	63	63	45
750	1.3	48	49	51	54	56	58	62	63	64	63	45
780	1.3	48	49	51	53	55	59	61	63	63	64	45
810	1.3	48	49	51	54	56	58	62	63	65	64	45
840	1.3	48	49	51	54	55	59	62	63	64	64	45
870	1.3	48	49	52	54	55	58	61	63	64	64	44
900	1.3	48	49	50	53	56	58	62	63	63	64	44
930	1.3	49	49	51	53	56	59	61	63	63	64	46
960	1.3	48	49	51	53	56	58	62	63	64	64	45
990	1.3	48	49	51	53	56	58	61	63	63	64	45
1020	1.3	48	49	51	54	56	59	62	63	64	64	46
1050	1.3	48	49	51	54	56	58	61	63	63	64	45
1080	1.3	48	49	51	53	56	58	62	62	63	64	45
1110	1.3	48	49	51	53	56	59	61	63	65	64	45
1140	1.3	48	49	50	54	56	58	61	63	63	64	45
1170	1.3	48	49	51	53	56	58	61	63	63	64	45
1200	1.3	49	49	51	54	56	58	61	63	63	65	45
1230	1.3	48	49	51	53	55	59	61	63	63	64	46
1260	1.3	48	49	50	53	56	58	61	63	64	64	46
1290	1.3	48	49	50	53	56	58	61	63	64	63	46
1320	1.3	49	49	50	53	55	59	61	63	63	64	45
1350	1.3	48	49	51	53	56	58	61	63	64	65	45
1380	1.3	49	49	51	53	55	58	61	63	63	64	45

1410	1.3	48	49	51	53	56	58	62	63	64	64	45
1440	1.3	48	49	50	53	55	58	61	63	64	65	44
1470	1.3	48	49	50	53	56	58	62	63	63	64	45
1500	1.3	48	50	51	54	56	58	62	63	64	64	47
1530	1.3	48	49	51	53	56	58	61	63	63	64	45
1560	1.3	48	49	51	53	56	58	62	63	63	64	47
1590	1.3	48	49	51	53	56	58	61	63	63	64	46
1620	1.3	48	49	52	54	56	59	61	63	64	64	45
1650	1.3	48	49	51	54	56	59	61	63	64	64	45
1680	1.3	48	49	51	54	56	58	61	63	64	64	45
1710	1.3	48	49	51	54	56	58	61	63	63	64	45
1740	1.3	48	49	51	54	56	59	62	63	64	64	45
1770	1.3	48	50	51	54	56	59	62	63	63	65	45
1800	1.3	49	50	51	54	56	59	61	63	63	65	45
1830	1.3	49	50	51	54	56	59	62	63	63	64	45
1860	1.3	48	50	51	54	56	59	62	63	63	64	46
1890	1.3	48	49	51	54	56	59	62	63	63	64	45
1920	1.3	49	49	51	54	56	59	61	63	64	64	45
1950	1.3	49	50	51	54	56	59	61	63	63	64	45
1980	1.3	49	50	51	54	56	59	62	64	64	65	45
2010	1.3	49	50	51	54	56	59	62	63	63	64	46
2040	1.3	49	50	52	54	56	59	62	64	64	64	48
2070	1.3	49	50	51	54	56	59	62	64	64	65	45
2100	1.3	48	50	51	54	56	59	62	63	64	64	46
2130	1.3	49	50	51	54	56	59	62	63	63	64	45
2160	1.3	49	50	51	54	56	59	62	63	65	66	45
2190	1.3	48	50	51	54	56	59	62	63	64	64	45
2220	1.3	49	50	51	54	56	59	62	63	64	64	47
2250	1.3	48	50	51	54	56	59	62	63	64	65	45
2280	1.3	49	50	51	54	56	59	62	64	64	65	45
2310	1.3	49	50	51	54	56	59	63	64	65	64	46
2340	1.3	49	49	51	54	57	59	62	63	64	64	45
2370	1.3	49	50	51	54	56	59	62	64	64	65	48
2400	1.3	49	50	51	54	57	59	62	64	64	65	45
2430	1.3	49	50	51	54	56	59	62	64	64	64	46
2460	1.3	49	50	51	54	57	59	62	64	64	66	46
2490	1.3	49	50	52	54	57	59	62	64	64	65	45

2520	1.3	49	50	51	54	57	59	63	64	64	65	46
2550	1.3	49	50	51	54	57	59	63	64	66	65	47
2580	1.3	49	50	52	54	56	59	63	64	64	64	47
2610	1.3	49	50	52	54	56	59	62	64	64	65	45
2640	1.3	49	50	51	54	56	59	62	63	64	65	45
2670	1.3	49	50	51	54	57	59	62	64	65	65	46
2700	1.3	49	50	51	54	56	59	62	64	64	65	45
2730	1.3	49	50	52	54	57	59	62	64	65	65	45
2760	1.3	49	50	51	54	56	59	62	64	64	64	45
2790	1.3	49	50	51	55	56	59	63	64	64	65	45
2820	1.3	49	50	52	54	56	59	62	64	64	65	45
2850	1.3	49	50	52	54	57	59	62	64	64	65	47
2880	1.3	49	50	51	54	57	59	62	64	64	64	46
2910	1.3	49	50	51	54	56	59	62	64	64	64	45
2940	1.3	49	50	51	54	57	59	62	64	64	64	45
2970	1.3	49	50	51	54	56	59	62	64	64	65	45
3000	1.3	49	50	51	54	56	59	62	64	64	64	46
3030	1.3	49	50	51	54	57	59	62	64	64	64	46
3060	1.3	49	50	51	54	56	60	64	64	64	64	46
3090	1.3	49	50	51	54	56	59	62	64	63	64	46
3120	1.3	49	50	51	55	56	59	62	64	65	64	45
3150	1.3	49	50	51	54	57	59	62	64	64	64	45
3180	0.15	48	49	51	53	56	59	62	64	64	64	46
3210	0	48	50	51	54	56	59	62	63	63	64	45
3240	0	48	49	51	53	56	58	61	63	66	64	44
3270	0	48	49	50	53	56	59	62	63	63	64	45
3300	0	48	49	51	53	56	58	61	63	63	63	45
3330	0	48	49	50	54	56	59	61	63	64	64	48
3360	0	48	49	51	53	56	58	62	63	63	64	45
3390	0	48	49	51	54	56	58	61	63	63	63	45
3420	0	48	49	51	53	56	58	62	63	63	64	45
3450	0	49	49	51	53	55	58	61	63	62	63	45
3480	0	48	50	50	53	55	58	61	63	63	63	45
3510	0	48	49	51	53	55	58	61	63	62	63	45
3540	0	48	49	50	53	55	58	61	63	62	63	46
3570	0	48	49	50	53	56	58	61	63	63	63	45

3600	0	48	49	50	53	55	58	61	63	63	63	44
3630	0	48	49	51	53	57	58	61	62	62	63	46
3660	0	48	49	51	53	55	58	61	63	64	63	45
3690	0	48	49	50	53	55	58	62	63	63	64	44
3720	0	48	49	51	53	55	58	61	62	62	63	45
3750	0	49	49	51	53	55	58	61	63	63	63	46
3780	0	48	49	50	53	55	58	61	62	62	63	45
3810	0	48	49	50	53	55	58	61	63	62	63	45
3840	0	48	49	50	53	55	58	61	62	62	64	45
3870	0	48	49	50	54	55	58	61	63	62	63	47
3900	0	48	49	50	53	55	58	61	63	63	63	45
3930	0	48	49	50	53	55	58	61	63	62	63	45
3960	0	48	49	50	53	56	58	61	62	62	63	45
3990	0	48	49	51	53	56	58	61	63	62	63	45
4020	0	48	49	50	53	55	58	61	62	62	63	45
4050	0	48	49	51	53	55	58	61	63	63	63	45
4080	0	48	49	50	53	55	58	60	63	62	63	45
4110	0	48	49	51	53	55	58	61	63	62	63	45
4140	0	48	49	50	53	55	58	61	63	63	63	45
4170	0	48	49	50	53	55	58	61	62	62	63	44
4200	0	48	49	50	53	55	58	61	63	62	64	47
4230	0	48	49	51	53	55	58	61	62	62	63	45
4260	0	48	49	50	53	55	58	61	63	62	63	44
4290	0	48	50	50	53	55	58	61	63	62	64	45
4320	0	48	49	51	53	55	58	61	62	63	64	45
4350	0	48	49	51	53	56	58	61	63	63	63	45
4380	0	48	49	50	53	55	58	61	63	63	63	45
4410	0	48	49	51	54	56	59	61	63	63	63	44
4440	0	48	49	50	53	55	58	61	63	62	63	45

VITA

Captain Lowell S. Hawthorne was born on 6 September 1966 in Irving, Texas, but spent most of his life in San Diego, California. He graduated from Fallbrook Union High School in Fallbrook, California, in 1984 and accepted an appointment to the United States Air Force Academy in Colorado Springs, Colorado, graduating in 1988 with a Bachelor of Science in Engineering Mechanics. Upon graduation, he received a regular commission in the USAF and served his first tour of duty as the 6960th Security Police Squadron's Officer in Charge of Security Police Administration at Electronic Security Command Headquarters, Kelly AFB, Texas. In this position he oversaw several multimillion dollar security construction projects as well as assisting Sandia National Laboratories in the design, installation and evaluation of a multimillion dollar alarm system for the Air Force Cryptologic Support Center's new Headquarters. He entered the School of Engineering, Air Force Institute of Technology, in May 1991.

Permanent Address: 100 Camino del Oeste
Bakersfield, CA 93309

REPORT DOCUMENTATION PAGE

1. AGENCY USE ONLY (Leave blank)		2. REPORT DATE DEC 92		3. REPORT TYPE AND DATES COVERED MASTER'S THESIS	
4. TITLE AND SUBTITLE REWET PERFORMANCE OF A RECTANGULAR GROOVED HEAT PIPE WICK AFTER GRAVITATIONALLY INDUCED DRYOUT				5. FUNDING NUMBERS	
6. AUTHOR(S) LOWELL S. HAWTHORNE, CAPTAIN, USAF					
7. PERFORMING ORGANIZATION NAME(S) AND ADDRESS(ES) AIR FORCE INSTITUTE OF TECHNOLOGY WPAFB OH 45433-6583				8. PERFORMING ORGANIZATION REPORT NUMBER AFIT/GA/ENY/92D-04	
9. SPONSORING MONITORING AGENCY NAME(S) AND ADDRESS(ES) AFWAL/POOS-3 WPAFB OH 45433				10. SPONSORING MONITORING AGENCY REPORT NUMBER	
11. SUPPLEMENTARY NOTES					
12a. DISTRIBUTION / AVAILABILITY STATEMENT APPROVED FOR PUBLIC RELEASE; DISTRIBUTION UNLIMITED				12b. DISTRIBUTION CODE	
13. ABSTRACT (Maximum 200 words) The effects of increased acceleration forces on the transient dryout and rewet performance of an axial groove heat pipe wick were experimentally studied using inclination to simulate increased acceleration forces. Two durations of increased acceleration were investigated, one being less than the time required for the groove to reach steady-state dryout conditions, the other being sufficient to ensure the groove had reached steady-state dryout conditions. The groove's extent of dryout was found to be greater at increased levels of acceleration. The period of time required for the groove to rewet after an acceleration induced dryout increased as acceleration increased. The period of time for rewet was independent of duration for higher acceleration levels. The time period required for the groove to return to starting steady-state temperatures was zero for short durations of increased acceleration, and increased as acceleration increased for short durations.					
14. SUBJECT TERMS HEAT PIPES, INCLINATION ANGLE, THERMOSYPHONS, RECTANGULAR AXIAL GROOVES, TRANSIENT RESPONSE, REWET, DRYOUT, WICKS, CAPILLARY FLOW, GRAVITATIONAL EFFECTS				15. NUMBER OF PAGES 141	
17. SECURITY CLASSIFICATION OF REPORT UNCLASSIFIED				16. PRICE CODE	
				20. LIMITATION OF ABSTRACT UL	
18. SECURITY CLASSIFICATION OF THIS PAGE UNCLASSIFIED		19. SECURITY CLASSIFICATION OF ABSTRACT UNCLASSIFIED			